PLASTIC ANTIBODIES FOR THE DETECTION OF BACTERIAL PROTEINS AND MICROORGANISMS

Azizur Rahman Khan

PLASTIC ANTIBODIES FOR THE DETECTION OF BACTERIAL PROTEINS AND MICROORGANISMS

Doctoral Thesis

Md. Azizur Rahman Khan

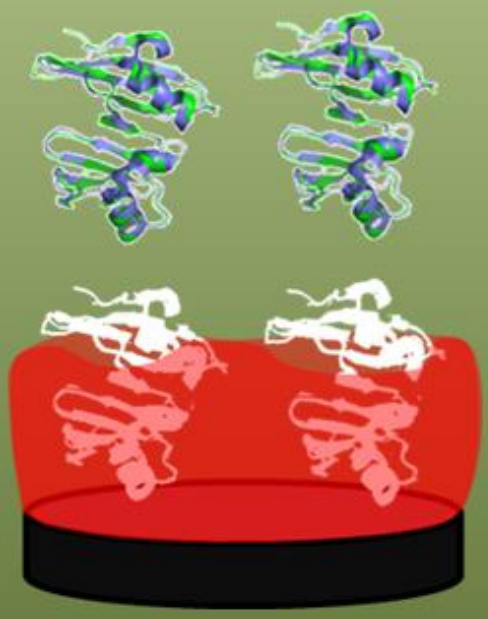

UNIVERSITAT ROVIRA I VIRGILI
Tarragona, Spain 2016

UNIVERSITAT ROVIRA I VIRGILI
PLASTIC ANTIBODIES FOR THE DETECTION OF BACTERIAL PROTEINS AND MICROORGANISMS
Azizur Rahman Khan

MD. AZIZUR RAHMAN KHAN

Plastic Antibodies for the detection of Bacterial Proteins and Microorganisms

DOCTORAL THESIS

supervised by

Dr. JORDI RIU RUSELL

UNIVERSITAT ROVIRA I VIRGILI

Department of Analytical Chemistry and Organic Chemistry

Tarragona, September 2016

UNIVERSITAT ROVIRA I VIRGILI
PLASTIC ANTIBODIES FOR THE DETECTION OF BACTERIAL PROTEINS AND MICROORGANISMS
Azizur Rahman Khan

MD. AZIZUR RAHMAN KHAN

Plastic Antibodies for the detection of Bacterial Proteins and Microorganisms

Tribunal members:

Prof. F. Xavier Rius Ferrús - Universitat Rovira i Virgili

Dr. Alicia Maroto Sánchez - Université de Bretagne Occidentale

Dr. Ana M. Benito - Consejo Superior de Investigaciones Científicas

External examiners:

Dr. Gustavo A. Zelada-Guillén - Universidad Nacional Autónoma de México

Dr. Felismina T.C. Moreira - Instituto Superior de Engenharia do Porto

UNIVERSITAT ROVIRA I VIRGILI

Department of Analytical Chemistry and Organic Chemistry

Tarragona, September 2016

UNIVERSITAT ROVIRA I VIRGILI
PLASTIC ANTIBODIES FOR THE DETECTION OF BACTERIAL PROTEINS AND MICROORGANISMS
Azizur Rahman Khan

UNIVERSITAT ROVIRA I VIRGILI

DEPARTAMENT DE QUÍMICA ANALÍTICA I QUÍMICA ORGÀNICA

Campus Sescelades, Marcel·lí Domingo, 1, 43007, Tarragona

Tel.: +34 977 55 84 91

E-mail: *jordi.riu@urv.cat*

Dr. Jordi Riu Rusell, Associate Professor at the Department of Analytical Chemistry and Organic Chemistry, Universitat Rovira i Virgili, Tarragona, Spain.

I STATE that the present study, entitled "*Plastic Antibodies for the detection of Bacterial Proteins and Microorganisms*", presented by *Md. Azizur Rahman Khan* for the award of the degree of Doctor, has been carried out under my supervision, in the Department of Analytical Chemistry and Organic Chemistry at the Universitat Rovira i Virgili. All the results presented in this thesis were obtained in experiments conducted by the above mentioned student, and meets the requirements to qualify for the International Doctorate mention.

Tarragona, 2 September 2016

Doctoral Thesis Supervisor

Dr. Jordi Riu Rusell

UNIVERSITAT ROVIRA I VIRGILI
PLASTIC ANTIBODIES FOR THE DETECTION OF BACTERIAL PROTEINS AND MICROORGANISMS
Azizur Rahman Khan

ACKNOWLEDGEMENTS

First of all, I want to express my deepest gratitude to my mentor, my supervisor Prof. Dr. Jordi Riu Rusell for his invaluable help, advice, enthusiasm and continuous support throughout this period of my life. He gave me constructive guidance and offered active discussion with his profound knowledge and rich research experiences throughout my research work. Additionally, his kindness and patience to students impressed me a lot. Sincerely, both his scientific and personal experience was really important in my personal development. I would thank to Prof. F. Xavier Rius Ferrús for allowing me to work in his group and whose guidance helped me to win the prestigious pre-doctoral fellowship (Grants for universities, research centres and hospital foundations to contract new research staff (FI-DGR) funded by Catalan Government, Spain.

I would also like to thank to Prof. M. Goreti F. Sales from Instituto Superior de Engenharia do Porto, Portugal for her invaluable suggestions, guidance, scientific and technical support during my research stay in Portugal. I am really grateful to her to help me in every aspect during my stay in Portugal. Additionally, special thanks go to Dr. Felismina T.C. Moreira, post-doctoral researcher, BioMark, Sensors Research Group, Porto, Portugal for her softness, helping mind and unconditional support during my stay in Portugal. To Prof. Susana Merino, University of Barcelona, for collaborating by providing flagella and bacterial kits.To Dr. Leonor G. Fernandez, National Polytechnic Institute, Mexico, who taught me culturing of bacteria and purification during her research stay in my group. To senior members of my research group Dr. Francisco J. Andrade, Dr. Pascal Blondeau and Dr. Santiago Macho, for their active co-operation for the research activities in the Group. Special thanks to my dearest friends Marc, Rocío, Marta, Tomas, Rafa, Par, Gabi, Rita and Carolina for their scientific and inventory discussion, valuable time, and mental support during this PhD period. My best wishes to all of you in your careers.

I would like to thank as well my parents my mother (Ma) and father, for their support and unconditional love, thanks for bringing me out in this world, Ma 'I love you both'. To my elder brother Md. Majibur Rahman Khan who is the person helps me in every step of my life, thanks for your unconditional support, help and love. You all serve my inspiration to push through. And above all, the Almighty Great Energy. Thanks for the wonderful life.

UNIVERSITAT ROVIRA I VIRGILI
PLASTIC ANTIBODIES FOR THE DETECTION OF BACTERIAL PROTEINS AND MICROORGANISMS
Azizur Rahman Khan

Dedicated to
My Beloved Parents

The woods are lovely, dark and deep,
But I have promises to keep,
And miles to go before I sleep,
And miles to go before I sleep.
-Robert Frost (1874-1963)

UNIVERSITAT ROVIRA I VIRGILI
PLASTIC ANTIBODIES FOR THE DETECTION OF BACTERIAL PROTEINS AND MICROORGANISMS
Azizur Rahman Khan

TABLE OF CONTENTS

SUMMARY

The diagnosis of most illnesses is of vital importance for providing the appropriate cure and hence controlling public health concerns. The standard methods that are used to confirm the presence of microorganisms typically consist of specific enrichment media to multiply, separate, identify and count bacterial cells. The duration of the process depends on the microorganism, but in most cases a confirmatory result can take from a few days to even weeks. One of the major objectives in this area is to detect microorganisms quickly, accurately and cheaply. Molecularly imprinted polymers (MIPs) offer in principle a robust, cost-efficient alternative to natural antibodies, but it is still a challenge to develop such materials for large molecule recognition. In this thesis we present a variety of molecular imprinting approaches for detecting bacterial proteins and/or microorganisms using techniques such as impedimetry, square wave voltammetry and potentiometry.

This doctoral thesis has been structured in chapters, each one of which contains the following information:

Chapter 1 gives a brief overview of general methods for detecting proteins and microorganisms, and an introduction to molecular imprinting approaches for detecting proteins and/or microorganisms. This chapter also includes a brief discussion about the detection techniques used in this thesis, and states its specific objectives.

Chapter 2 is the experimental part and describes the reagents, materials, protocols, instruments and techniques.

Chapter 3 demonstrates the detection of bacterial surface proteins from *Staphylococus aureus.*

Chapter 4 demonstrates a simple, cost-effective way for manually fabricating paper-printed electrodes including their application.

Chapter 5 describes the detection of bacterial flagella and *Proteus mirabilis*. The chapter is divided into three subsections: in the first, the bacterial flagella are detected based on impedimetry and/or square wave voltammetry techniques; the second is the extension of the first to detect whole cell of *Proteus mirabilis* and the third section describes the potentiomeric detection of flagella from *Proteus mirabilis* along with its whole cell.

Finally, **Chapter 6** reports the conclusions of the thesis including trends for the future work. In addition, the personal attributes and skills acquired during the doctoral period are briefly mentioned at the end of this chapter.

Chapter 1

Introduction

UNIVERSITAT ROVIRA I VIRGILI
PLASTIC ANTIBODIES FOR THE DETECTION OF BACTERIAL PROTEINS AND MICROORGANISMS
Azizur Rahman Khan

Chapter 1

This chapter contains three main sections: section **1.1** describes the state of the art of general methods for detecting proteins and microorganism and introduces molecularly imprinted polymers (MIPs), the sensing material used in this thesis; section **1.2** describes the techniques which have been used for detecting the target analytes during this doctoral thesis; and section **1.3** describes the specific objectives of this doctoral thesis.

1.1 Background

The purpose of section **1.1.1** is to give an overview of general analytical methods for detecting proteins and microoganisms and, where relevant, a brief description of their advantages and limitations. Section **1.1.2** focuses on molecularly imprinted polymers (MIPs), also known as plastic antibodies, as recognition elements in the detection of proteins and microorganisms.

1.1.1 General methods for detecting proteins and microorganisms

Detection of proteins is of great importance for making diagnoses and point of care testing. Protein detection can be classified into four major groups: a) electrophoretic separations; b) techniques that measure variations in surface properties due to molecular recognition events between a molecular receptor and its target (e.g. surface plasmon resonance, surface-enhanced Raman spectroscopy and others); c) mass spectrometry-based techniques; and d) immunoassay-based methods. In immunoassay-based methods, an antigen-antibody interaction is detected by electrochemically active labels, luminescence, fluorescence or radioactivity (Walker, 2002). The most common methods in diagnostics use western-blot assays, immunoblotting techniques, immunoprecipitation, immunofluorescence and immunosorbent assays (Barber and Eichler, 1985; Kurien and Scofield, 2009; Walker, 2002). These methods are widely used in research since they have the general advantages of high sensitivity and specificity but they are labor-intensive, time-consuming and require highly trained technical staff. Another limitation of these methods is the use of expensive instrumentation which is unsuited for point-of-care diagnostics applications. Of the immunoassay-based methods, probably the most widely used is the enzyme-linked immunosorbent assay (ELISA), developed by Engvall and Perlmann (Engvall E. and Perlmann, 1971) in 1971, a major turning point in protein detection in the past decades. Since then it has been adapted for the detection of a large number of target proteins. An overview of ELISA is presented in **Figure 1.1** (adapted from http://www.epitomics.com/products/product_info/1257).

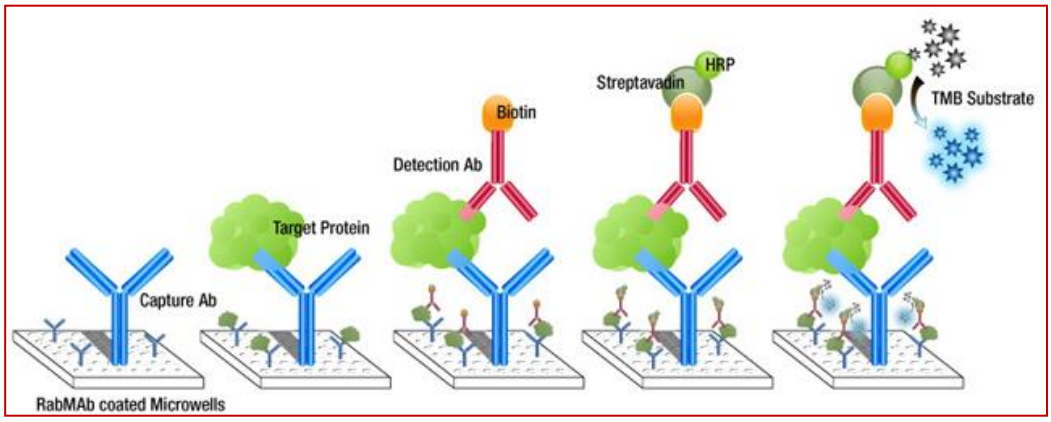

Figure 1.1. An overview of ELISA: Primary antibody (capture antibody) binds with the target by specific interaction and subsequently the same target binds with the secondary antibody (detection antibody). The secondary antibody is tagged with the enzyme. The product of the reaction of the enzyme produces the signal to be measured, being an indirect measurement of the target.

This technique is the tool of choice in both clinical diagnostics and protein research protocols (Engvall, 2010). ELISA assays have the advantage of being completely customizable towards different targets. They are affordable and can achieve very low detection limits. However, they also require highly qualified personnel and special equipment. Furthermore, the reproducibility of antibodies is not always guaranteed and the analyte cannot always be accurately quantified. False negative results can also be obtained if the target protein is not extracted from the matrix effectively (Taylor et al., 2009).

Several methods have been proposed to date to detect microorganisms. Among many others, the conventional culture is a standard method used in both the food and medical sectors. It relies on specific microbiological media to isolate and enumerate viable cells. Media contains both specific substrates and inhibitors that allow only the targeted strains to grow (Lazcka et al., 2007). They are very sensitive and inexpensive and can give both qualitative and quantitative information on the microorganisms present in a sample. However, the main disadvantage of traditional methods is that they are labor intensive and require several days (or even weeks or months depending on the specific microorganism) to give results and, meanwhile, the microorganism multiplies and produces visible colonies (Boer and Beumer, 1999). Moreover, biochemical tests are normally required to confirm the species of the microorganism.

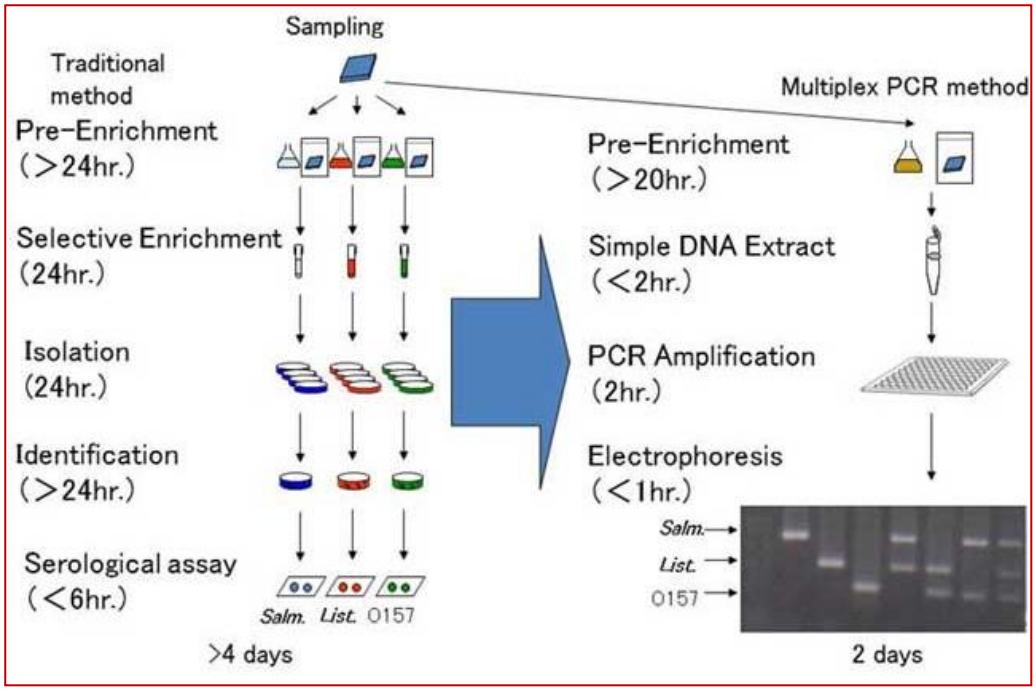

Figure 1.2. Schematic representation of conventional culture-based detection and the PCR method (Kawasaki et al., 2005).

In recent years there have appeared several biosensing platforms and strategies which incorporate nanobased materials to decrease the detection limit and the length of the assay for detecting bacteria (Yang et al., 2010). Various approaches have been employed for detecting bacteria, including physicochemical methods for bacteriological metabolite measurements (Mazza, 1983), capillary electrophoresis (Turenne et al., 1999), ELISA (González et al., 1993) and fluorescence resonance energy transfer assays (Ko and Grant, 2006). Another group of methods are electrochemical-based platforms, such as chip-based devices with electrochemical impedance spectroscopy detection (Maalouf et al., 2007), and amperometric (Kim et al., 2006) and potentiometric (Ivnitski et al., 2000) devices that use natural antibodies as capture probes. Nowadays, several biosensors show very low detection limits in short assay times for instance, carbon nanotube-based field effect transistors can detect 100 CFU/mL of *Salmonella Infantis* in a 1 h assay (Villamizar et al., 2008), interesting ultrafast PCR detection methods can detect 5 CFU in only 7 min (Belgrader et al., 1999), and PCR methods using a B cell-based sensor can detect 500 CFU/g in less than 5 min (Rider et al., 2003). With these developments in mind, our group reported a potentiometric aptamer-based biosensor that can selectively detect 1 CFU living

bacteria in 1 min (Zelada-Guillen et al., 2009). However, these methods for high-throughput microorganism detection require trained people and expensive equipments and/or tools and/or receptor materials (Yang and Bashir, 2008). Overall, these detection techniques are time consuming, and they require sample preparation, particular reagents, and costly equipment and/or recognition materials. Therefore, there is a need in society for more rapid, cost effective, and sensitive tests which can identify whole bacteria and be used at the point of care.

1.1.2 Molecularly imprinted materials (MIPs) and detection of proteins and microorganisms

The field of molecular imprinting in synthetic polymers is one of the most exciting areas in chemistry and materials science today. Molecular imprinting may be described as the formation of sites or cavities within the polymer that are receptive to a specific molecule or group of related molecules. These cavities are formed by the synthesis of the polymer in the presence of a specific molecule. The molecule around which the polymer is synthesized is known as the template, and the subsequent removal of the template after the polymer has formed creates the selective sites. These sites are then available for rebinding the template on the basis of shape, size and, perhaps most importantly, functionality, all of which combine to promote a high degree of molecular recognition. The polymer thus formed is known as a molecularly imprinted polymer (MIP) or plastic antibody. The purpose of this section (**1.1.2**) is to introduce molecular imprinting and its approach to creating recognition elements for the detection of proteins and microorganisms using materials which may replace natural antibodies and have advantages of cost-effectiveness, reusability and long term stability.

1.1.2.1 The history of molecular imprinting

Excellent reviews of molecular imprinting are available (Alexander et al., 2006; Mayes and Whitcombe, 2005). These reviews and the MIP database (Whitcombe, 2011) make it possible to present a brief account of this rapidly growing field. Nowadays, it is generally accepted (Alexander et al., 2006; Andersson and Nicholls, 2001) that the Soviet chemist M.V. Polyakov gave the first example of molecular imprinting in 1930s when he mentioned the interesting adsorption behavior of silica gel matrices (Polyakov, 1931). In these matrices, benzene, toluene or xylene were added to the silica matrix prior to drying and adsorption was carried out on dried silica, from which the additives had been removed by

extensive washing. Interestingly, this research showed selective adsorption for the additive that was present during the formation of the gel. Subsequently, Polyakov published a number of other papers (Polyakov et al., 1937, 1933) in the same decade but his work remained largely unnoticed by the wider scientific community (Alexander et al., 2006). In the late forties, a graduate student of Linus Pauling, Frank Dickey, introduced the term, 'specific adsorption' of methyl orange dye in silica gels, which attracted greater attention (Dickey, 1949). Dickey stated that the adsorption of methyl orange led to the formation of "pockets that fit closely enough to the foreign molecule to hold it in by Van der Waal's forces, hydrogen bonds, ionic attraction and other types of intermolecular interaction". Dickey went on to publish a more detailed paper investigating such topics by studying the amount of reactive surface and the yield of fabricated cavities (Dickey, 1955). Also at that time, other researchers applied Dickey's work to the separation of stereoisomers (Bernhard, 1952; Curti and Colomb, 1952; Haldeman and Emmett, 1955). In 1959 Morrison et al. challenged Dickey's suggestions about the cause of selective adsorption (Morrison and Worsley, 1959). Despite this, in the 1960s research continued and extended into the parallel line of "stereoselective adsorbents", outlining the use of the imprinting process. An example of imprinting of bacteria to investigate the optical activity of receptors in dissymmetric organisms was carried out by Patrikeev et al. which was early work continued by Beckett and Youssef (Beckett and Youssef, 1963; Patrikeev et al., 1960). Work on molecular imprinting in organic polymers was initiated by Wulff and Sarhan in the seventies, and continued by Arshady and Mosbach in the eighties, leading to "the new era of molecular imprinting" (Mayes, 2005; Mosbach and Arshady, 1981; Wulff and Sarhan, 1972).

1.1.2.2 MIPs as recognition elements

Molecular recognition may be described as a set of phenomena under the control of specific non-covalent interactions (Gellman, 1997). These interactions, and the subsequent 'recognition' events at a molecular level, are often necessary in order to perform or induce specific functions or effects. Nobel laureate, J.M. Lehn states that binding alone is not recognition but that recognition can be considered to be "binding with a purpose" (Lehn, 1995). Given the high degree of specificity involved in the molecular recognition that takes place in biological systems, coupled with the myriad functions of this recognition, it is little wonder that the incorporation of these properties into MIP materials has been the focus of much scientific and technological research.

Introduction

Molecular recognition by molecularly-imprinted polymers (MIPs) is a challenging area in supramolecular chemistry and a promising alternative to natural materials, such as antibodies, enzymes or other biological receptors that display selective affinity to specific targets. These natural biological receptors are used in a multiplicity of applications, ranging from analytical and preparative chemistry to nanomedicine, including diagnostics, drug development, and drug delivery. The stability of such natural receptors is, however, limited, and they are also expensive. This has led to a considerable number of research work that aimed to create more stable synthetic systems that mimic highly selective and sensitive recognition processes in nature. Although nature's selectivity and sensitivity have not yet been matched, steady progress is being made in creating synthetic systems for molecular recognition (Ravelet and Peyrin, 2006).

Molecular imprinting (MI) is typically the 3-D imprint of a particular molecule in a rigid polymeric matrix. The overall process can be seen in **Figure 1.3**, consists of a pre-arrangement between target compound and selected monomers, followed by suitable polymerization that lead to the formation of a rigid matrix. The template molecule is subsequently removed, without disturbing the geometry of the solid. The resulting material keeps the ability to rebind the template because of its 3-D functional arrangement (Ravelet and Peyrin, 2006).

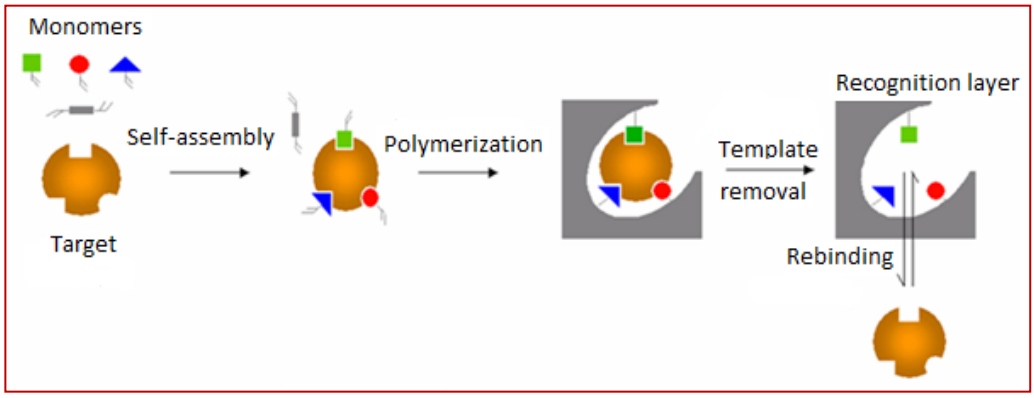

Figure 1.3. Molecular imprinting approach: creation of recognition layer.

The synthesis of imprinting materials can often be modified or improved (Vogtle, 1991) since the sensing mechanism is typically based on "simultaneous non-covalent interactions between single binding sites" (Schneider and Yatsimirsky, 2000). The presence of a

number of binding sites is needed by the inherently weak nature of non-covalent interactions and recognition is achieved by concurrent interaction between the individual binding sites. Lehn (Lehn, 1995) states a number of factors necessary to induce the large difference in binding energies between those of a given substrate and other substrates that are required to achieve the desired level of recognition and they include the following:

- Steric complementarity between substrate and site
- Interactional complementarity within three-dimensional sites
- Large contact areas
- Multiple interaction sites
- Strong overall binding
- Solvent effects

With these considerations firmly in mind, plus the advantages of readily synthesized artificial receptors, the appeal and potential for utilizing polymeric material in which these receptor sites can be created and maintained is readily seen.

While imprinting target compounds of low molecular weight is today reasonably established, protein imprinting is still a challenge due to the typical flexibility and instability of proteins. The 3-D structure of proteins depends on the surrounding environment (which induces conformational changes), and this dependence can lead to a mismatched imprint. Special care must be taken when selecting the experimental conditions, including the way the MIP is integrated at the transducer surface. To date, molecularly imprinted proteins have been integrated in biosensors by many different approaches. These approaches may vary from the target to be imprinted (total compound or only epitope region) and to the way the polymerization is conducted (*in situ* – bulk – or surface, being photochemically or thermally initiated) (Henry et al., 2008). They all have advantages and drawbacks. Bulk protein imprinting is easier to achieve, because the experimental procedures are fairly simple, but surface-imprinting methods provide a controlled modification of the imprinted surface in thin films of specific polymers. The template is much easier to remove, which gives good access to the imprinted sites, and provides lower non-specific binding, while the bulk approach may suffer from poor template extraction, slow binding kinetics, template entrapment and bleeding. The main drawback of surface imprinting is the number of binding sites, which is limited by the reduced surface available. Consequently, the choice of the material and the signal transduction method to be used should made very carefully.

Several approaches for imprinting proteins and microorganisms have been presented in the literature. Most of these involve bulk or surface imprinting of the entire protein target molecule, but a few use epitope imprinting, which can also include bulk or surface techniques. These studies are detailed in the next section (section **1.1.2.3**).

1.1.2.3 MIPs for detecting proteins and microorganisms

Molecular imprinted materials have been widely used for small molecule separation, extraction and detection in different fields and for different purposes. But MIPs for large molecules, despite being promising, are still a relatively unexplored field. This section describes different approaches of MIPs that can be used to detect proteins and microorganisms.

- Bulk imprinting

Of the various types of imprinting processes, bulk imprinting is interesting because of the ease with which 3-D binding sites can be obtained for the entire target. Target proteins, monomers and/or cross linkers are mixed together and subsequent polymerization imprints the target. Removal of the target creates imprinted sites. The interaction between monomers, cross linkers and target proteins in bulk imprinting is schematically presented in **Figure 1.4.**

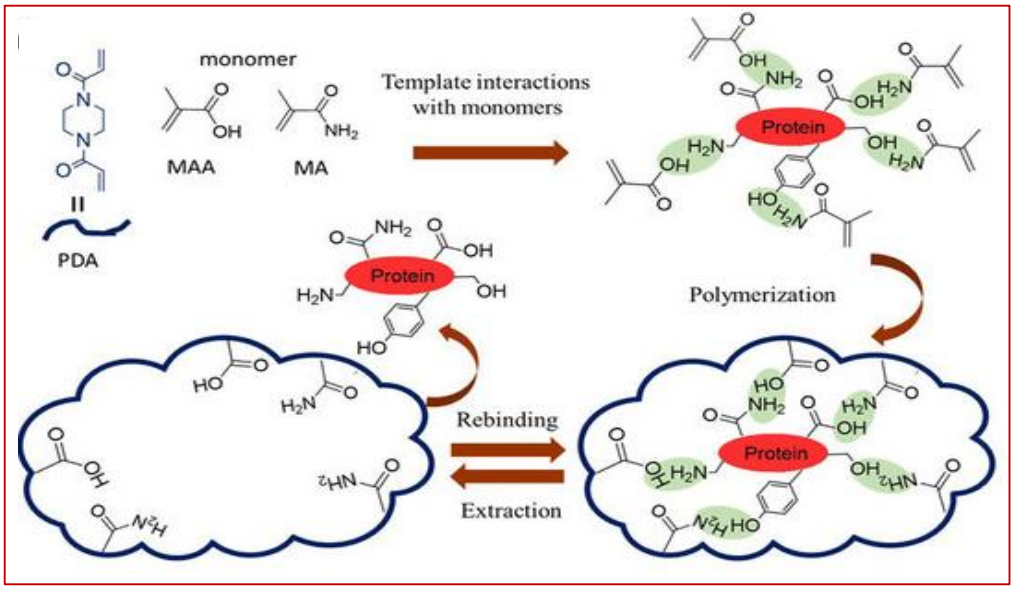

Figure 1.4. Bulk imprinting approaches ((methacrylamide (MA), methacrylic acid (MAA), piperazine diarylamide (PDA)) adapted from (Liu et al., 2014).

The literature reports many facile procedures for synthesising this type of material (Kryscio and Peppas, 2012), which include the use of acrylate, hydrogel and /or sol-gel chemistry (Turner et al., 2006).

- *Acrylate*

Few reports have been published on acrylate-based bulk imprinting of proteins. Among the ones that have, Turan et al. synthesized acrylate-based imprinting materials using 2-acrylamido-2-methylpropanesulfonic acid as monomer that also included isopropylacrylamide because of the good biocompatibility of acrylamide (AAM) environments with proteins. They employed free-radical cross link copolymerization, and the sensing performance of the imprinted materials was selectively better than that of non-imprinted materials (Turan, 2009). Recently, (Liu et al., 2014) methacrylamide and methacrylic acid have been used as monomers with piperazine diarylamide as hydrophilic and biological compatibility cross linkers. Liu et al. were able to selectively deplete albumin from human serum. In this case, methacrylamide and methacrylic provide carboxyl amide and hydroxyl groups, which can interact with the functional groups (such as amino, carboxyl and hydroxyl groups) of the template proteins, through the hydrogen bonding interactions to form the recognition sites.

Conventionally, acrylate imprinting is carried out in non-aqueous solvents, normally at high temperature (above 37°C). The major limitation of acrylate imprinting is the dissolution or dispersion of proteins in non-aqueous solvents because the protein shape or conformation normally changes during imprinting due to the dissolution media and the effect of temperature (Turner et al., 2006). Therefore, this is a harsh environment for protein imprinting and other milder environments such as hydrogels are usually more suitable for bulk imprinting.

- *Hydrogel/Sol Gel*

Hydrogels are “smart” or “stimulus responsive” materials that can change a property, such as shape, in response to a change in the environment, and which can substitute conventional polymeric materials in molecular imprinting (MI). Common stimuli for smart hydrogels in biological applications are pH, temperature and ionic strength and changes in these parameters can change the hydrogel dimension or structure which can be used to control the uptake and release of the templates with little effect on the polymeric network, which memorizes the imprinting shape.

Hjerten et al. imprinted proteins such as hemoglobin, cytochrome C, and the sensors made with these imprinting approaches were able to successfully detect the target proteins. (Hjerten et al., 1997). Wang et al. investigated the electrochemical and electrocatalytic behavior of immobilized hemoglobin at the carbon paste electrode for the first time prepared by sol-gel film derived from tetraethyl orthosilicate. This work showed a suitable pathway of silica-based sol-gel entrapping of proteins (Wang et al., 2004). Recently, S.M. Reddy et al. detected bovine hemoglobin by dual polarisation interferometry using a polyacrylamide-based MIP obtained from hydrogels. They were able to detect up to 2 µg/mL of bovine haemoglobin. The hydrogel MIPs retained their selectivity after exposure to real biological samples when used in 1:100 diluted serum (Reddy et al., 2013).

One advantage of sol-gel materials over other types of protein imprinting is that the preparation conditions are milder and the protein can be entrapped with well conserved physical and chemical properties inside the polymer network. Also in sol-gel imprinting approaches, the cross-linking network tends to make rigid structures which can help the cavities to retain their shape after the templates have been removed. By varying the reaction time, type of monomer and template composition ratio, the surface porosity and thickness can be easily controlled. But the drawback of these imprinted materials is that they form flimsy polymer networks which may lose the imprinting cavities and hence be less robust than other types of bulk and/or surface imprinting (Lahav et al., 2001; Marx and Liron, 2001; Tripathi et al., 2006).

Harvey *et al.* reported the imprinting of microorganisms in organic media. They took *Bacillus thuringiensis* and *Bacillus anthracis* as the target bacteria and the obtained sensing materials acted as a semi-selective matrix to capture and concentrate the specific spores of the target (Harvey et al., 2006).

- *Electropolymerization*

The main drawback of the synthesis of imprinted materials based on sol-gel is the amount of time the process takes. A faster and easier way is to use electropolymerization (Syritski et al., 2008). The various optimization parameters of sol-gel processes can be easily controlled and optimized in electropolymerization processes by the number of cycles or the current applied and by a suitable selection of the solvent. In the bulk imprinting approach, electropolymerization typically requires electroactive monomers along with the conductive support surface, but not an initiator, UV light or heat. The mechanism behind

polymer formation with molecular recognition cavities directly on the conductive support surface involves the generation of a radical by an electro-oxidation reaction, and a subsequent polymerization reaction (Sharma et al., 2012). A general example of an electropolymerization-based bulk imprinting approach can be seen in **Figure 1.5.**

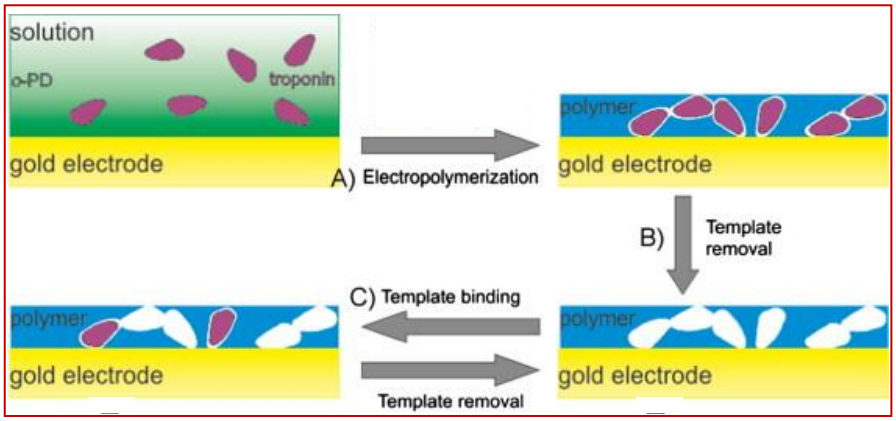

Figure 1.5. Electropolymerization-based bulk imprinting approach (Karimian et al., 2013).

Karimian et al. used electrochemical bulk imprinting to fabricate artificial receptors for the cardiac protein troponin T. They used electropolymerization of the functional monomer, o-phenylenediamine (o-PD) in the presence of troponin T as target molecules. The resulting materials showed high affinity (similar to when a natural receptor was used) to the target in cyclic voltammetry (CV) or square wave voltammetry-based detection (SWV) (Karimian et al., 2014, 2013). Very recently, Rebelo et al. reported a novel biosensor that had been fabricated by electrochemical bulk imprinting of the Annexin A3 protein. They selectively detected the target protein using SWV (Rebelo et al., 2016). Tokonami et al. used MIP-based sensors built over oxidizing pyrrole to selectively detect *bacilliforms.* They reported that a novel combination of dielectrophoresis coupled with QCM technologies offered a highly sensitive and selective bacterial detection platform (Tokonami et al., 2013).

- Surface imprinting

Conventional bulk imprinting is a straightforward approach but their highly cross linked structures and irregular shapes limit their application as artificial receptors. The specific disadvantages of bulk imprinting are the following: (1) it is difficult to remove the target molecules from the inner binding sites; (2) their rebinding capacity is limited by the small

number of binding sites on/near the surface; and (3) target molecules are easily prevented from accessing binding sites deep in the interior of the particles (Vasapollo et al., 2011). These problems can be solved by surface imprinting (2D) which is widely used as an imprinting strategy (Turner et al., 2006), because it requires a smaller amount of target than the conventional bulk approaches. Surface imprinting consists of immobilizing the template on a solid support surface and subsequently polymerizing around it, thus create binding sites close to the surface (**Figure 1.6**) afterward template removal. These binding sites are more accessible than in bulk-based approaches and target/polymer interactions are not hindered by diffusion (Mirsky et al., 1999). Generally, diffusion decreases equilibrium time and increases binding kinetics.

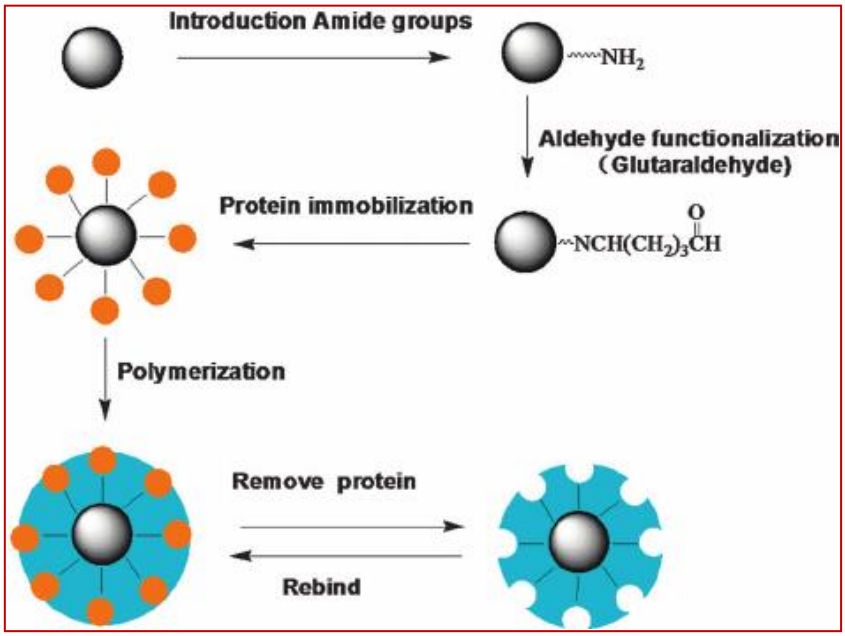

Figure 1.6. An example of the surface imprinting approach (Chen and Li, 2011).

The imprinting of small molecules is a well-established field which has previously been reviewed but the imprinting of large molecules still faces many challenges. The imprinting of protein is particularly tricky because of the dependence on the temperature, pH and ionic strength of the buffer. Surface imprinting always takes place on a suitable receptor surface acting as support for the imprinted material and different technical approaches can be used for this purpose (for example, stamp-coating/micro-contact, polymer-brush imprinting, and

surface grafting).

- *Stamp-coating/micro-contact*

In the stamp imprinting approach, the stamp is used to physically position the template moiety during the imprinting process (Bernard et al., 1998). Recently an article by Kuwata el al. reported a transcription-type molecular imprinting that used protein-immobilized dots as stamps (**Figure 1.7**). In this case, the protein stamp was prepared by the avidin-biotin interaction with the target proteins. It was then transcribed onto the methacrylate glass substrate after photoirradiation for polymerization. The authors reported that they were able to selectively detect multiple proteins such as cytochrome C, lysozyme, myoglobin, and ribonuclease by a labeled fluorescence technique which was also supported by surface plasma resonance (Kuwata et al., 2015).

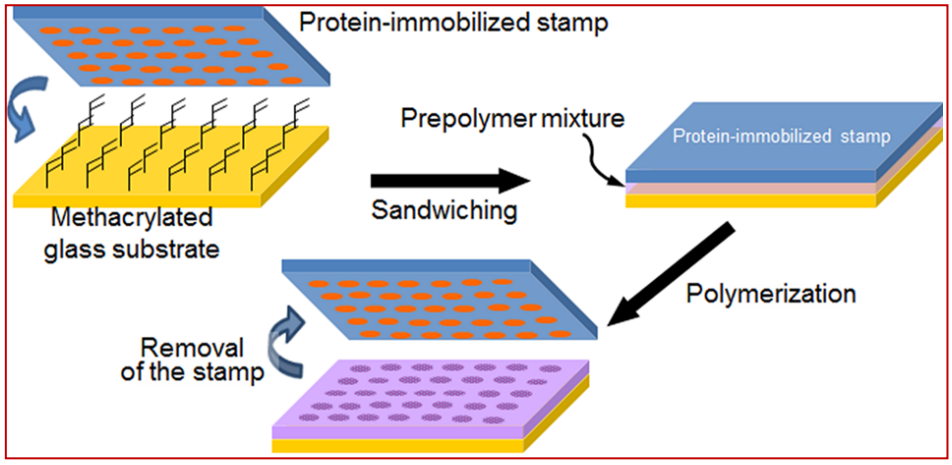

Figure 1.7. Stamp imprinting approach (Kuwata et al., 2015).

The imprinting of microorganisms has been gaining in importance in recent years as a new way of making affinity biosensors and improving the detection of microorganisms. Hayden and Dickert et al. imprinted round bacteria and yeast on quartz crystal microbalance (QCM) electrodes using the stamp imprinting approach. The detection limit of their imprinted sensors was 1×10^4 cells/mL (Dickert and Hayden, 2002; Hayden and Dickert, 2001). Their imprinted materials showed high selectivity against various yeasts and bacteria using QCM-based sensors. However, the stamping technique has only been

applied to round bacteria and yeasts, because of the technical difficulty of removing more complex-shaped templates, such as bacilli, from the cavities. A similar strategy was used by Hayden et al. to imprint viruses, and they selectively detected various viruses such as *tobacco mosaic*, *human rhino* and *parapox ovis* (Hayden et al., 2006). The same group reported that synthetic polymer receptors for the online monitoring of bioanalytes were directly formed on quartz crystal microbalances using surface imprinting techniques and molded materials. These polymers are capable of enriching whole cells, viruses and enzymes on the sensor layer surface by dual QCM coupled to two electrodes on a single piezocrystal (Hayden et al., 2003). Recently, Eersels at el. also used stamp imprinting for the specific identification of viable cells (macrophages and cancer cell lines MCF-7 and Jurkat). The various cell types are detected by changes in the heat transfer resistance at the solid-liquid interface of a thermal sensor device induced by the cells binding to a surface imprinted polymer. The detection limit was found to be in the order of 1×10^4 cells/mL (Eersels et al., 2013).

Protein imprinting based on the micro-contact approach requires a minimal mass of proteins which form a monolayer over the recognition substrate on which they are imprinted. An interesting article by Chou et al. used the micro-contact imprinting process to imprint C–reactive protein and the procedure they used can be regarded as a general example of the micro-contact imprinting approach (**Figure 1.8**). In this case, template proteins and functional monomers adhere to a cover glass and another support glass contains cross linkers and radical initiators. After placing one glass above the other and exposing UV light at the glass assemblies allow polymerization. Removal of the cover glass and successive washing of the imprinted surface creates imprinting sites to further rebind with the target template (Chou et al., 2005).

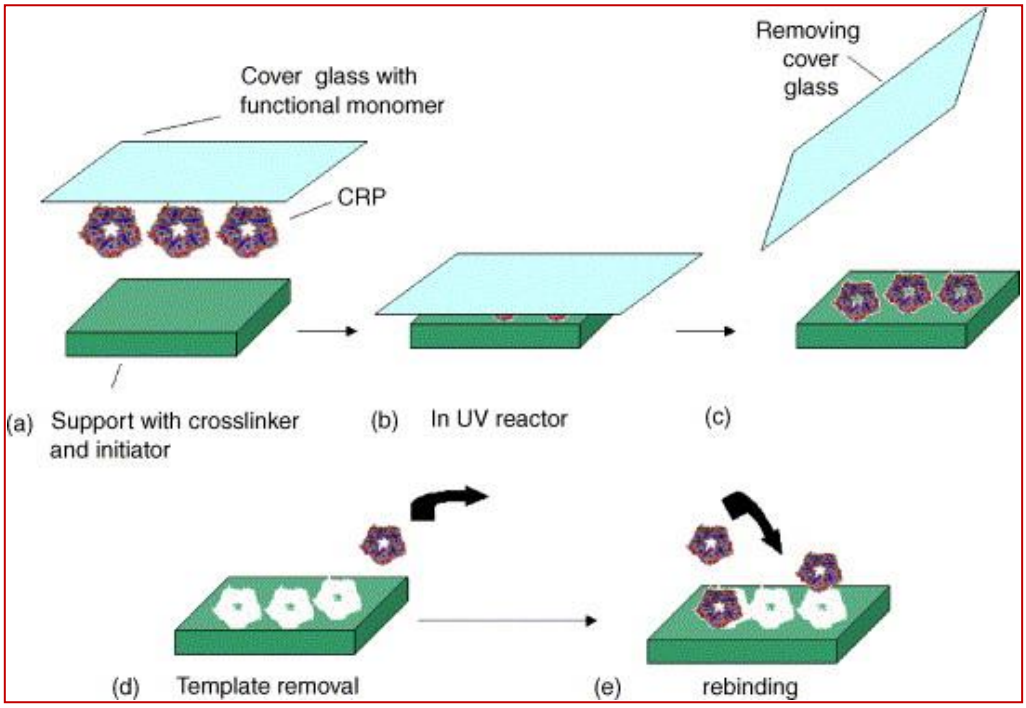

Figure 1.8. Surface micro-contact imprinting method (Chou et al., 2005).

Another study by Chou et al. carried out a micro-contact imprinting process using biomarkers such as C-reactive protein, ribonuclease, lysozyme and myoglobin as templates. They created the nanocavities in the MIPs by optimizing the composition ratio between the lowest affinity cross-linker and the highest affinity functional monomer, which allowed them to prepare highly selective recognition sites for a wide variety of template proteins (Chou et al., 2007). A systematic approach to form micro-contact imprints of creatine kinase was described by Chen et al, in which they used PEG (poly(ethylene glycol)) dimethacrylate as crosslinker and methacrylic acid as functional monomer. The resulting polymer showed excellent imprint recognition (Chen et al., 2009).

- *Polymer-brush imprinting*

Zdyrko et al. described an original approach to surface imprinting of protein that used the grafting of polymer brushes. Protein molecules were first chemically bound to an ultrathin polyglycidylmethacrylate reactive polymer layer and later removed by protease treatment. Unlike the PEG-coated surface, the imprinted surfaces were able to absorb the

protein template. They were also able to differentiate between bovine serum fibrinogen and bovine serum albumin (BSA) (Zdyrko et al., 2009).

- *Surface grafting*

The major problem with the imprinting of large templates, such as proteins, lies in the restricted mobility of those molecules within highly cross-linked polymer networks and their poor reversibility and efficiency in binding. Despite the laborious procedure, polymer grinding can also destroy affinity sites. Surface grafting seems to be the most promising way of overcoming these difficulties.

Hongyan et al. synthesized imprinted materials via surface grafting on silica support with the model protein lysozyme as template (**Figure 1.9**). They reported that these films had greater rebinding capacity selectively towards the target than the non imprinted film (Hongyan et al., 2010).

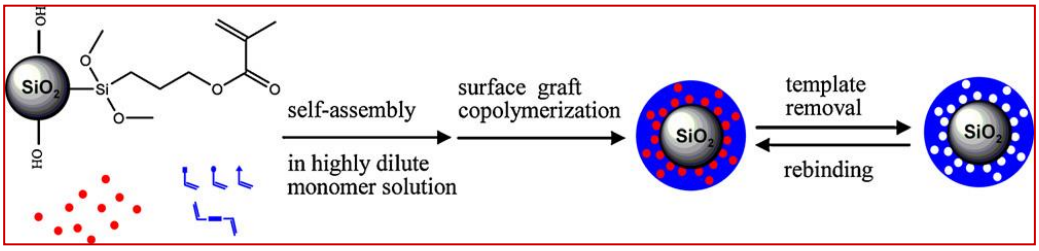

Figure 1.9. Schematic illustration of the imprinting of lysozyme over 3-Methacryloxypropyl trimethoxysilane-modified silica nanoparticles via surface graft copolymerization (Hongyan et al., 2010).

Wang et al. reported a potentiometric protein sensor based on molecular imprinting using self-assembled monolayers of alkanethiol with hydroxyl terminal groups as the matrix material. The sensing layer was created on the surface of gold-coated silicon chips, acting as an electrochemical transducer. Potentiometric measurement demonstrated that the sensor could selectively detect target proteins such as myoglobin and hemoglobin (Wang et al., 2008). Yin et al. developed surface grafting imprinted materials for protein recognition and reported the molecular imprinting of a functional polymer layer with lysozyme as the template in a two-step grafting procedure by a novel initiation approach on a track-etched

polyethylene terephthalate membrane surface. This approach is based on surface functionalization with aliphatic C–Br groups which can be used as initiators for surface-initiated atom transfer radical polymerization and photo-initiated copolymerization (Yin and Ulbricht, 2013).

Recently, Xiangjie et al reported the synthesis of imprinted materials based on ZnO rods by surface grafting copolymerization. The shell of the imprinting process was composed of acrylamide, methacrylic acid and *N*, *N'*- methylenebisacrylamide. Acrylamide was chosen as the functional monomer because of the affinity of amide groups to carboxyl groups of BSA. They were able to selectively detect BSA by fluorescence measurement (Xiangjie et al., 2015).

- *Electropolymerization*

Bulk imprinting (3D) of protein based on electrochemical processes could be termed as one-step process to imprint the target but this process may be limited by the irreversible binding of proteins with the imprinted polymers. Sometimes is therefore more convenient to use surface imprinting (2D) which can be termed as a two-step process. In this case, the protein is first immobilized and then a suitable monomer is electrochemically polymerized to imprint the target protein. The rest of the process is similar to bulk imprinting.

Sharma et al. reported surface imprinting of antibodies and /or similar analogues on amino ($-NH_2$) functionalized solid support surfaces where the target is covalently attached and then imprinted (Sharma et al., 2012). The direct physical adsorption of the protein and then the electrochemical imprinting is the most straightforward process according to Moreira et al. (Moreira et al., 2014).

Bacterial endospores from the *Bacillus subunit* were imprinted on conductive polymer films (Namvar and Warriner, 2007) and the subsequent electrochemical detection of bound spores using these films was reported. The imprinted films were prepared by absorbing the spores on the surface of glassy carbon electrodes upon which a polypyrrole layer with a dopant (sodium dodecyl sulphate) and proton donor (lactic acid), followed by a poly(3-methylthiophene) layer were deposited electrochemically. The target was detected impedimetrically using Mn(II) as signal mediator with a detection limit of 10^2 CFU/mL.

- Epitope imprinting

As described above, one of the main difficulties in protein and microorganism imprinting is the complex process involving large templates. This difficulty could be solved by using epitope imprinting. Proteins and microorganisms have specific binding sites called epitopes. It is interesting to apply the imprinting approach using these specific regions of the proteins or microorganisms to create cavities in the recognition layer (i.e. the MIP) for those specific epitopes. These epitope-based MIPs should not prevent whole proteins or microorganisms from being detected. This approach is still not fully developed and it has only been used in a few studies.

The C-terminus of such proteins as cytochrome C, alcohol dehydrogenase and BSA was used for epitope imprinting by Nishino et al. (Nishino et al., 2006). The authors used stamp imprinting and acrylamide/bisacrylamide to make polymer films. They reported that it is better to use the terminal peptides of these proteins as an imprinting strategy than other regions of the target proteins, and because they are less susceptible to post translational modification (Polevoda and Sherman, 2000). Another interesting related technique is fingerprint analysis, which uses a pool of peptides from distinct proteins. Bossi et al. combined fingerprint and epitope imprinting approaches to rationally select and determine NT-pro BNP (N-terminal pro b-type natriuretic peptide) with good imprinting factors and binding capacity in a complex sample, composed of the whole digests of NT-pro BNP (Bossi et al., 2012).

Tai et al. developed a quantitative method using artificial antibodies to detect creatine kinase in which linear epitope sequences were selected using an artificial-epitope mapping strategy and MIPs corresponding to the peptides selected were fabricated on QCM chips (Tai et al., 2011).

In brief, the advantage of epitope imprinting over whole protein and/or microorganism imprinting is that a tiny part of the target analyte can be imprinted, as readily as if it is a small molecule. This makes it easy to remove the template from the polymeric network, a crucial stage in creating the recognition layer for further rebinding with the target template. The disadvantage of this approach is that it is difficult to select the perfect specific part (epitope) of the target to be imprinted.

1.2 Detection techniques

MIP-based recognition layers were introduced in section **1.1.2.2**, and they can be used as a sensing layer in bio-sensing devices. Electrochemical biosensors, like other sensors, are composed of three different parts. The first is the recognition/sensing layer. The second is the transducer element or transducer layer, which converts the electrochemical event to electronic current or vice versa. And the third is the detection system. Various techniques can be used to detect the target analyte, and in this section we aim to explain the fundamental concepts of the techniques used in this thesis.

1.2.1 Transducer

The transducer element is an essential part of any biosensor. In electrochemical biosensors, the electrochemical event that takes place on the biosensor must be transformed into an electronic current. Subsequently, electronic processing makes it possible to record the relevant analytical signal. Conventionally, semiconducting and conducting materials are used as the transducer (Düzgün et al., 2013; Hernández et al., 2012; Liang et al., 2015) because of their high capacities or the high charge transfer generated at their interfaces. The process of assembling transducers into sensors can be seen in **Figure 1.10** (adapted from, http://www.nanoscience.imdea.org/molecular-nanoscience/chemical-synthesis/developing-biosensors-based-nanomaterials)

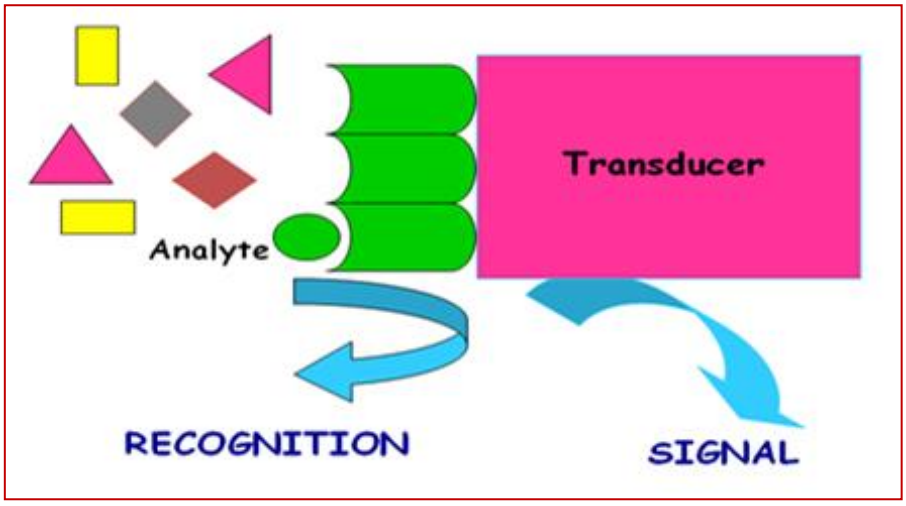

Figure 1.10. Sensors system including the role of the transducer.

In this thesis, SWNCTs-COOH/MWCNTs-COOH, graphene oxide and conductive polypyrrole were used as transducers due to their exceptional electrical properties and signal transformation.

1.2.2 Electrochemical sensors

The change in the electrical signal can be observed as current (fixed potential, amperometry), potential (fixed current, potentiometry), current with a variable potential (voltammetry) or impedance (impedimetry). These techniques are widely used to detect a wide range of molecules, from small to large ones. In this section we describe the techniques which have been used in this thesis.

1.2.2.1 Potentiometric sensors

Potentiometry is a simple electro-analytical tool which measures the potential between two electrodes (reference and working) while the electric current between these two electrodes is nearly zero (Christopher and Brett, 1993). The electrochemical cell is constructed by dipping these two electrodes into the solution and completing the circuit. The potential of the reference electrode is known and stable, and the cell potential is variable because of the variable potential of the working electrode due to the biochemical interactions between the working electrode and the target analyte. This electrode is covered by a polymeric membrane (for instance in the case of the ion-selective electrodes) or by a wide range of receptors which allow the target analyte to interact with it based on the charge and size. The most widely used potentiometric electrodes are ion-selective electrodes (ISEs) in which the concentration of the target analyte is related to the potential created at the sample/membrane interface (Bakker et al., 2004). The cell potential derived as the potential difference between the reference and the working electrode is produced due to free energy changes (ΔG, *Equation 1.1*) after interaction between the target analyte and the electrode.

$$\Delta \mathrm{G} = -nF\mathrm{E} \qquad \textit{Equation 1.1}$$

In this equation, E is the maximum potential difference between two electrodes, *F* is Faraday's constant (96,485 C mol-1) and *n* is the number of electrons exchanged. When the reaction takes place in non-standard conditions, the Nernst equation is as follows (*Equation 1.2*).

$$\mathrm{E} = E_0 + \frac{2.303RT}{Z_A F} \log\left[a_A + \sum_{i-1}^{n} K_{A,Bi}^{pot} \left(a_{Bi}\right)^{Z_A/Z_{Bi}}\right] \qquad \textit{Equation 1.2}$$

Where E_0 is the cell potential in standard conditions, R is the universal gas constant (8.314 J/(Kmol)), T is the temperature (in Kelvin), n is the charge of the ion or number of electrons participating in the reaction and K is the selectivity coefficient.

The key part of potentiometric ion selective sensors is fabricating the membrane containing the selective ionophore plus cationic and/or anionic additives and plasticizers.

This membrane (the sensing layer of the sensor) is casted over the substrate of the working electrode (Amemiya, 2007; Buck and Lindneri, 1994). This technique is widely used to detect small molecules but for detecting large molecule such as proteins and microorganisms it would face harsh condition due to difficulty of penetration of large molecules to the receptors of the membrane. So in our case the ion-selective membrane has been substituted by molecularly imprinted polymers. And because we do not use the ion-selective membrane, the sensing mechanism is completely different to that of the ISEs. While an equilibrium system is established between the two immiscible layers (polymeric membrane/water sample) in ISEs, a change in the electrical charges at the surface of the biosensor during the target recognition event is the origin of the EMF in our sensors. The advantages of potentiometric sensors are their low cost, low energy consumption, rapid response and regeneration.

1.2.2.2 Impedimetric sensors

Impedimetric sensors use electrochemical impedance spectroscopy (EIS) which is a favorite tool for monitoring changes on the surface of the biosensor (for example, in surface charge, electrode/electrolyte interaction, electrode kinetics, or absorption of the target on the surface). Although the basic principle of EIS is complex, it is easier to apply and the data is easier to interpret. Resistance is defined, according to Ohm's law, by the ratio of voltage (E) and current (I) by *Equation 1.3.*

$$R = \frac{E}{I} \qquad \textit{Equation 1.3}$$

This equation is followed by ideal resistors which are limited because it is assumed that they follow Ohm's law at all current and voltage levels, that the resistance value is independent of the frequency, and that the AC current and voltage signals are in phase with

each other. EIS measure the ability of a circuit to resist the flow of electrical current not limited by the above assumptions. In EIS, a small sinusoidal excitation signal is applied to the working electrode that is under investigation and measures the subsequent response of the system in steady-state. The sum of the sinusoidal functions helps to analyse the current signal state (Yuan et al., 2010) (Yuan et al., 2010).

The changes in potential and current over time are represented each one by a sinusoidal function in **Figure 1.11**, which shows a typical graph that illustrates the relationship between two related sinusoidal signals– AC (*I*) and voltage (*E*) –rotating at the same angular frequency (adapted from https://www.eeweb.com/blog/andrew_carter/P60/).

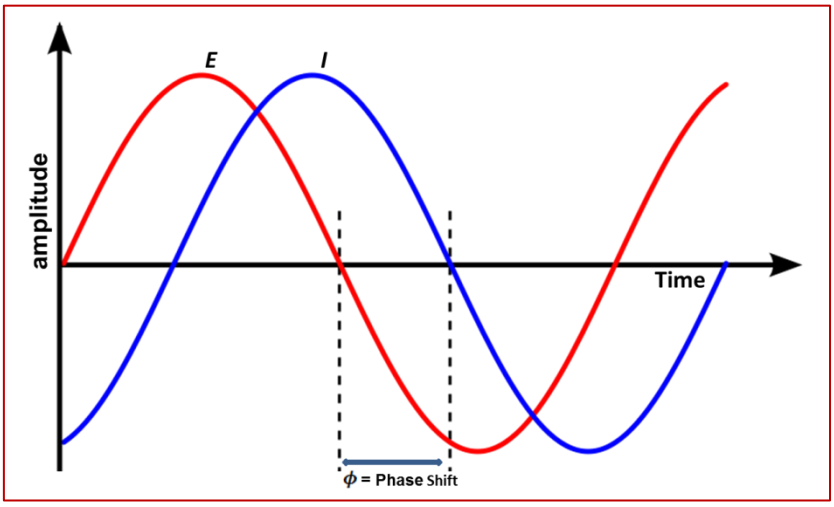

Figure 1.11. Two sinusoidal waves (voltage and current) offset from each other by a phase shift ϕ.

The phase of two sinusoidal waves is separated by the phase angle ϕ, and the application of a purely sinusoidal voltage to the electrode/electrolyte solution interface, expressed as a function of time, has the form

$$E(t) = E_0 \, sin(\omega t) \qquad \textit{Equation 1.4}$$

where *E (t)* is the applied voltage at a time *t*, E_0 is the oscillation amplitude of the excitation signal, and ω is the angular frequency of the sinusoidal excitation. ω is *2π* times higher than the conventional frequency *f* (Hz) in agreement with equation:

$$\omega = 2\pi f \qquad \textit{Equation 1.5}$$

In linear systems, the current response (I), which has a different oscillation amplitude (I_0), and is shifted in phase (ϕ) relative to the excitation signal, is expressed by:

$$I(t) = I_0 \, sin \, (\omega t + \phi) \qquad \textit{Equation 1.6}$$

The electrical impedance of the system (Z) is defined as the proportionality factor between the applied potential perturbation and the current response. Using an expression analogous to the Ohm´s law, the impedance of the sinusoidal system is calculated as follows:

$$Z = \frac{E(t)}{I(t)} = \frac{E_0 sin(\omega t)}{I_0 sin(\omega t + \phi)} = Z_0 \frac{sin(\omega t)}{sin(\omega t + \phi)} \qquad \textit{Equation 1.7}$$

Where the impedance (Z) is characterized by the magnitude (Z_0) and phase angle (ϕ). Remember Euler´s equation:

$$exp(j\phi) = \cos(\phi) + j sin(\phi) \qquad \textit{Equation 1.8}$$

It is possible to express the impedance as a complex function. In this way, the potential is described as:

$$E(t) = E_0 \, exp(j\omega t) \qquad \textit{Equation 1.9}$$

where j is the imaginary number defined as $j = (-1)^{1/2}$. In the same way, the current response is defined as:

$$I(t) = I_0 \exp(j\omega t - j\phi) \qquad \textit{Equation 1.10}$$

Thus, the impedance can be represented as a complex number:

$$Z = Z_0 \frac{exp(j\omega t)}{exp(j\omega t - j\phi)} = \left|Z\right| \exp(j\phi) = \left|Z\right| (cos\phi + j sin\phi) \qquad \textit{Equation 1.11}$$

Equation 1.11 states that in the complex plane, the impedance is composed of real ($Z' = Z_0 \, cos\phi$) and imaginary parts ($Z'' = Z_0 \, sin\phi$), at any value of ω, as follows,

$$Z = Z' + jZ'' \qquad \textit{Equation 1.12}$$

The Nyquist plot of the real part in X-axis and the imaginary part in Y-axis can be seen in **Figure 1.12.** In this plot, the Y-axis indicates impedance at each point of angular frequency, ω. However, the Nyquist plot shows impedance as the vector length of $\left|Z\right|$ and the angle between this vector length and X-axis is the phase angle, $\phi = arg$ Z (Yuan et al., 2010).

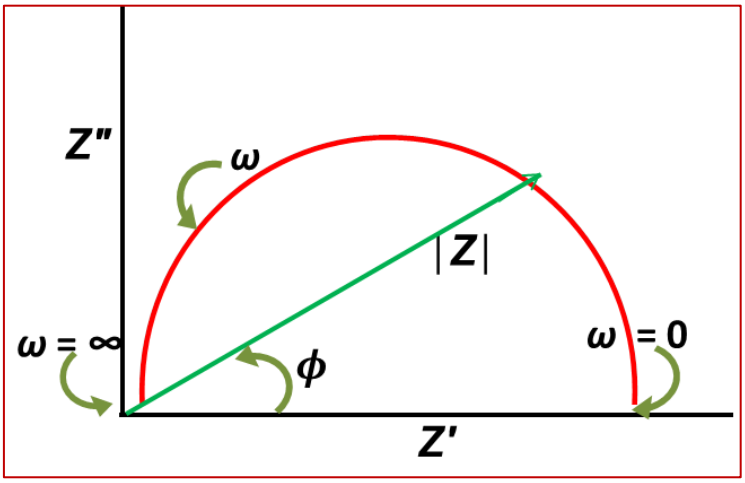

Figure 1.12. Nyquist plot by illustrating real (Z') and imaginary (Z'') components of impedance at each ω.

The Nyquist plot gives an overview of the EIS data, so that qualitative interpretations can be made. The semicircle in **Figure 1.12** is characteristic of a simple equivalent circuit (i.e. the Randles equivalent circuit). The data point closest to the origin indicates the resistance value of the solution, and the intercept farthest from the origin indicates the total resistance (solution plus charge transfer resistance). The diameter of the semicircle is therefore equivalent to the charge transfer resistance (Billah et al., 2008). This technique is widely used to detect a wide range of small to large molecules with the advantage of one spot and label free detection (Wang et al., 2012).

1.2.2.3 Square wave voltammetry-based sensors

Voltammetry is a common tool in analytical chemistry, and it is widely used in different fields for different purposes. However, it is particularly useful in biosensors. In all kinds of voltammetry, a potential sweep is applied and the electrical current generated is measured. Depending on the alteration mode of applied potential, voltammetry can be divided into sweep voltammetry (i.e. linear sweep voltammetry and cyclic voltammetry), and pulse voltammetry (i.e., differential pulse voltammetry, normal pulse voltammetry and square wave voltammetry). In the case of sweep voltammetry, the potential is applied as a sweep/linear function of time and in pulse voltammetry the potential is applied by pulsing one potential to another rather than sweeping. And as an example, the pulse and potential wave form for square wave voltammetry (SWV) can be seen in **Figure 1.13** (Chen and

Shah, 2013). Of all the types of voltammetry, SWV has significant advantages because of the sensitivity and speed of measurement.

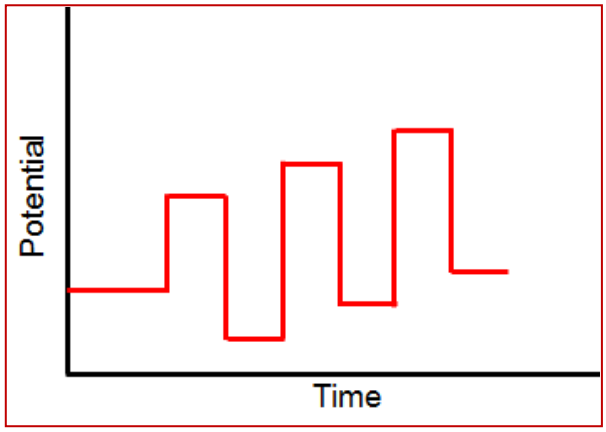

Figure 1.13. Potential alteration mode over time in SWV.

In SWV, the reverse waveform is subtracted from the forward waveform and the differential wave form is plotted as current against the applied potential. The peak current corresponds to *Equation 1.13*, where the intensity is proportionally related to the concentration of the redox active species. Since the reverse wave is subtracted from the forward wave, SWV can be used in the presence of oxygen because the reduction signal is excluded from the analyte response by background subtraction, which is another advantage of SWV over other types of voltammetry (Bard and Faulkner, 2001).

$$\Delta i_p = \frac{nFAD_0^{1/2}C_0^*}{(\pi t_p)^{1/2}}\,\Delta\Psi p \qquad \textit{Equation 1.13}$$

Δi_p is the differential current peak value, A is the surface area of the electrode, C_0^* is the concentration of the target species, D_0 is the coefficient of diffusion of the target species, t_p is the pulse width, and $\Delta\Psi_p$ is a dimensionless parameter which gauges the peak height in SWV relative to the limiting response in normal pulse voltammetry.

1.3 Final considerations and objectives

The literature has yet to report a method for detecting bacterial surface proteins based on artificial antibodies, and only a few studies have investigated how to make artificial antibodies for microorganisms using a complicated process of stamp imprinting (Dickert and Hayden, 2002; Eersels et al., 2013; Hayden and Dickert, 2001; Hayden et al., 2006, 2003) which followed sophisticated quartz crystal microbalance (QCM)/heat flow measurement as detection techniques. The main focus and objective of this thesis is to develop a new approach for detecting bacterial surface proteins and microorganisms based on artificial antibodies for the construction of label-free and cost-effective portable devices. These general objectives are achieved by implementing a series of specific objectives:

- Development of an easy pathway to make artificial antibodies by molecular imprinting process.
- Application of SWV, EIS and potentiometry as detection techniques using molecularly imprinting polymers as the sensing layer.
- Use of homemade and commercially available screen-printed electrodes for the electrochemical detection of targets in the search for disposable and portable devices.
- Electrochemical imprinting and detection of bacterial surface proteins and/or micro-organisms.

1.4 References

Alexander, C., Andersson, H.S., Andersson, L.I., Ansell, R.J., Kirsch, N., Nicholls, I.A., O'Mahony, J., Whitcombe, M.J., 2006. Molecular imprinting science and technology: a survey of the literature for the years up to and including 2003. J. Mol. Recognit. 19, 106–180.

Amemiya, S., 2007. Potentiometric ion-selective electrodes. Elsevier Science, Amsterdam, The Netherlands, p. 261.

Andersson, H., Nicholls, I., 2001. Chapter 1. In molecularly imprinted polymers: man made mimics of anitibodies and their applications. Elsevier, Amsterdam, The Netherlands.

Bakker, E., Buhlmann, P., Pretsch, E., 2004. The phase-boundary potential model. Talanta

63, 3–20.

Barber, M.J., Eichler, D.C., 1985. Immunodetection of spin-labelled proteins. Biochem. Soc. Trans. 13, 624–625.

Bard, A.J., Faulkner, L.R., 2001. Electrochemical Methods: Fundamentals and Applications. John Wiley and Sons, Inc, New York, p. 427.

Beckett, A., Youssef, H., 1963. Active sites in stereoselective adsorbents as models of drug receptors and enzyme active sites. J. Pharm. Pharmacol. 15, 253T–266T.

Belgrader, P., Benett, W., Hadley, D., Richards, J., Stratton, P., Mariella, R., Milanovich, F., 1999. PCR detection of bacteria in seven minutes. Science 284, 449–450.

Bernard, A., Delamarche, E., Schmid, H., Michel, B., Bosshard, H.R., Biebuyck, H., 1998. Printing patterns of proteins. Langmuir 14, 2225–2229.

Bernhard, S., 1952. The preparation of specific adsorbents. J. Am. Chem. Soc. 74, 4946–4947.

Billah, M., Hays, H.C.W., Millner, P.A., 2008. Original paper development of a myoglobin impedimetric immunosensor based on mixed self-assembled monolayer onto gold. Microchim Acta 160, 447–454.

Boer, D.E., Beumer, R.R., 1999. Methodology for detection and typing of foodborne microorganisms. Int. J. Food Microbiol. 50, 119–130.

Bossi, A.M., Sharma, P.S., Montana, L., Zoccatelli, G., Laub, O., Levi, R., 2012. Fingerprint-imprinted polymer: Rational selection of peptide epitope templates for the determination of proteins by molecularly imprinted polymers. Anal. Chem. 84, 4036–4041.

Buck, R.P., Lindneri, E.R.N., 1994. Recomendations for nomenclature of ion-selective electrodes. Pure Appl. Chem. 66, 2527–2536.

Chen, A., Shah, B., 2013. Electrochemical sensing and biosensing based on square wave voltammetry. Anal. Methods 5, 2158–2173.

Chen, L., Li, J., 2011. Recent advances in molecular imprinting technology : current status, challenges and highlighted applications. Chem. Soc. Rev. 40, 2922–2942.

Chen, Y.-W., Rick, J., Chou, T.C., 2009. A systematic approach to forming micro-contact

imprints of creatine kinase. Org. Biomol. Chem. 7, 488–494.

Chou, P.C., Rick, J., Chou, T.C., 2005. C-reactive protein thin-film molecularly imprinted polymers formed using a micro-contact approach. Anal. Chim. Acta 542, 20–25.

Chou, T.-C., Rick, J., Weng, Y.-C., 2007. Nanocavity protein biosensor - fabricated by molecular imprinting. IEEE, 7th Ieee Conf. Nanotechnol. 1-3, 16–20.

Christopher, M.A., Brett, A.M.O.B., 1993. Electrochemistry: Principles, Methods, and Applications. Oxford University Press, Incorporated, p. 427.

Curti, R., Colomb, U., 1952. Chromatography of stereoisomers with “tailor made” compounds. J. Am. Chem. 74, 3961–3961.

Dickert, F.L., Hayden, O., 2002. Bioimprinting of polymers and sol-gel phases. Selective detection of yeasts with imprinted polymers. Anal. Chem. 74, 1302–1306.

Dickey, F.H., 1955. Specific adsorption. J. Phys. Chem. 58, 695–707.

Dickey, F.H., 1949. The preparation of specific adsorbents. Proc. Natl. Acad. Sci. U. S. A. 35, 227–229.

Düzgün, A., Imran, H., Levon, K., Rius, F.X., 2013. Protein detection with potentiometric aptasensors : a comparative study between polyaniline and single-Walled carbon nanotubes transducers. Sci. World J. 2013, 1–8.

Eersels, K., Grinsven, B. Van, Ethirajan, A., Timmermans, S., Bogie, J.F.J., Punniyakoti, S., Vandenryt, T., Hendriks, J.J.A., Cleij, T.J., Daemen, M.J.A.P., Somers, V., Ceuninck, W. De, Wagner, P., 2013. Selective identification of macrophages and cancer cells based on thermal transport through surface-imprinted polymer layers. ACS Appl. Mater. Interfaces 5, 7258–7267.

Engvall E., E., Perlmann, P.E., 1971. Enzyme-linked immunosorbent assay (ELISA) quantitative assay of immunoglobulin G. Immunochemistry 8, 871.

Engvall, E., 2010. The ELISA, enzyme-linked immunosorbent assay. Clin. Chem. 56, 319–320.

Gellman, S., 1997. Introduction: molecular recognition. Chem. Rev. 97, 1231–1232.

González, I., Martín, R., García, T., Morales, P., Sanz, B., Hernández, P.E., 1993. A sandwich enzyme-linked immunosorbent assay (ELISA) for detection of Pseudomonas

fluorescens and related psychrotrophic bacteria in refrigerated milk. J. Appl. Bacteriol. 74, 394–401.

Haldeman, R.G., Emmett, P.H., 1955. Specific adsorption of alkyl orange dyes on silica gel. J. phys. Chem 59, 1039–1043.

Harvey, S.D., Mong, G.M., Ozanich, R.M., Mclean, J.S., Goodwin, S.M., Valentine, N.B., Fredrickson, J.K., 2006. Preparation and evaluation of spore-specific affinity-augmented bio-imprinted beads. Anal Bioanal Chem 366, 211–219.

Hayden, O., Bindeus, R., Haderspo, C., Wirl, B., Dickert, F.L., 2003. Mass-sensitive detection of cells , viruses and enzymes with artificial receptors. Sensors Actuators B Chem. 91, 316–319.

Hayden, O., Dickert, F.L., 2001. Selective microorganism detection with cell surface imprinted polymers. Adv. Mater. 13, 1480–1483.

Hayden, O., Lieberzeit, P.A., Blaas, D., Dickert, F.L., 2006. Artificial antibodies for bioanalyte detection-sensing viruses and proteins. Adv. Funct. Mater. 16, 1269–1278.

Henry, O.Y.F., Piletsky, S.A., Cullen, D.C., 2008. Fabrication of molecularly imprinted polymer microarray on a chip by mid-infrared laser pulse initiated polymerisation. Biosens. Bioelectron. 23, 1769–1775.

Hernández, R., Riu, J., Bobacka, J., Vallés, C., Jiménez, P., Benito, A.M., Maser, W.K., Rius, F.X., 2012. Reduced graphene oxide films as solid transducers in potentiometric all-solid-state ion-selective electrodes. J. Phy. Chem. C 116, 22570–22578.

Hjerten, S., Liao, J.L., Nakazato, K., Wang, Y., Zamaratskaia, G., Zhang, H.X., 1997. Gels mimicking antibodies in their selective recognition of proteins. Chromatographia 44, 227–234.

Hongyan, H., Guoqi, F., Wang, Y., Chai, Z., Jiang, Y., Chen, Z., 2010. Imprinting of protein over silica nanoparticles via surface graft copolymerization using low monomer concentration. Biosens. Bioelectron. 26, 760–765.

Ivnitski, D., Wilkins, E., Tien, H.T., Ottova, A., 2000. Electrochemical biosensor based on supported planar lipid bilayers for fast detection of pathogenic bacteria. Electrochem. commun. 2, 457–460.

Karimian, N., Turner, A.P.F., Tiwari, A., 2014. Electrochemical evaluation of troponin T

imprinted polymer receptor. Biosens. Bioelectron. 59, 160–165.

Karimian, N., Vagin, M., Hossein, M., Zavar, A., Chamsaz, M., Turner, A.P.F., Tiwari, A., 2013. An ultrasensitive molecularly-imprinted human cardiac troponin sensor. Biosens. Bioelectron. 50, 492–498.

Kawasaki, S., Horikoshi, N., Okada, Y., Takeshita, K., Sameshima, T., Kawamoto, S., 2005. Multiplex PCR for simultaneous detection of Salmonella spp., Listeria monocytogenes, and Escherichia coli O157:H7 in meat samples. J. Food Prot. 68, 551–556.

Kim, H.J., Bennetto, H.P., Halablab, M.A., Choi, C., Yoon, S., 2006. Performance of an electrochemical sensor with different types of liposomal mediators for the detection of hemolytic bacteria. Sensors Actuators B Chem. 119, 143–149.

Ko, S., Grant, S.A., 2006. A novel FRET-based optical fiber biosensor for rapid detection of Salmonella typhimurium. Biosens. Bioelectron. 21, 1283–1290.

Kryscio, D.R., Peppas, N.A., 2012. Critical review and perspective of macromolecularly imprinted polymers. Acta Biomater. 8, 461–473.

Kurien, B.T., Scofield, R.H., 2009. Protein Blotting and Detection: Methods and Protocols. Humana Press, Totowa New Jersey, p. 588.

Kuwata, T., Uchida, A., Takano, E., Kitayama, Y., Takeuchi, T., 2015. Molecularly imprinted polymer arrays as synthetic protein chips prepared by transcription-type molecular imprinting by use of protein-immobilized dots as stamps. Anal. Chem. 87, 11784–11791.

Lahav, M., Kharitonov, A.B., Katz, O., Kunitake, T., Willner, I., 2001. Tailored chemosensors for chloroaromatic acids using molecular imprinted TiO2 thin films on ion-sensitive field-effect transistors. Anal. Chem. 73, 720–723.

Lazcka, O., Campo, F.J. Del, Munoz, F.X., 2007. Pathogen detection: a perspective of traditional methods and biosensors. Biosens. Bioelectron. 22, 1205–1217.

Lehn, J.-M., 1995. Supramolecular chemistry: Concepts and perspectives. Wiley-VCH, Weinheim.

Liang, R., Yin, T., Qin, W., 2015. A simple approach for fabricating solid-contact ion-selective electrodes using nanomaterials as transducers. Anal. Chim. Acta 853, 291–296.

Liu, J., Deng, Q., Tao, D., Yang, K., Zhang, L., Liang, Z., Zhang, Y., 2014. Preparation of protein imprinted materials by hierarchical imprinting techniques and application in selective depletion of albumin from human serum. Sci. Rep. 4:5487, 1–6.

Maalouf, R., Fournier-wirth, C., Coste, J., Chebib, H., Saı, Y., Vittori, O., Errachid, A., Cloarec, J., Martelet, C., Jaffrezic-renault, N., Cnrs, U.M.R., Cnrs, U.M.R., Lyon, E.C. De, Collongue, G. De, 2007. Label-free detection of bacteria by electrochemical impedance spectroscopy : comparison to surface plasmon resonance. Anal. Chem. 79, 4879–4886.

Marx, S., Liron, Z., 2001. Molecular imprinting in thin films of organic-inorganic hybrid sol-gel and acrylic polymers. Chem. Mater. 13, 3624–3630.

Mayes, A., 2005. Chapter 2. In Molecularly imprinted materials: Science and Technology. Marcel Dekker, New York.

Mayes, A.G., Whitcombe, M.J., 2005. Synthetic strategies for the generation of molecularly imprinted organic polymers. Adv. Drug Deliv. Rev. 57, 1742–1778.

Mazza, G., 1983. Rapid assay for detection of microorganisms producing DNA-damaging metabolites. Appl. Environ. Microbiol. 45, 1949–1952.

Mirsky, V.M., Hirsch, T., Piletsky, S.A., Wolfbeis, O.S., 1999. A Spreader-bar approach to molecular architecture : formation of stable artificial. Angew. Chem. Int. Ed. 3, 1108–1110.

Moreira, F.T.C., Sharma, S., Dutra, R.A.F., Noronha, J.P.C., Cass, A.E.G., Sales, M.G.F., 2014. Protein-responsive polymers for point-of-care detection of cardiac biomarker. Sensors Actuators B Chem. 196, 123–132.

Morrison, J., Worsley, M., 1959. The nature of the specificity of adsorption of alkyl orange dyes on silica gel. Can. J. Chem. 37, 1986–1995.

Mosbach, K., Arshady, R., 1981. Synthesis of substrate-selective polymers by host-guest polymerization. Macromol. Chem. Phys. 182, 687–692.

Namvar, A., Warriner, K., 2007. Microbial imprinted polypyrrole/poly (3-methylthiophene) composite films for the detection of Bacillus endospores. Biosens. Bioelectron. 22, 2018–2024.

Nishino, H., Huang, C., Shea, K.J., 2006. Selective protein capture by epitope imprinting.

Angew. Chem. Int. Ed. 45, 2392–2396.

Patrikeev, V., Balandin, A., Klabunovski, E., Mardashev, Y., Maksimova, G., 1960. Selectivity of an adsorbent produced in the presence of bacteria with respect to optical isomers. Dokl . Akad. Nauk SSSR 132, 850–852.

Polevoda, B., Sherman, F., 2000. N -terminal acetylation of eukaryotic proteins. J. Biol. Chem. 275, 36479–36482.

Polyakov, M., 1931. Adsorption properties and structure of silica gel. Zhurnal Fizieskoj Khimii 2, 799–805.

Polyakov, M., Kuleshina, L., I, N., 1937. On the dependence of silica gel adsorption properties on the character of its porosity. Zhurnal Fizieskoj Khimii 10, 100–112.

Polyakov, M., P, S., Paryckij, M., Malkin, I., Duchina, F., 1933. On the structure of silica. Zhurnal Fizieskoj Khimii 4, 454–456.

Ravelet, C., Peyrin, E., 2006. Recent developments in the HPLC enantiomeric separation using chiral selectors identified by a combinatorial strategy. J. Sep. Sci. 29, 1322–1331.

Rebelo, T.S.C.R., Pereira, C.M., Sales, M.G.F., Noronha, J.P., Silva, F., 2016. Protein imprinted material electrochemical sensor for determination of Annexin A3 in biological samples. Electrochim. Acta 190, 887–893.

Reddy, S.M., Hawkins, D.M., Phan, Q.T., Stevenson, D., Warriner, K., 2013. Protein detection using hydrogel-based molecularly imprinted polymers integrated with dual polarisation interferometry. Sensors Actuators B Chem. 176, 190–197.

Rider, T.H., Petrovick, M.S., Nargi, F.E., Blanchard, D.J., Bortolin, L.T., Young, A.M., Chen, J., Hollis, M. a, 2003. A B cell – based sensor for rapid identification of pathogens. Science 301, 5–8.

Schneider, H.-J., Yatsimirsky, A., 2000. Principles and Methods in Supramolecular Chemistry. Wiley, Chichester.

Sharma, P.S., Pietrzyk-le, A., D'Souza, F., Wlodzimierz, K., 2012. Electrochemically synthesized polymers in molecular imprinting for chemical sensing. Anal Bioanal Chem 402, 3177–3204.

Syritski, V., Reut, J., Menaker, A., Gyurcsanyi, R.E., Opik, A., 2008. Electrosynthesized

molecularly imprinted polypyrrole films for enantioselective recognition of l-aspartic acid. Electrochim. Acta 53, 2729–2736.

Tai, D.-F., Ho, Y.-F., Wu, C.-H., Lin, T.-C., Lu, K.-H., Lin, K.-S., 2011. Artificial-epitope mapping for CK-MB assay. Analyst 136, 2230.

Taylor, S.L., Nordlee, J.A., Niemann, L.M., Lambrecht, D.M., 2009. Allergen immunoassays-considerations for use of naturally incurred standards. Anal. Bioanal. Chem. 395, 83–92.

Tokonami, S., Nakadoi, Y., Takahashi, M., Ikemizu, M., Kadoma, T., Saimatsu, K., Dung, L.Q., Shiigi, H., Nagaoka, T., 2013. Label-free and selective bacteria detection using a film with transferred bacterial configuration. Anal. Chem. 85, 4925–4929.

Tripathi, V.S., Kandimalla, V.B., Ju, H., 2006. Preparation of ormosil and its applications in the immobilizing biomolecules. Sensors Actuators B Chem. 114, 1071–1082.

Turan, E., 2009. Dependence of protein recognition of temperature-sensitive imprinted hydrogels on preparation temperature. Macromol. Biosci. 9, 421–428.

Turenne, C.Y., Sanche, S.E., Hoban, D.J., Karlowsky, J.A., Kabani, A.M., 1999. Rapid identification of fungi by using the ITS2 genetic region and an automated fluorescent capillary electrophoresis system. J. Clin. Microbiol. 37, 1846–1851.

Turner, N.W., Jeans, C.W., Brain, K.R., Allender, C.J., Hlady, V., Britt, D.W., 2006. From 3D to 2D : a review of the molecular imprinting of proteins. Biotechnol. Prog. 22, 1474–1489.

Vasapollo, G., Sole, R. Del, Mergola, L., Lazzoi, M.R., Scardino, A., Scorrano, S., Mele, G., 2011. Molecularly imprinted polymers: present and future prospective. Int. J. Mol. Sci. 12, 5908–5945.

Villamizar, R.A., Maroto, A., Rius, F.X., Inza, I., Figueras, M.J., 2008. Fast detection of *Salmonella infantis* with carbon nanotube field effect transistors. Biosens. Bioelectron. 24, 279–283.

Vogtle, F., 1991. Supramolecular Chemistry. Wiley, Chichester.

Walker, J.M., 2002. The protein protocols handbook. Humana Press, Totowa New Jersey, p. 1146.

Wang, Q., Lu, G., Yang, B., 2004. Direct electrochemistry and electrocatalysis of hemoglobin immobilized on carbon paste electrode by silica sol–gel film. Biosens. Bioelectron. 19, 1269–1275.

Wang, Y., Ye, Z., Ying, Y., 2012. New trends in impedimetric biosensors for the detection of foodborne pathogenic bacteria. Sensors 12, 3449–3471.

Wang, Y., Zhou, Y., Sokolov, J., Rigas, B., Levon, K., Rafailovich, M., 2008. A potentiometric protein sensor built with surface molecular imprinting method. Biosens. Bioelectron. 24, 162–166.

Whitcombe, M., 2011. Whitcombe MJ: MIPDATABASE.COM 2011.

Wulff, G., Sarhan, A., 1972. The use of polymers with enzyme-analogous structures for the resolution of racemates. Angew. Chem. Int. Ed. 11, 364–364.

Xiangjie, L., Jingjing, Z., Lei, T., Wei, L., Zhang, B., Zhang, H., Qiuyu, Z., 2015. Bovine serum albumin surface imprinted polymer fabricated by surface grafting copolymerization on zinc oxide rods and its application for protein recognition. J. Sep. Sci. 38, 3477–3486.

Yang, L., Bashir, R., 2008. Electrical/electrochemical impedance for rapid detection of foodborne pathogenic bacteria. Biotechnol. Adv. 26, 135–150.

Yang, W., Ratinac, K.R., Ringer, S.R., Thordarson, P., Gooding, J.J., Braet, F., 2010. Carbon nanomaterials in biosensors: should you use nanotubes or graphene. Angew. Chem. Int. Ed. 49, 2114–2138.

Yin, D., Ulbricht, M., 2013. A novel two-step surface grafting method. J. Mater. Chem. B 1, 3209–3219.

Yuan, X., Wang, H., C., S., Zhang, J., 2010. Electrochemical Impedance Spectroscopy in PEM Fuel Cells. Fundamentals and Applications. Springer London Dordrecht Heidelberg, New York.

Zdyrko, B., Hoy, O., Luzinov, I., 2009. Toward protein imprinting with polymer brushes. Biointerphases 4, FA17–21.

Zelada-Guillen, G.A., Riu, J., Düzgün, A., Rius, F.X., 2009. Immediate detection of living bacteria at ultralow concentrations using a carbon nanotube based potentiometrie aptasensor. Angew. Chem. Int. Ed. 48, 7334–7337.

Chapter 2

Experimental Part

UNIVERSITAT ROVIRA I VIRGILI
PLASTIC ANTIBODIES FOR THE DETECTION OF BACTERIAL PROTEINS AND MICROORGANISMS
Azizur Rahman Khan

This chapter lists the materials, reagents and instruments used in this thesis, and describes the protocols used to construct the electrodes or their parts. The techniques, devices and protocols described have been taken from the experimental part of the various chapters of the thesis. Finally, the characterization techniques used throughout the study are reported.

2.1 General materials, reagents and instruments

2.1.1 Carbon nanotubes, graphene oxide and graphite powder

Multi-walled carbon nanotubes (MWCNTs) with a purity of > 99%, an average length of 150 μm and diameters of 10-20 nm were obtained from HEJI, Inc. (Zengcheng City, China). They were refluxed in H_2SO_4/HNO_3 (3:1) for 30 min to obtain carboxylated MWCNTs (Kerric et al., 2012). Then they were filtered on a Millipore membrane (polycarbonate PC, 0.10 μm) and the solid on the filter was washed with Milli-Q water, dried to get MWCNTs-COOH and stored under dry conditions until used. Graphene oxide solution in water was provided by ICB (Instituto de Carboquímica CSIC), Zaragoza, Spain. Graphite powder (<20 μm) was purchased from Sigma Aldrich.

2.1.2 Screen-printed and home-made electrodes

Single-walled carbon nanotube-based screen-printed electrodes (SWCNTs-SPE) or gold screen-printed electrodes (Au-SPE) were purchased from DropSens, Oviedo, Spain. Home-made carbon-printed electrodes (HP C-PE) were fabricated on wax-modified filter paper by manually printing carbon ink from Creative Materials, USA.

2.1.3 Monomers, proteins and flagella for MIP synthesis

Monomers such as acrylamide, *N,N'*-methylenebis(acrylamide) (NMMA), pyrrole, 3-aminophenol (AP), 3-aminopheny boronic acid (ABA) and phenol were purchased from Sigma Aldrich for synthesizing the MIP-based recognition layer and/or receptors. Protein A (PA) from *Staphylococcus aureus* was purchased from Sigma Aldrich and flagella from *Proteus mirabilis* (FPM) was received from the Department of Microbiology, University of Barcelona, Spain.

2.1.4 Lipophilic salts

Various selectophore-grade lipophilic salts were obtained from Fluka: sodium tetrakis[3,5-bis(trifluoro-methyl)phenyl]borate (NaTFPB), potassium tetrakis(4-chlorophenyl)borate (KTClPhB) and tridooctylammonium bromide (TOBr).

2.1.5 Analytical grade salts

In order to prepare the standard solutions, analytical grade salts were purchased from Fluka: sodium chloride (NaCl), potassium chloride (KCl) sodium acetate ($NaCH_3COO$), sodium monohydrogen phosphate (Na_2HPO_4), sodium dihydrogen phosphate (NaH_2PO_4).

2.1.6 Culturing media and microorganism

The culturing media tryptic soy broth (TSB) and tryptic soy agar (TSA) were purchased from Becton, Dickinson and Company (Sparks, USA), and they were prepared according to indications. These non-selective media were used in the enumeration and cultivation of pure strains of *Proteus mirabilis* (Gerhardt et al., 1981).

2.1.7 Other materials and reagents

Unless otherwise indicated, the following molecular biology grade reagents (>99.5% purity) were purchased from Sigma-Aldrich and were used as received:

- *N*-ethyl-*N'*-(3-dimethylaminopropyl)carbodiimide hydrochloride (EDAC).
- *N*-hydroxysuccinimide (NHS).
- 2-(*N*-morpholino) ethanesulfonic acid (MES).
- (2-aminoethyl methacrylate hydrochloride)
- Vinyl benzoate (VB)
- Ammonium persulphate (APS)
- Benzoyl peroxide (BOP)
- *N,N,N',N'*-Tetramethylethylenediamine (TEMED)
- Tetrahydrofuran (THF)
- *o*-Nitrophenyloctyl ether (oNPOE), poly(vinylchloride) (PVC) of high molecular weight
- (Vinylbenzyl)trimethylammonium chloride 97% (VTA)
- 4-(2-hydroxyethyl)-1-piperazineethanesulfonic acid (HEPES)
- Trypsin
- Proteinase K
- Bovin serum albumin (BSA)
- Glucose oxidase
- Tris(hydroxymethyl)aminomethane
- Potassium ferricyanide and potassium ferrocyanide

2.1.8 Materials and instruments

The following materials and instruments have been used:

- Double junction reference electrode (Ag/AgCl/KCl 3 M) containing a 1 M LiAcO electrolyte bridge, type 6.0729.100, Metrohm AG, Herisau, Switzerland.
- Glass filtration system with a capacity for 250 mL, model 5810, Fisher Scientific, Madrid, Spain.
- Glassy carbon cylindrical rods, length 50 mm and diameter 3 mm, HTW Hochtemperatur-Werkstoffe GmbH, Thierhaupten, Germany.
- High speed micro centrifuge, model 5417 R, Eppendorf AG, Hamburg, Germany.
- High-input impedance voltmeter (1015 Ω), model EMF-16, Lawson Laboratories Inc, Malvern, PA, USA.
- Metrohm Autolab and a PGSTAT302N (Utrecht, The Netherlands), equipped with a FRA module and controlled by Nova software.
- Infrared sterilizer, model Sterilbio, JP Selecta, Barcelona, Spain.
- Integral water purification system, model Milli-Q plus, Millipore, Molsheim, France.
- Magnetic stirring system, model Agimatic-N, JP Selecta, Barcelona, Spain.
- Magnetic stirring system, model ANM-10006, SBS SL, Sabadell-Barcelona, Spain.
- Microbiological incubator with natural convection system, model 100-800, Memmert GmbH Co KG, Schwabach, Germany.
- Nylon and polycarbonate filtration membranes, 47 mm diameter, pore size 0.45 μm, Albet Lab science, Dassel, Germany.
- Silica furnace chamber, HST 12/600, Carbolite, Hope Valley, UK.
- pH selective electrode, Model GLP 21, Crison Instruments SA, Barcelona, Spain.
- Polishing alumina, 25 and 1 micron grain size, Buehler, Lake Bluff, USA.
- Steam sterilizer (autoclave), model Med 12, JP Selecta, Barcelona, Spain.
- Teflon rods, 7 mm in diameter and 1000-2000 mm in length, Amidata SA, Madrid, Spain.
- Tip-sonicator, Ultraschallprocessor UP200S, Dr. Hielscher, Teltow, Germany.
- Triple vent polystyrene Petri dishes, 90x16 mm, model P101VR20, Sterilin Ltd, Newport, UK.

- Variable volume micropipettes, models 3111 000.157, 3111 000.165 and 3111 000.181 (capacities 20-200 µL, 100-1000 µL and 0.1-10.0 µL, respectively), Eppendorf AG, Hamburg, Germany.
- Bacteriological transfer and inoculating loop, model S-33, JP Selecta, Barcelona, Spain.
- Balance, model GR-120-EC, A&D Instruments, Abingdon, UK.
- Biosafety level II cabinet, model BIO II A, Telstar Industrials, Terrassa, Spain.
- Fourier transform infrared spectroscopy (FTIR), Waltham, USA.
- Raman spectrometer,Waltham, USA.
- Environmental scanning electron microscope (ESEM) FEI Quanta 400FEG, USA.
- Atomic force microscope (AFM), Keysight 5500, USA.
- Transmission electron microscope (TEM), Jeol 1011, Japan.
- Common laboratory glassware and plasticware such as volumetric pipettes, volumetric flasks, boiling flasks, Erlenmeyer flasks, filtering flasks, volumetric burettes, graduated cylinders, glass funnels, centrifuge tubes, watch glasses, beakers, non-sterile and sterile test tubes, weighing bottles, vials, condensers, microcentrifuge tubes, Teflon stirring rods, as well as other materials such as support stands, clamp holders, sterile plastic syringes of several sizes, stainless steel needles of different lengths and gauges, micropipette tips, sterilization indicator labels and tapes, latex and silicon rubber tubing of different gauges were purchased from Fisher Scientific, Madrid, Spain.

2.2 General procedures

2.2.1 Preparation of MIP-based recognition layer or receptors

This section is subdivided into two sections, one for each type of detection technique: a) EIS- and/or SWV-based detection of bacterial proteins, flagella and/or *Proteus mirabilis*; b) potentiometric detection of bacterial flagella and/or *Protein mirabilis*.

2.2.1.1 Synthesis of the MIP-based recognition layer for EIS- and/or SWV-based detection of the target

- Electrochemical: Bulk imprinting

Prior to electropolymerization, the SWCNTs-SPEs were cleaned by chronoamperometry (1.7 V, for 60s, in KCl 0.1M solution) and later stabilized by cyclic voltammetry (–0.2 to 0.8

V, 10 cycles, 50 mV/s, in MES buffer). Then, 75 µL of a solution containing PA 2.38×10^{-6} mol/L and AP 1.0×10^{-2} mol/L in acetate buffer pH 5.0 was placed over the SPE to cover the three electrodes and polymerization was performed by CV (between -0.2 and 0.8 V at a scan rate of 50 mV/s) for a variable number of cycles. The resulting film was thoroughly washed with de-ionized water and incubated next in proteinase K (500 µg/mL in PBS pH 7.4) for 2.5 h at room temperature. The surface was then washed thoroughly with Milli-Q water and subjected to electrochemical cleaning by 25 CV cycles in MES buffer (potential range -0.2 to 0.8 V, scan rate 0.05 V/s). This part can be seen in Chapter **3**, section **3.1**.

- Electrochemical: Surface imprinting

The SWCNTs-SPEs were cleaned using chronoamperometry in the same way as was discussed at the beginning (Electrochemical: bulk imprinting) of this section. Also, home-made carbon-printed electrodes (HP C-PEs) were cleaned by cyclic voltammetry (potential from -2.0 and +2.0 V, 40 cycles, scan-rate of 100 mV/s with KCl 0.1M in Milli-Q water), and stabilized electrochemically in the same way as for SWCNTs-SPE.

For the SWCNTs-SPE, 10 µL of 1.22×10^{-6} mol/L FPM solution prepared in MES buffer was exposed to the working area of the electrode for 30 min at room temperature and gently washed with Milli-Q water. Then 75 µL of phenol solution (3.55×10^{-3} mol/L prepared in acetate buffer 1.0×10^{-2} mol/L pH 5.0) was deposited onto the SPE to cover the three-electrodes for around 10s and polymerization was performed by CV between -0.2 and 0.8 V (scan rate of 50 mV/s, 15 CVs cycles was found to be optimal). For the HP C–PE the total procedure was the same as for the SWCNTs-SPE but the potential range for electropolymerization was -0.2 to 1.2V. The resulting film (either in SWCNTs-SPEs or in HP C-SPEs) was thoroughly washed with deionized water and incubated with proteinase K (500 µg/mL in PBS pH 7.4) for 2.5h at room temperature. The surface was then thoroughly washed with Milli-Q water and subject to subsequent electrochemical cleaning by 25 CV cycles in MES buffer (potential range -0.2 to 0.8 V, scan rate 50 mV/s). The results of this work can be seen in Chapter **5,** section **5.1** and **5.2**.

2.2.1.2 Synthesis of MIP-based receptors for potentiometric detection of the target

- Electrochemical: Surface imprinting

Prior to electropolymerization, the Au-SPE electrodes were cleaned with ethanol and then cleaned electrochemically with 0.5 M H_2SO_4 by cycling at a potential −0.2 to1.2 V, for 15 cycles, at a scan-rate of 50 mV/s. Subsequently, FPM were deposited in the working

area of the Au-SPE via nonspecific adsorption. In this case, 10 µL of 2.44×10^{-6} mol/L FPM solution prepared in MES buffer was exposed to the working area of the electrodes for 30 minutes at room temperature and gently washed with Milli-Q water. Then the three electrodes were covered with 75 µL of pyrrole solution (1×10^{-3} mol/L) in acetate buffer (1×10^{-2} mol/L, pH 5.0) and polymerization was performed from -0.2 to 1.2 V. Subsequently, FPM were removed by the action of trypsin (500 µg/mL in Tris buffer, 37°C, 3 h) and electrochemical cleaning (-0.6 to 1 V, 50 mV/S, 10 CV cycles in MES buffer) to create imprinted cavities. This electrode was directly used for potentiometric detection of flagella and *Proteus mirabilis* **(**Chapter **5,** section **5.3)**.

2.2.2 Microorganism culturing

The bacteria strains were cultured using standard microbiological techniques, and appropriately sterilized materials, solutions and culturing media.

Pure cultured strains of *Proteus mirabilis* bacteria in agar (TSA) were received from the Department of Microbiology, University of Barcelona, Spain. These pure cultured strains were further incubated in broth (TSB) for 24-48 h at 37°C to re-culture, and then further cultured in agar medium (24 h at 37°C) to obtain characteristic colonies. The colonies obtained in agar cultures were then transferred to glycerol/TSB 20:80 and stored at -20°C until needed and the bacteria were re-cultured in 10 mL of sterile broth medium (TSB) at 37°C for 24 h.

For the bacteria enumeration assays, the testing of biosensors and the preparation of standard solutions, the selected bacteria were inoculated in 10 mL of sterile broth medium at 37°C for 24 h. Then, 1 mL of the bacteria samples was centrifuged at 15000 rpm for 10 minutes (repeated three times) and the supernatant was discarded. The precipitate was suspended in 10 mL of sterile distilled water/buffer (HEPES 1×10^{-4} mol/L, pH 7.3) (Chapter **5,** section **5.2** and **5.3)** and the resulting solution was 1:10 diluted ninefold to provide a series of 10^{-1} to 10^{-9} stock solutions of bacteria. Each stock solution was quantified with the standard plate count method in triplicate (Gerhardt et al., 1981) in the appropriate culturing agar medium (TSA).

2.3 Electrode characterization

2.3.1 Electrochemical characterization

The surface was characterized by CV, EIS and SWV by observing the blocking behavior of polymers and/or target using Metrohm Autolab.

2.3.2 Spectroscopic and microscopic characterization

FTIR (attenuated total reflectance mode) and Raman spectroscopy analysis were carried out to see the chemical changes on the surface of the electrodes. FTIR spectroscopy generates absorbance peaks on the spectrum indicate functional groups of different types of bonds. Although the analysis is performed in absorbance, it can be converted to transmittance, since they are simply inversions of each other. Raman spectroscopy employed to see the defect properties of the surface. The electrode surfaces were microscopically characterized by ESEM and AFM. TEM was used to observe the shape and size of the flagella from *Proteus mirabilis*.

2.4 References

Gerhardt, P., Murray, R.G.E., Costilow, R.N., Nester, E.W., Wood, W.A., Krieg, N.R., 1981. Manual of methods for general bacteriology. American Society for Microbiology, p. 524.

Kerric, G., Parra, E.J., Crespo, G.A., Xavier Rius, F., Blondeau, P., 2012. Nanostructured assemblies for ion-sensors: functionalization of multi-wall carbon nanotubes with benzo-18-crown-6 for Pb^{2+} determination. J. Mater. Chem. 22, 16611.

UNIVERSITAT ROVIRA I VIRGILI
PLASTIC ANTIBODIES FOR THE DETECTION OF BACTERIAL PROTEINS AND MICROORGANISMS
Azizur Rahman Khan

Chapter 3

Molecular imprinting of protein A from *Staphylococcus aureus*

UNIVERSITAT ROVIRA I VIRGILI
PLASTIC ANTIBODIES FOR THE DETECTION OF BACTERIAL PROTEINS AND MICROORGANISMS
Azizur Rahman Khan

As first approach for the detection of bacterial surface proteins (protein A from *Staphylococcus aureus*) we proposed to make MIPs to be used as the sensing part in the construction of potentiometric sensors based on conductive materials (oxidized multi-walled carbon nanotubes (MWCNTs-COOH), graphene oxide (GO), polypyrrole). But since the obtained results were not good, we decided to change the detection method from potentiometry to impedimentary. In this chapter (section **3.1**), electrochemical bulk imprinting and electrochemical impedance spectroscopy have been used to capture and detect protein A from *Staphylococcus aureus,* and the results were published in 'Sensors and Actuators B: Chemical', year 2011, volume 233, pages 697-704.

3.1 Article: Plastic antibody for the electrochemical detection of bacterial surface proteins

This work presents a novel molecularly imprinted polymer (MIP) for the indirect detection of bacteria, by targeting an outer membrane protein on a disposable device. Protein A (PA) was selected for this purpose, as a representative protein of the outer surface of *Staphylococcus aureus*. The imprinted polymer was assembled directly on a film of single walled carbon nanotubes (SWCNTs), placed on screen-printed electrodes (SPEs). The MIP material was produced by electropolymerizing 3-aminophenol in the presence of the protein template (PA) using cyclic voltammetry (CV). The proteins entrapped at the polymeric backbone were digested by the action of proteolytic activity of proteinase K and then washed away to create vacant sites.

The performance of the corresponding imprinted and non-imprinted electrodes was evaluated by EIS and the effect of several variables, such as monomer and template concentrations, thickness of imprinting surface, was controlled and optimized by the number of CV cycles. The detection limit of the MIP-based sensors was 0.60 nM in MES buffer. High repeatability and good selectivity was observed in the presence of a model protein BSA. The sensor performance was also tested to check the effect of inorganic ions in tap water. The detection limit observed was 16.83 nM, with a recovery factor of 91.1±6.6%. The sensor described in this work is a potential tool for screening PA on-site, due to the simplicity of fabrication, disposability, short response time, low cost, good sensitivity and selectivity.

Keywords: Plastic antibody; Molecularly imprinted polymer; Electropolymerization; Bacterial surface proteins, *Staphylococcus aureus;* Screen-printed electrodes; Disposable device.

3.1.1 Introduction

In our daily life, diseases and productivity losses caused by bacteria are very common, and *Staphylococcus aureus* (*S. aureus*) is the responsible for a spectrum of pathologic conditions, including circumscriptive suppurations, bloodstream invasion, a variety of toxic syndromes, and serious skin diseases (Sompolinsky et al., 1985). *S. aureus* can produce several types (A, B, C, D, and E) of enterotoxins that cause gastroenteritis (Halpin-Dohnalek and Marth, 1989; Minor and Marth, 1976). The presence of the bacterium in water is also a health hazard if the water is held at a temperature that allows bacterial growth, which permits synthesis of enterotoxins. Not surprisingly, *S. aureus* has several virulence factors including cytotoxic hemolysins, leukocidins, enterotoxins, teichoic acid, and protein A (Sompolinsky et al., 1985).

Protein A (PA) is a cell wall constituent (Lofkvist and Sjoquist, 1962) of S. *aureus* and is covalently linked to the peptidoglycan structure of the bacterium. Around 99% of S. *aureus* strains have PA on the cell wall (Chang and Huang, 1995) and between 8-30% of it is secreted during the exponential growth phase (Movitz, 1976; Sjoquist et al., 1972). This extracellular protein can thus be detected and it can be used as an indicator of the presence of the microorganism in clinical or food specimens (Chang and Huang, 1995; Song et al., 1997). In this context, the detection of protein A is of great importance and may constitute a simple way to detect the presence of *S. aureus* in a given sample.

Surface proteins of pathogenic bacteria can serve as protective antigens and malignity markers, though they can be technically challenging to detect. Several biochemical and microbiological techniques have been employed to detect bacterial surface proteins, including fluorescent labeling (Anaya et al., 2007), stable isotope labeling (Zhu et al., 2002), LC-MS coupled biotinylation (Hempel et al., 2010), surface shaving approaches (Tjalsma et al., 2008), genome analyses and protein and antibody arrays (Cahill, 2001) or enzyme-linked immunosorbent assay (ELISA) (Burkovski, 1997). The antigen/antibody reaction is highly preferred in this context due to the high selectivity of the affinity reaction taking place between these biomolecules. However, the use of natural antibodies for protein detection is expensive due to the high cost of the material, the need for special handling and storage, and the poor stability of the antibodies.

These constraints would be overcome by replacing natural antibodies by artificial receptors such as molecularly imprinting polymers (MIPs), also known as plastic antibodies (Masqué et al., 1998; Mayes and Mosbach, 1997). Although the development of MIP

materials is a technology from the 70s, protein and/or microorganism imprinting has faced many difficulties within time (Algieri et al., 2014; Lv et al., 2013; Vasapollo et al., 2011; Verheyen et al., 2011; Whitcombe et al., 2011). Few reports have been published for microorganism detection based on stamp imprinting. The most remarkable ones need a pre-polymerization step to make a gel which can be then deposited by a controlled way over the electrode surface (Eersels et al., 2013; Hayden and Dickert, 2001; Hayden et al., 2006). The detection technique used is QCM (quartz crystal microbalance) (Hayden and Dickert, 2001; Hayden et al., 2006) which is limited by externally induced mechanical vibrations and large overall footprint, and heat flow measurements (Eersels et al., 2013) which could be limited by temperature control. But most of the MIP materials obtained so far are used for separation and binding (Piletsky et al., 2001), and the detection of protein based on imprinted materials is not so much explored yet, although it remains as a promising field (Algieri et al., 2014; Vasapollo et al., 2011; Verheyen et al., 2011; Whitcombe et al., 2011). As far as we know molecular imprinting-based bacterial surface protein detection is still now missing.

In MIPs, a polymeric network is assembled (2-D or 3-D) and molded around a suitable template molecule (i.e. the target analyte), which upon removal (Almeida et al., 2012; Moreira et al., 2014; Rebelo et al., 2014) yields nano/micro cavities of specific size, shape, and/or chemical functionality in a matrix. Such molecularly designed cavities show affinity for the imprinted molecule over other structurally and chemically related compounds. Preparation of thin films by this method is very attractive for chemical and biological sensing applications, due to long term stability with respect to pH or temperature changes. Several strategies have been used for the fabrication of MIPs, such as vinyl-based (Rebelo et al., 2014) or sol-gel polymerizations (Almeida et al., 2012), that are chemically or physically initiated/sustained (i.e., by electromagnetic radiation or and electrical stimulus) (Moreira et al., 2014). Any of these may be achieved by surface imprinting (2-D) and bulk imprinting (3-D). Usually electrochemical imprinting offers the advantaged of controlling the thickness of the imprinting layer easily, by adjusting the time or the number of cycles during polymerization. Electrochemical MIPs preparation is also a green synthesis process, since it is made without using any type of free radical formation agent (Sharma et al., 2012), as most of the conventional polymerization processes. Between the 3-D and 2-D electrochemical imprinting, the former offers a higher number of rebinding positions, while needing less optimization procedures to control the surface polymerization thickness (which is the crucial part of the imprinting stage in surface imprinting).

The production of an electropolymerized MIP film is however confined to the existence of suitable monomers. Many monomers have been used so far for this purpose agent (Sharma et al., 2012). In this regard, and having in mind that a protein is being targeted, aminophenol would be a good choice. The growth of an electropolymerized aminophenol film is self-limiting, and therefore its thickness may be easily controlled (Moreira et al., 2014). Furthermore, the presence of amino groups at the imprinting polymeric matrix would attract the target protein by permselectivity during the sensing stage which would presumably contribute to an increased sensitivity and better detection ability.

In this paper, we used electrochemical bulk imprinting (3-D) for the fabrication of MIPs over single walled carbon nanotubes-based disposable screen printed electrodes (SWCNT-SPEs) for PA detection. The PA from the outer surface of *Staphylococcus aureus* was mixed with 3-aminophenol monomers and electropolymerized by cyclic voltammetry to entrap PA in the polymeric backbone. PA was removed in a later stage by proteolytic activity of proteinase K and subsequent electrochemical washing by cyclic voltammetry. Electrochemical impedance spectroscopy (EIS) was employed to follow the changes in the electrical features of the working electrode as well as to detect PA with high selectivity and precision.

3.1.2. Experimental section

3.1.2.1 Apparatus

The electrochemical measurements were conducted with a potentiostat/galvanostat from Metrohm Autolab and a PGSTAT302N (Utrecht, The Netherlands), equipped with a FRA module and controlled by Nova software. The SWCNTs-SPEs were purchased from DropSens (Oviedo, Spain), and composed by a working electrode made of carboxylated SWCNTs, a counter electrode made of carbon and a reference electrode made of silver; electrical contacts were also made of silver. The diameter of the working electrode was 3.80 mm. The SWCNTs-SPEs were connected to a portable switch box, also from DropSens (DRP-DSC), allowing their interface with the potentiostat/galvanostat.

Fourier transform infrared spectroscopy (FTIR) measurements were performed using a Thermo Scientific Smart iTR Nicolet iS10, coupled to a SAGA smart accessory, also from Thermo Scientific (Waltham, USA). Raman measurements were performed in a Thermo Scientific DXR Raman spectrometer with confocal microscopy (Waltham, USA), with a 10

mW 532 nm excitation laser. Images of the materials were taken with an Environmental Scanning Electron Microscope (ESEM) FEI Quanta 400FEG.

3.1.2.2 Reagents

All chemicals were of analytical grade and water was de-ionized or ultrapure Milli-Q laboratory grade. Potassium hexacyanoferrate III, potassium hexacyanoferrate II trihydrate, and sodium acetate anhydrous were obtained from Riedel-deHäen; bovine serum albumin (BSA), and proteinase K from Fluka; 3-aminophenol (AP) 99%, and 2-(*N*-morpholino)ethanesulphonic acid monohydrate 98% (MES) from Alfa Aesar; PA (from *Staphylococcus aureus*) from Sigma Aldrich; and potassium chloride (KCl) from Merck.

3.1.2.3 Solutions

Stock solutions of 2.38×10^{-5} mol/L PA were prepared in HEPES buffer (1.0×10^{-4} mol/L, pH 5.0). Standards were obtained by accurate dilution of the previous solution in MES buffer (1.0×10^{-2} mol/L, pH 5.0, KCl 0.1M) or in sodium acetate buffer (1.0×10^{-2} mol/L, pH 5.0) depending on the study. Electrochemical assays were performed with 5.0×10^{-3} mol/L $[Fe(CN)_6]^{3-}$ and 5.0×10^{-3} mol/L $[Fe(CN)_6]^{4-}$ prepared in MES buffer. The selectivity study was made by a competitive assay in MES buffer and using BSA in a concentration of 7.1×10^{-7} mol/L.

3.1.2.4 Electrochemical synthesis of molecular imprinted (MIP) and non-imprinted polymer (NIP) films

Prior to electropolymerization, the SWCNTs-SPEs were cleaned by chronoamperometry (1.7 V, for 60s, in KCl 0.1M solution) and later stabilized by cyclic voltammetry (–0.2 to 0.8 V, 10 cycles, 50 mV/s, in MES buffer). Then, 75 µL of a solution containing PA 2.38×10^{-6} mol/L and AP 1.0×10^{-2} mol/L in acetate buffer pH 5.0, was placed over the SPE to cover the three electrodes and polymerization was performed by CV (between -0.2 and 0.8 V at a scan rate of 50 mV/s) for a variable number of cycles. The resulting film was thoroughly washed with de-ionized water and incubated next in proteinase K (500 µg/mL in PBS pH 7.4) for 2.5 h at room temperature. The surface was then washed thoroughly with Milli-Q water and subjected to electrochemical cleaning by 25 CV cycles in MES buffer (potential range -0.2 to 0.8 V, scan rate 0.05 V/s). The overall process has been presented schematically in **Figure 3.1**.

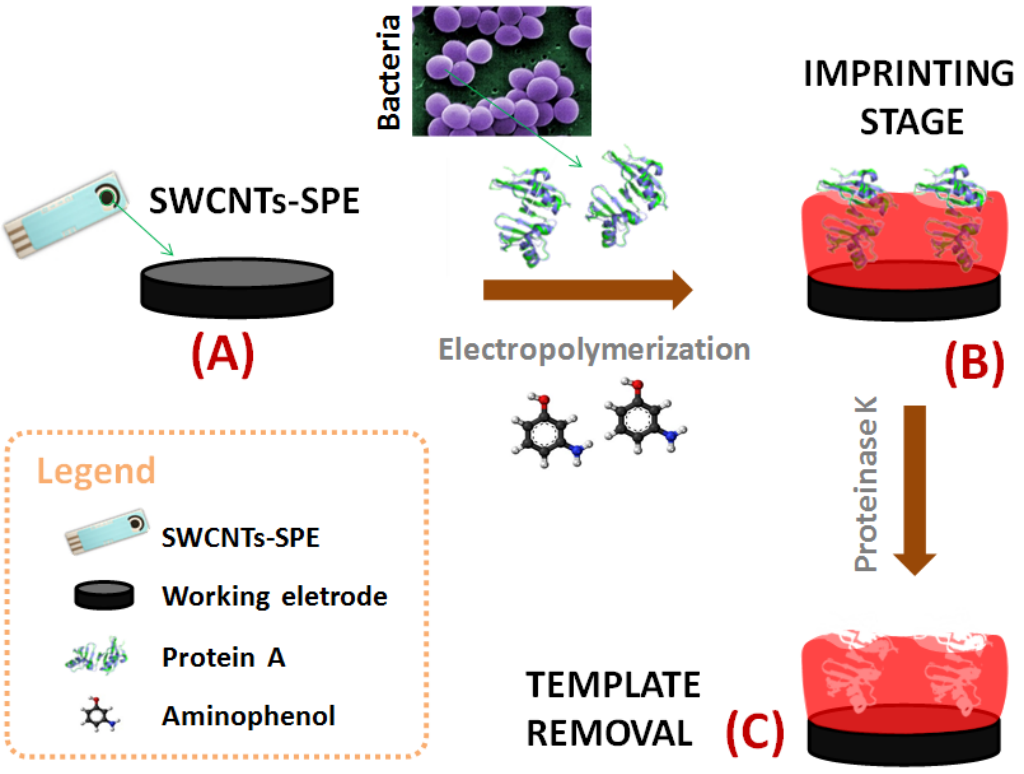

Figure 3.1. Schematic representation of the synthetic process. (A) Working area of SWCNTs-SPE; (B) Imprinting stage after electropolymerization of AP along with PA and (C) Binding site formation after template removal by proteinase K.

In parallel, non-imprinted polymers (NIPs) have been synthesized in a similar mode, but without presence of PA. Therefore NIPs are similar than MIPs but without the cavities for the target analyte.

3.1.2.5 Qualitative characterization of the films

All qualitative analyses were directly performed on the SPE without any treatment. MIP films with PA and after PA removal with proteinase K treatment, and NIP films at different stages of fabrication were analysed by Raman spectroscopy, where the average signal-to-noise ratio (peak height/RMS noise) was set automatically along 5 min of maximum measuring time, for a 5 mW laser power on the sample, and 50 µm slit aperture. FTIR analysis was performed before and after the electropolymerization of MIP and NIP film formation. The FTIR (from 400 to 4000 cm^{-1}) number of scans was set to 256, the

resolution to 8, apodization of Happ-Genzel, Mertz Phase correction, and a background gain of 8. ESEM analysis was done at high vacuum and 1×10^5 magnification at 15 kV.

3.1.2.6 Binding isotherm

The adsorption dynamics of MIPs and NIPs were studied by incubating increasing concentrations of PA standards, prepared in MES buffer, ranging from picomolar to micromolar level. The incubation time was set to 20 min at room temperature before adding the redox probe for subsequent EIS measurements.

A Langmuir isotherm model (*Equation 3.1*) was applied to the experimental data, where R_{ct} is the normalized charge transfer-density (kΩ/cm^2), S the concentration of PA (in M) and $R_{ct}^{máx}$ is the maximum charge transfer density observed (kΩ/cm^2). The apparent dissociation constant (K_D in M) and the maximum binding capacity ($R_{ct}^{máx}$) were calculated from the fitting of the experimental data to the model in *Equation 3.1*. K_D is the protein concentration required to provide half of the maximum response produced by the device.

$$R_{ct} = \frac{R_{ct}^{máx}}{1 + K_D/[S]} \qquad \textit{Equation 3.1}$$

3.1.2.7 Electrochemical assays

The redox probes in all CV and EIS measurements were 5.0 mmol/L $[Fe(CN)6]^{3-}$ and 5.0 mmol/L $[Fe(CN)6]^{4-}$ prepared in MES buffer at pH 5.0. In CV assays, the potential ranged from −0.5 to +0.7 V with a scan rate of 50 mV/s. In EIS, an open circuit potential was set using a sinusoidal potential perturbation of 0.01 V amplitude and 50 frequency values logarithmically distributed over a frequency range of 0.1 Hz to100 kHz.

Calibration curves were performed by EIS measurements for PA in the range from 23.8 pM to 4.76 µM level. At each concentration level, 10µLof PA standard solution in MES buffer was exposed to the imprinted sensors for 20 min at room temperature. The values of precision corresponded to the standard deviation of triplicate experiments. Selectivity studies were conducted by checking the response of a PA 7.1×10^{-7} mol/L solution prepared in MES buffer at pH 5.0, with or without BSA (7.1×10^{-7} mol/L). Real sample analysis was done by spiking PA in tap water diluted with MES buffer (1:3, tap water/buffer).

3.1.3 Results and discussion

3.1.3.1 Electropolymerization and imprinting stage

For a successful imprinting, the selection of the polymer has an important role depending on several parameters, such as the degree of polymerization, the selected potential for electropolymerization, and the functional groups of the polymer with ability to increase permselectivity. Polyaminophenol (PAP) exhibits several advantages, including an easy control of the polymer thickness due to a self-limiting growth, and a high degree of permselectivity (Tucceri et al., 2012). The amine and hydroxyl functional groups linked to the aromatic ring may also contribute to establish electrostatic interactions with the target protein at the rebinding event, thereby contributing for its stability at the rebound position, even after washing.

The electropolymerization was established by imposing consecutive CV cycles over the clean-SPE. In the first cycle, the current increased in the direction of the oxidation potentials, evidencing a peak at around 0.6 V. This peak indicated the oxidation of AP, thereby allowing the occurrence of electropolymerization (**Figure 3.2A**). In the reverse scan, down to negative potentials, no peak was present showing the irreversibility of the reaction. The subsequent CV cycles showed a continuous decrease in the current of the system, which confirmed the growing of a non-conductive layer.

The CV profiles of the iron redox probe obtained for the SPE coated with the polymeric film (MIP or NIP) on top of the working electrode clearly confirmed the presence of a highly *blocked* surface (**Figure 3.2B**). The redox peaks of the iron probe at the clean SPEs almost disappeared after formation of the polymeric layer. This was coupled with a higher peak-to-peak potential separation, also evidencing that the surface was *blocked*.

The electrical changes occurring at the SPEs by polymerization were also followed by EIS. In general, the electrochemical properties occurring at the electrode-solution interface were related to simplified Randles cell (Daniels and Pourmand, 2007; Suni, 2008). The circuit consisted of one resistor (solution resistance, R_s) in series with one parallel circuit comprised of a resistor (charge transfer resistance, R_{ct}) and a capacitance of double layer (C_{dl}) (inset, **Figure 3.2C**) (Daniels and Pourmand, 2007; Ding et al., 2005a, 2005b). In this circuit, the Nyquist plot consists of a single semicircle. Such semicircle intersects the real axis (Z') in two spots: the data point closest to the origin indicates the resistance value of the solution (R_s), while the intercept farthest from the origin indicates the total resistance

(R_{ct}+R_s). Thus, the charge transfer resistance (R_{ct}) corresponds to the diameter of the observed semicircle. The clean SPE showed very little R_{ct} value, when compared to the polymeric modifications of the surface. As may be seen in **Figure 3.2C**, the polymer on the surface cause a huge increase of the charge-transfer resistance of a clean SPE. This was due to the non-conductive properties of the PAP.

In parallel, the control film (NIP) was synthesized without the presence of PA during electropolymerization. The NIP polymer yielded a lower R_{ct} compared to MIP (**Figure 3.2C**), and this difference could only be attributed to the presence of PA in the MIP polymerization stage. As PA was within the growing polymer, two interrelated events occur: the presence of PA on the matrix changes the electrical properties of the surface where the polymer is growing (when compared with AP growing alone in NIP), which is turn affects the polymer growth as the polymer is being formed by an electrical stimulus applied to the electrode surface. In other words, the differences reflect the direct impact of the protein on the electrical properties of the surface and its indirect impact by promoting a differentiated polymer growth by such different electrical features.

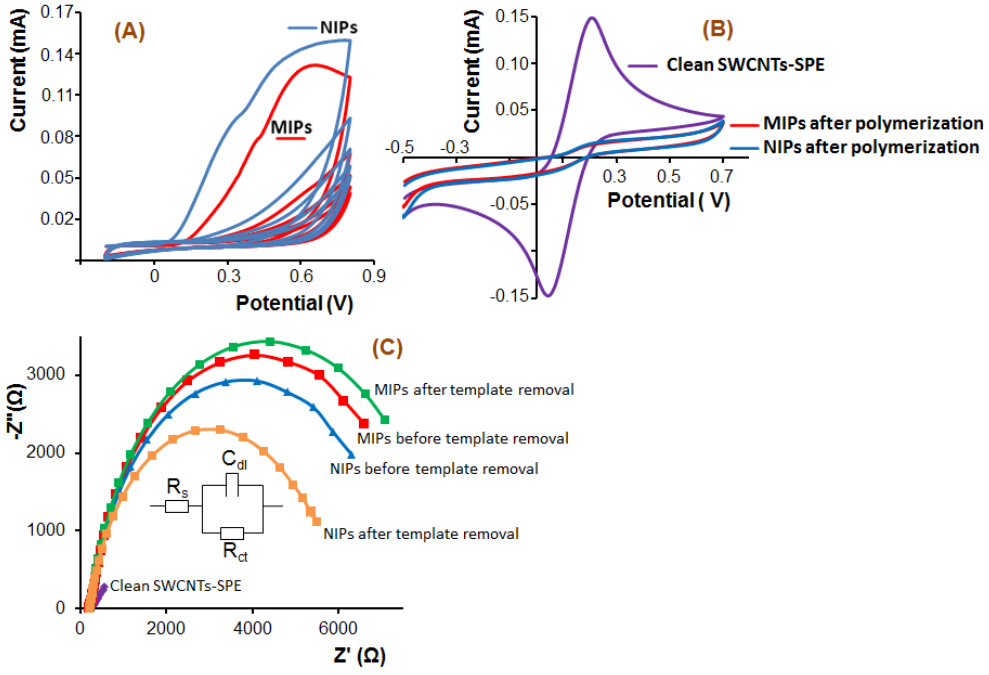

Figure 3.2. (A) Electrochemical synthesis of MIPs and NIPs. Electrochemical control of the subsequent modification steps in 5.0 mM $[Fe(CN)_6]^{3-}$ and 5.0 mM $[Fe(CN)_6]^{4-}$, in MES buffer pH 5, carried out by (B) CV and (C) EIS (Nyquist plots) assays for MIPs/NIPs, and Randles circuit (inset).

3.1.3.2 Protein removal

PA biomolecules hanging at the surface of the imprinted polymer, and exposed to the solution, were removed as peptide fragments by the proteolytic activity of proteinase K. The protein removal changed the typical electrical features of the redox probe, as this additional element no longer existed at the surface. The changes of charge transfer resistance (R_{ct}) are different in MIPs and NIPs after the action of proteinase K and the electrochemical cleaning (**Figure 3.2C**).

When the NIP material was subject to proteinase K, the R_{ct} value of the iron redox probe decreased significantly. This was most probably related to the partial loss of polymer along this process, as no protein existed to be digested. In this case, the enzyme could have partially digested the polymer lying at the surface, because one of its predominant sites of cleavage is peptide bonds near aromatic amino acids with blocked alpha amino groups, and the PAP is likely to have many nitrogen and oxygen related groups linked to aromatic groups.

But the MIP material increased its R_{ct} value after proteinase K action. In a first glance, this seemed a strange behavior, because the enzyme decreased the R_{ct} of the control polymer and protein removal generally decreases the resistance of a given surface. However, the effect of a given protein also depends of its protonation, compared to the redox probe. If PA would be positively protonated, the concentration of the iron redox probe at the surface could increase by ionic interaction, thereby reducing the R_{ct}, despite the fact that a higher amount of a non-conductive compound existed at the surface. Indeed, this was verified in practice, when different concentrations of PA were incubated at the surface of a blank electrode and the resistance decreased. Thus, the increase of the R_{ct} in the MIP layer after protein removal was a combination of opposite events: a decrease caused by polymer loss and an increase caused by protein loss.

3.1.3.3 Follow-up of the surface modification

- Raman spectroscopy

Raman spectra were recorded for MIP and NIP materials at different stages of the assembly of the sensing surface. The spectra obtained are shown in **Figure S3.1** (Supplementary Information), displaying the typically observed G and D bands of carbon-based materials.

The I_D/I_G ratio of the clean SWCNTs-SPE was 0.658. After polymerization without template (NIPs), the I_D/I_G ratio changed to 0.738 and after formation of MIPs the I_D/I_G ratio was 0.755. Overall, an increase in the defect band D was observed after polymerization, suggesting the modification of SWCNTs with a less organized carbon material, and this change was not the same in MIPs than in NIPs, accounting for the presence of the protein. Interestingly, after the template removal by the proteolytic activity of proteinase K, the I_D/I_G ratio decreased to 0.724 for MIPs. In the case of NIPs, after the action of proteinase K (in this case there was no template to remove) the I_D/I_G ratio was 0.735, almost similar to the ratio without the action of proteinase K. The difference in the I_D/I_G ratio for MIPs before and after the template removal, and the quasi constant values in the I_D/I_G ratio for NIPs before and after the template removal, is a strong evidence of the successful imprinting.

- Fourier transformed infrared spectroscopy

The AP electropolymerization is expected to yield polymers which contain phenyl, quinoid and benzenoid ring (Franco et al., 2008; Gopalasamy et al., 2014; Verma et al., 2015) and the FTIR analysis was conducted directly over the SPEs directly over the SPEs at before and after polymerization of sensors fabrication to find out their existence. The results are presented in **Figure S3.2** (Supplementary Information).

After polymerization, the MIPs and NIPs showed a characteristic broad peak at ~3000-3700 cm^{-1} for the N–H and O–H stretching in the polymeric network, which is absent in the clean SWCNTs-SPEs. The peak position also changed from 1571 cm^{-1} (clean SWCNTs-SPE) to 1589 cm^{-1} (after polymerization) with high intensity and broad peak, which is the indication of a mixture of the C=C and C=N stretching vibrations in the quinoid ring.

- Electron microscopy

The surface morphology was investigated by environmental scanning electron microscope at different stages of the MIP fabrication. The collected images are presented in **Figure S3.3** (Supplementary information). The clean SWCNTs-SPE evidenced the presence of carbon nanotubes well distributed within the carbon structure and several pores of different sizes, randomly distributed over the surface. Such porous surface disappeared after assembling the MIP layer on top of SWCNTs; the microscopic image of the MIP evidenced a compact structure, with no pores and, apparently, homogenous. After the template removal, the surface of MIP materials evidenced several pores, of small dimension. In addition the MIP surface became more rough which could indicated the exit

of oligomer fractions of the polymer and/or polymer degradation derived by the enzymatic action.

3.1.3.4 Analytical performance of the sensor

The analytical performance of the sensor was evaluated by incubating the sensing surface (MIP or NIP) with a PA standard solution of increasing concentration. For this purpose, a drop of standard solution was casted on top of the working electrode and let stand there for 20 min. During this period, PA rebinding was allowed. After this, the electrode surface was washed and the three electrode system of the SPE covered with the standard iron redox probe for electrical reading.

Figure 3.3 shows the EIS detection (ranging from pmol·L^{-1} to μmol·L^{-1}) recorded for MIP and NIP-based electrodes. **Figures 3.3A** and **B** showed the impedance responses upon the addition of different PA concentrations for the MIP and NIP-based devices respectively. Both MIP and NIP devices displayed decreasing charge-transfer resistances when the PA concentration increased (**Figures 3.3A** and **C**). This lowering of R_{ct} with increasing PA concentration was probably related to the positive protonation of the imprinted surface by the interaction of PA with the amino or hydroxyl groups of the imprinted polymers, under the conditions in which the assay was performed. The imprinted polymer contains –NH and –OH groups (FTIR in **Figure S3.2** of the Supplementary Information), and probably the electrostatic interaction of these groups with the PA functional groups create protonation over the imprinted surface. Such interaction between PA and MIP increased the density of positive charges over the receptor surface, which in turn increased the number of negatively charged iron redox probe molecules attracted over the surface.

For low level concentrations (up to 23.8 nM) the NIP-based devices presented a random behaviour against increasing protein A (PA) concentrations (**Figures 3.3B** and **C**). For higher concentrations, the NIP R_{ct} values start to decrease, thereby confirming the existence of non-specific binding of PA to the receptor surface. The MIP surface displayed a similar behaviour, but the linear response was extended over a wider range of PA concentrations, including lower concentrations of protein.

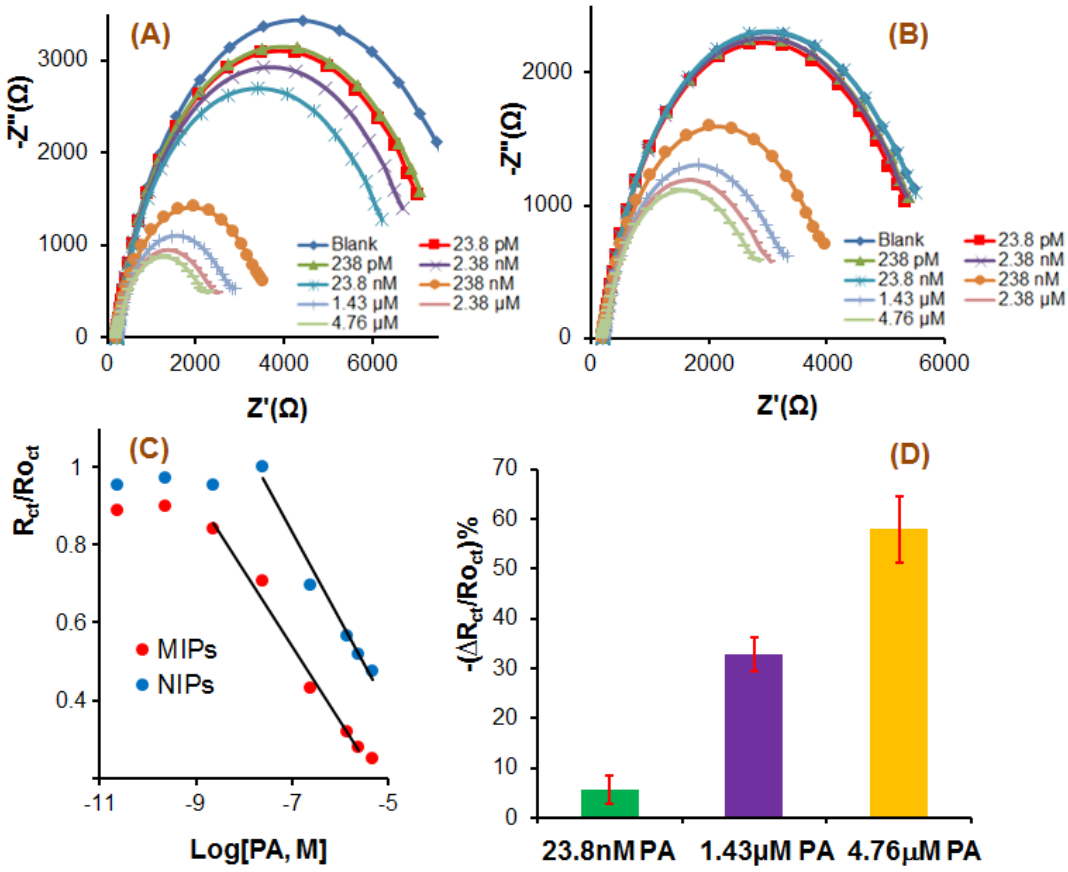

Figure 3.3. EIS measurements of (A) MIPs and (B) NIPs based sensors and the corresponding calibration curves (C) in 5.0 mM $[Fe(CN)_6]^{3-}$ and 5.0 mM $[Fe(CN)_6]^{4-}$, in MES buffer pH 5, with different concentrations of PA; (D) Precision of MIPs-based device. The error bars correspond to ± the standard deviation of the three results.

The detection limit (LOD) of MIPs was 0.60 nM, considering three times the standard deviation of the blank response. The precision of the MIP-based devices (results based on three different measurements using three different devices), at different levels of concentration is shown in **Figure 3.3D.**

3.1.3.5 Binding isotherm

The isotherm based on EIS results of MIPs follows a hyperbolic response (**Figure 3.4A**) approaching the typical behaviour of antibody/interactions (Ding et al., 2005b). The

parametric data over the Langmuir equation ($\Delta R_{ct}^{máx}$ and K_D, in *Equation 3.1*) assesses the performance of the sensor in terms of template rebinding. $\Delta R_{ct}^{máx}$ reflects the differences in the amount of PA bound to the sensor surface and K_D (the dissociation constant) shows the concentration of PA providing half of the maximum response ($\Delta R_{ct}^{máx}$), thus measuring how well PA form complexes with MIPs and the affinity with which it occurs. If the K_D is low it indicates a large binding affinity, as there action will approach the maximum response more rapidly. On the contrary, a high K_D indicates that the sensor does not efficiently bind with PA.

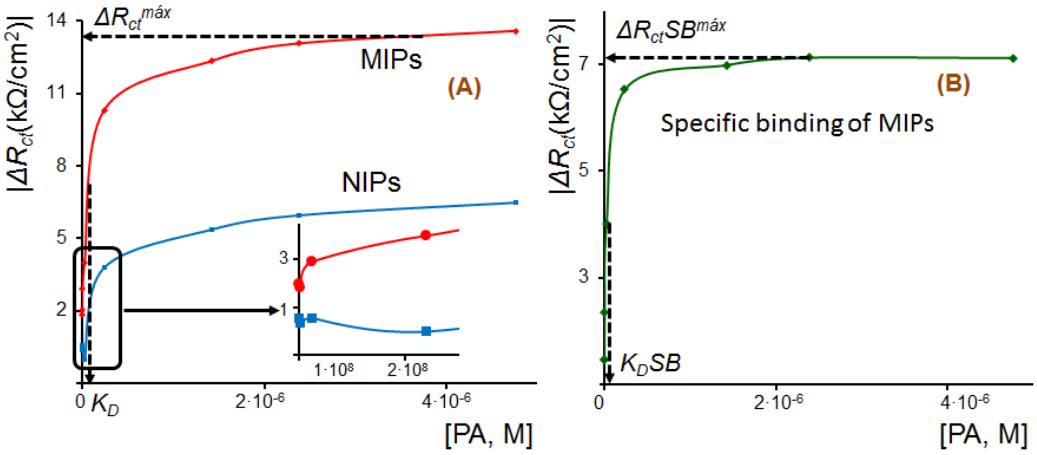

Figure 3.4. Graphical representation of the Langmuir isotherm plot: (A) comparison of signal density and maximum binding capacity ($\Delta R_{ct}^{máx}$) of MIPs and NIPs; (B) Binding isotherm of MIPs after subtracted NIPs signal density.

In general, the MIP $\Delta R_{ct}^{máx}$ and K_D values should be distinguishable from control NIPs. R_{ct} and Ro_{ct} respectively indicates normalized and baseline charge transfer resistance of the sensor, and hence the signal density ΔR_{ct} (where $\Delta R_{ct} = R_{ct} - Ro_{ct}$) represents the binding adsorption for each concentration of PA. The signal density (ΔR_{ct} *per* unit area of electrode) for MIPs increases after each addition of PA (until a saturation) whereas for NIPs the signal density is scattered at low concentration and it suffers from non-specific binding at high concentration of PA (**Figure 3.4A**). $\Delta R_{ct}^{máx}$ for MIPs is 13.34 kΩ/cm^2 and for NIPs is 6.21 kΩ/cm^2 ($\Delta R_{ct}^{máx}$ of MIPs is 2.15 times higher than the NIPs one). The dissociation constant (K_D) is 119 nM for MIPs. NIPs showed a random affinity at low concentration of PA (inset in **Figure 3.4A**) whereas the MIP signal density was regularly increasing over all the

range of concentrations. The most interesting information from the binding isotherms is found after subtracting the NIP signal density from the MIP signal: the subtracted signal density ΔR_{ct}SB (where ΔR_{ct}SB = ΔR_{ctMIP} - ΔR_{ctNIP}) also follows a hyperbolic response (**Figure 3.4B**) which reflects the amount of specific binding that occurs with MIPs without considering non-specific binding. The dissociation constant for the specific binding (K_DSB) of MIPs is 23.8 nM with maximum specific binding ($\Delta R_{ct}SB^{máx}$) of 7.12 kΩ/cm^2 what shows the difference between MIPs and NIPs.

3.3.3.6 Selectivity

The selectivity of the sensor was evaluated by EIS measurements using the competitive method (Moreira et al., 2014). In this case, the time and conditions were set as like the calibration of the sensors, and BSA was chosen to check the interferences as a model protein. Negligible interference effect was found, with a signal variation of only 1.7 % when the PA and BSA concentration ratio was 1:0.1, and 0.35 %, when the PA and BSA concentration ratio was 1:1(**Figure 3.5**).

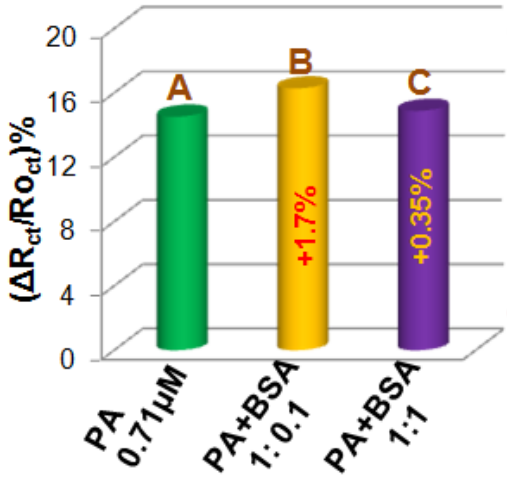

Figure 3.5. Selectivity test of the sensor by competitive method; signal for (A) only PA, (B) mixture of PA and BSA 1: 0.1 (in M), and (C) mixture of PA and BSA 1: 1 (in M).

3.1.3.7 Application to real samples

Tap water, as a general source of bacteria, was selected as a proof-of-concept for the detection of PA. We spiked PA in tap water (tap water four times diluted in MES buffer) and

checked the performance of the sensors. Using this matrix, the LOD is 16.83 nM (**Figure 3.6**) which is a little bit higher than when detecting PA in pure MES buffer. This probably indicates that some inorganic ions may have some impact on the sensors performance by electrostatic interaction with the protein rebinding site or with the target protein.

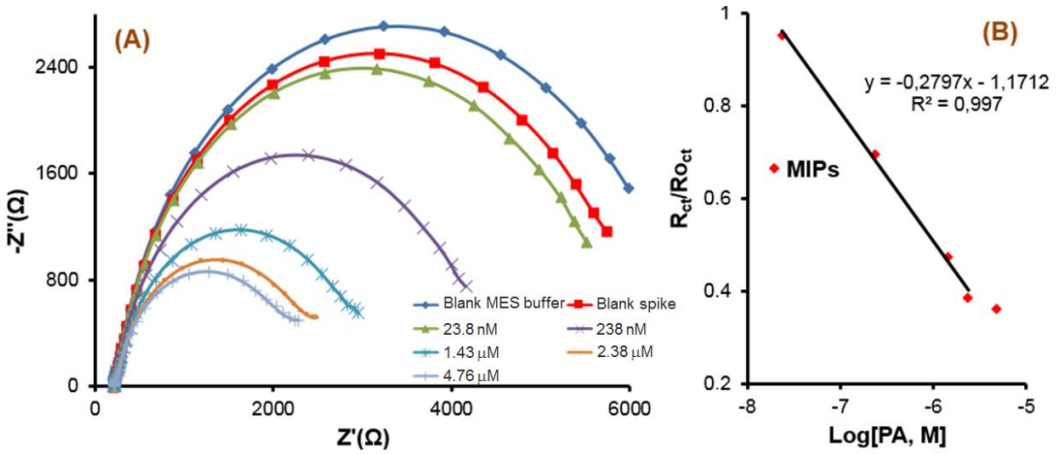

Figure 3.6. EIS measurements of (A) MIPs based sensor and the corresponding calibration curves (B) in 5.0 mM $[Fe(CN)_6]^{3-}$ and 5.0 mM $[Fe(CN)_6]^{4-}$ by spiking PA in tap water.

We tested the recovery factors after spiking of PA in tap water. The spiked value was 2.38 µM and the recovered value was 2.17 µM, what means a recovery value of 91.08% with a standard deviation (calculated from the propagation of errors from the regression line) of 6.60%.

3.1.4. Conclusions

In this paper we present a molecularly imprinting-based analytical device for the direct electrical detection of the PA from *S. aureus.* This device concerns a simple and low cost assembly. It displays a good precision, selectivity, low detection limit, offering also the advantages of disposability, simple instrumentation and easy preparation for the detection of PA from the outer surface of *S. aureus.* This device can be seen as a first step for the detection of bacteria using molecularly imprinted polymer-based devices. Before using the device in field-conditions, further experiments are necessary to ensure its successful application to water holding bacterial contamination.

Acknowledgements

Catalan Government and European Research Council are acknowledged for the financial support of MARK PhD Fellowship (2013FI_B 00842) and Starting Grant, 3P's, GA 311086 respectively. The URV team thanks the financial support from the Spanish Ministerio de Economía y Competitividad (Project CTQ2010-18717).

3.1.5 References

Algieri, C., Drioli, E., Guzzo, L., Donato, L., 2014. Bio-Mimetic sensors based on molecularly imprinted membranes. Sensors 14, 13863–13912.

Almeida, S.A.A., Truta, L.A.A.N.A., Queirós, R.B., Montenegro, M.C.B.S.M., Cunha, A.L., Sales, M.G.F., 2012. Optimizing potentiometric ionophore and electrode design for environmental on-site control of antibiotic drugs: application to sulfamethoxazole. Biosens. Bioelectron. 35, 319–26.

Anaya, C., Church, N., Lewis, J.P., 2007. Detection and identification of bacterial cell surface proteins by fluorescent labeling. Proteomics 7, 215–219.

Burkovski, A., 1997. Rapid detection of bacterial surface proteins using an enzyme-linked immunosorbent assay system. J. Biochem. Biophys. Methods 34, 69–71.

Cahill, D.J., 2001. Protein and antibody arrays and their medical applications 250, 81–91.

Chang, T.C., Huang, S.H., 1995. Evaluation of coagulase activity and protein A production for the identification of *Staphylococcus aureus*. J. Food Prot. 58, 858–862.

Daniels, J.S., Pourmand, N., 2007. Label-Free Iimpedance biosensors: opportunities and challenges. Electroanalysis 19, 1239–1257.

Ding, S.J., Chang, B.W., Wu, C.C., Lai, M.F., Chang, H.C., 2005a. Impedance spectral studies of self-assembly of alkanethiols with different chain lengths using different immobilization strategies on Au electrodes. Anal. Chim. Acta 554, 43–51.

Ding, S.J., Chang, B.W., Wu, C.C., Lai, M.F., Chang, H.C., 2005b. Electrochemical evaluation of avidin-biotin interaction on self-assembled gold electrodes. Electrochim. Acta 50, 3660–3666.

Eersels, K., Grinsven, B. Van, Ethirajan, A., Timmermans, S., Bogie, J.F.J., Punniyakoti, S.,

Vandenryt, T., Hendriks, J.J.A., Cleij, T.J., Daemen, M.J.A.P., Somers, V., Ceuninck, W. De, Wagner, P., 2013. Selective identification of macrophages and cancer cells based on thermal transport through surface-imprinted polymer layers. ACS Appl. Mater. Interfaces 5, 7258–7267.

Franco, D.L., Afonso, A.S., Vieira, S.N., Ferreira, L.F., Gonçalves, R.A., Brito-Madurro, A.G., Madurro, J.M., 2008. Electropolymerization of 3-aminophenol on carbon graphite surface: Electric and morphologic properties. Mater. Chem. Phys. 107, 404–409.

Gopalasamy, T., Gopalswamy, M., Gopichand, M., Raj, J., 2014. Poly Meta-Aminophenol: chemical synthesis, characterization and Ac impedance study. J. Polym. 2014, 11 pages.

Halpin-Dohnalek, H.I., Marth, E.H., 1989. Staphylococcus aureus: production of extracellular compounds and behavior in foods - a review. J. Food Prot. 52, 267–82.

Hayden, O., Dickert, F.L., 2001. Selective microorganism detection with cell surface imprinted polymers. Adv. Mater. 13, 1480–1483.

Hayden, O., Lieberzeit, P.A., Blaas, D., Dickert, F.L., 2006. Artificial antibodies for bioanalyte detection — sensing viruses and proteins. Adv. Funct. Mater. 16, 1269–1278.

Hempel, K., Pane, J., Otto, A., Sievers, S., Hecker, M., 2010. Quantitative cell surface proteome profiling for sigB-dependent protein expression in the human pathogen *Staphylococcus aureus* via biotinylation approach. J. Proteome Res. 17, 1579–1590.

Lofkvist, T., Sjoquist, J., 1962. Chemical and serological analysis of antigen preparations from *Staphylococcus aureus*; a comparison between the products obtained by Verwey's and Jensen's techniques. Acta Pathol. Microbiol. Scand. 56, 295–304.

Lv, Y., Tan, T., Svec, F., 2013. Molecular imprinting of proteins in polymers attached to the surface of nanomaterials for selective recognition of biomacromolecules. Biotechnol. Adv. 31, 1172–1186.

Masqué, N., Marcé, R.M., Borrull, F., 1998. New polymeric and other types of sorbents for solid-phase extraction of polar organic micropollutants from environmental water. TrAC - Trends Anal. Chem. 17, 384–394.

Mayes, A.G., Mosbach, K., 1997. Molecularly imprinted polymers: useful materials for analytical chemistry. TrAC - Trends Anal. Chem. 16, 321–332.

Minor, T.E., Marth, E.H., 1976. Staphylococci and Their Significance in Foods, Elsevier

Scientific Publishing Inc., Amsterdam.

Moreira, F.T.C., Sharma, S., Dutra, R.A.F., Noronha, J.P.C., Cass, A.E.G., Sales, M.G.F., 2014. Protein-responsive polymers for point-of-care detection of cardiac biomarker. Sensors Actuators B Chem. 196, 123–132.

Movitz, J., 1976. Formation of extracellular protein A by *Staphylococcus aureus*. Eur. J. Biochem. 68, 291–299.

Piletsky, S.A., Alcock, S., Turner, A.P.F., 2001. Molecular imprinting: At the edge of the third millennium. Trends Biotechnol. 19, 9–12.

Rebelo, T.S.C.R., Santos, C., Costa-Rodrigues, J., Fernandes, M.H., Noronha, J.P., Sales, M.G.F., 2014. Novel prostate specific antigen plastic antibody designed with charged binding sites for an improved protein binding and its application in a biosensor of potentiometric transduction. Electrochim. Acta 132, 142–150.

Sharma, P.S., Pietrzyk-le, A., D'Souza, F., Wlodzimierz, K., 2012. Electrochemically synthesized polymers in molecular imprinting for chemical sensing. Anal Bioanal Chem 402, 3177–3204.

Sjoquist, J., Movitz, J., Johansson, I.-B., Hjelm, H., 1972. Localization of protein A in the bacteria. Eur. J. Biochem. 30, 190–194.

Sompolinsky, D., Samra, Z., Karakawa, W.W., Vann, W.F., Schneerson, R., Malik, Z., 1985. Encapsulation and capsular types in isolates of *Staphylococcus aureus* from different sources and relationship to phage types. J. Clin. Microbiol. 22, 828–834.

Song, J., Kang, X., Guo, W., 1997. Determination of hemoglobin in plasma and serum by linear-sweep polarography. Fresen. J. Anal. C. 357, 127–129.

Suni, I.I., 2008. Impedance methods for electrochemical sensors using nanomaterials. TrAC - Trends Anal. Chem. 27, 604–611.

Tjalsma, H., Lambooy, L., Hermans, P.W., Swinkels, D.W., 2008. Shedding & shaving : disclosure of proteomic expressions on a bacterial face. Proteomics 8, 1415–1428.

Tucceri, R., Arnal, P., Scian, A., 2012. Electrosynthesis and spectroscopic characterization of poly(o -Aminophenol) film electrodes. ISRN Polym. Sci. 2012, 1–26.

Vasapollo, G., Sole, R. Del, Mergola, L., Lazzoi, M.R., Scardino, A., Scorrano, S., Mele, G., 2011. Molecularly imprinted polymers: present and future prospective. Int. J. Mol. Sci.

12, 5908–5945.

Verheyen, E., Schillemans, J.P., Van Wijk, M., Demeniex, M.-A., Hennink, W.E., Van Nostrum, C.F., 2011. Challenges for the effective molecular imprinting of proteins. Biomaterials 32, 3008–3020.

Verma, S.K., Kar, P., Yang, D.J., Choudhury, A., 2015. Poly(m-aminophenol)/functionalized multi-walled carbon nanotube nanocomposite based alcohol sensors. Sensors Actuators B Chem. 219, 199–208.

Whitcombe, M.J., Chianella, I., Larcombe, L., Piletsky, S.A., Noble, J., Horgan, A., 2011. The rational development of molecularly imprinted polymer-based sensors for protein detection. Chem. Soc. Rev. 40, 1547–1571.

Zhu, H., Pan, S., Gu, S., Bradbury, E.M., Chen, X., 2002. Amino acid residue specific stable isotope labeling for quantitative proteomics. Rapid Commun Mass Spectrom 16, 2115–2123.

3.1.6 Supplementary Information

- Raman spectroscopy

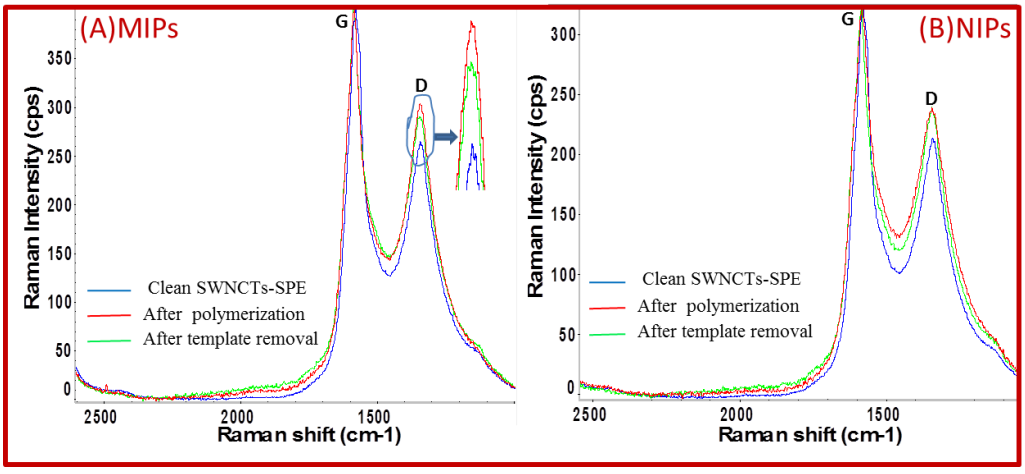

Figure S3.1. Raman spectrum at different stages of the sensors fabrication, (A) MIPs; (B) NIPs; inset: zoom of MIPs D peaks.

For polyaminophenol (PAP) films, the peaks (**Figure S3.1**) at about 1341 and 1583 cm^{-1} is expected correspond to quinoid groups and to the aromatic ring –C=N– in quinonimine units, respectively (Franco et al., 2008; Gopalasamy et al., 2014; Verma et al., 2015).

- Fourier transformed infrared spectroscopy

When FTIR analysis (**Figure S3.2**) was conducted with an attenuated total reflectance (ATR) accessory, the transmittance data was always accounted as major signal the background Au layer at the working electrode. So, a SAGA accessory as tried out because it enabled that the optical beam focused the electrode tangentially, thus allowing identifying small changes taking place at the outer surface of this active layer. The major drawback of such procedure was the decrease of the signal intensity, but this was compensated by an increased number of readings.

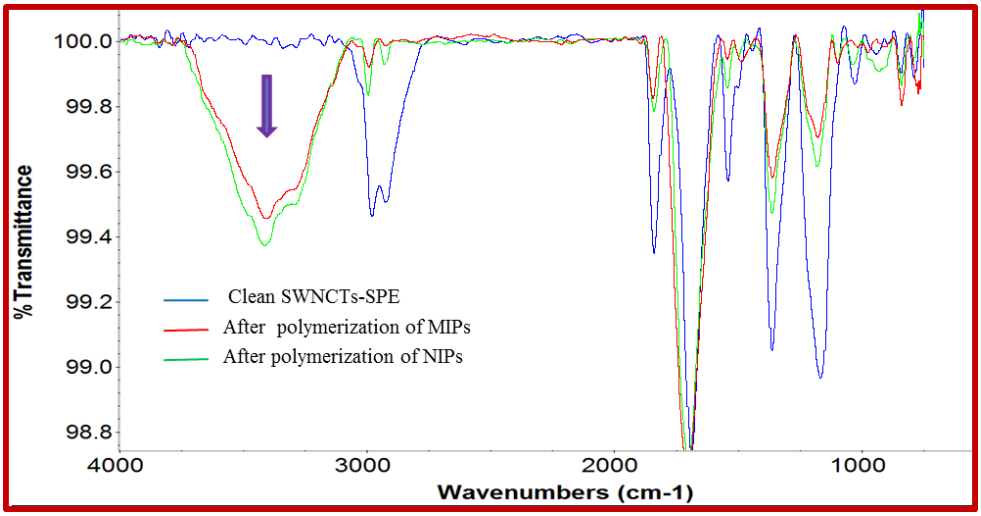

Figure S3.2. FTIR Spectrum at different stages of the sensors fabrication.

- Environmental scanning electron microscopy

The surface morphology was investigated at different stages of MIP fabrication by ESEM which are presented in **Figure S3.3.**

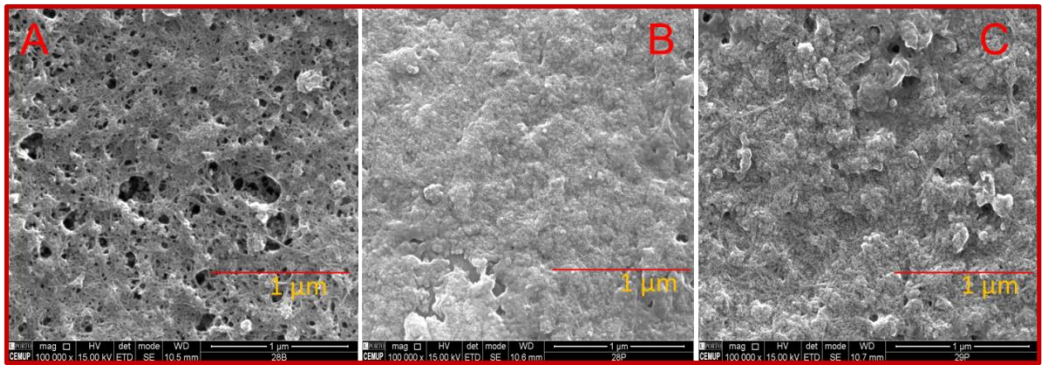

Figure S3.3. ESEM images at different stages of the sensors fabrication, (A) Clean SWNCTs SPE, (B) MIP after polymerization and (C) MIP after template removal.

- **References**

Franco, D.L., Afonso, A.S., Vieira, S.N., Ferreira, L.F., Gonçalves, R.A., Brito-Madurro, A.G., Madurro, J.M., 2008. Electropolymerization of 3-aminophenol on carbon graphite surface: Electric and morphologic properties. Mater. Chem. Phys. 107, 404–409.

Gopalasamy, T., Gopalswamy, M., Gopichand, M., Raj, J., 2014. Poly Meta-Aminophenol: chemical synthesis , characterization and Ac impedance study. J. Polym. 2014, 11 pages.

Verma, S.K., Kar, P., Yang, D.J., Choudhury, A., 2015. Poly(m-aminophenol)/functionalized multi-walled carbon nanotube nanocomposite based alcohol sensors. Sensors Actuators B Chem. 219, 199–208.

Chapter 4

Homemade paper-based electrode

UNIVERSITAT ROVIRA I VIRGILI
PLASTIC ANTIBODIES FOR THE DETECTION OF BACTERIAL PROTEINS AND MICROORGANISMS
Azizur Rahman Khan

This chapter (section **4.1**) shows a simple, cost-effective way for manually fabricating paper-based electrodes. The fabricated three-electrode system has also been used in chapter **5** section **5.1** for the construction of biosensors to detect flagella from *Proteus mirabilis.*

4.1 Fabrication of homemade paper-based electropolymerized printed electrodes (*Manuscript submitted*).

This chapter reports the fabrication of electrodes in inexpensive paper-based substrates (homemade paper-based carbon-printed electrodes, HP C-PEs). Standard filter paper was modified with wax to make it hydrophobic and the electrodes were manually printed over the hydrophobic paper at a close distance (≈ 1 mm). Two different configurations of devices are presented: two electrodes (to be used for instance in potentiometric measurements) or three electrodes (for instance to be used in voltammetry experiments). The three-electrode system shows similar electrochemical characteristics as the commercial ones, but a reduced cost. Electropolymerization performance with various electroactive monomers has been thoroughly studied on the HP C-PEs for the first time when three electrodes are assembled together. Moreover, the ability of these manually printed electrodes to be used as reference electrodes has been tested (in the two electrodes configuration) by adding a model protein (bovine serum albumin, BSA) in the potentiometric cell and observing stable potential upon BSA additions.

Keywords: Paper substrate, Carbon-printed electrodes, Homemade paper-based electrodes, Electropolymerization, Pseudo reference electrode.

4.1.1 Introduction

Photolithography is a frequently used method to fabricate electrodes in many devices, but their use is limited by the expensive cost, the high operational time and complex operations associated to these processes (Lin et al., 2009, 2008; Zhu et al., 2011). Another limitation of these techniques is that the fabricated electrodes can be easily damaged or even disabled by being bent and/or folded. Recently, research is going on to develop and fabricate low-cost devices, using for instance paper-based supports, but nowadays this technology is mainly promising as it has not been so much explored and/or commercialized yet (Oh and Chow, 2015).

Presently, polymeric thin films are very attractive for many technological applications such as coatings, adhesives, electronic devices or sensors and detectors (Berkes et al., 2015; Samet et al., 2010). This type of films are made by electropolymerization over various types of surfaces, and a great control over the film thickness is achieved varying the parameters of electropolymerization (Lipatov et al., 2015). Constructing a new wave of low-cost, flexible, portable and robust electrodes that need small volume of sample is also highly interesting to meet the demand in laboratory use and in point-of-care applications. Nowadays, a variety of electrochemical electrodes such as glassy carbon (GC), gold or indium tin oxide (ITO) electrodes on glass and plastic substrates are available. Recently the use of much more affordable materials such as paper is being significantly increased using various types of fabrication such as inkjet printing (Sjberg et al., 2016), direct printing and pressure-assisted ball pen (Li et al., 2015), with all of them needing an electronic instrument assistance to print. But these processes can be limited by the viscosity of the ink, and the lack of enough rigidity of the fabricated device for the easy and quick connection with the electrochemical instrument.

In the case of manual printing, impurity in ink materials used during the fabrication of the electrodes can severely interfere and retard polymerization. It is remarkable that even considering that homemade electrodes are cheap, these need proper conditioning, especially in cases of electropolymerization, which demand clean surfaces with high conductivity. As far as we know, proper cleaning and conditioning of homemade paper-based three-electrode system with a monitorization of electropolymerization performance has not been yet thoroughly studied.

In this work we present the manual fabrication of homemade paper-based carbon-printed electrodes (HP C-PEs) on wax-modified standard filter paper, including the study of electropolymerization performance over the working electrode and the pseudo reference characteristics of the reference electrode. Two different configurations of devices are presented: two electrodes (to be used for instance in potentiometric measurements) or three electrodes (for instance to be used in voltammetry experiments). Electrochemical characterization of these electrodes show that they present very attractive characteristics, similar to the ones obtained using commercial electrodes, being able also to bend without losing their performance characteristics.

4.1.2 Experimental

4.1.2.1 Reagents and chemicals

All chemicals were of analytical grade and water was de-ionized or ultrapure Milli-Q laboratory grade. Potassium hexacyanoferrate III, potassium hexacyanoferrate II trihydrate, and sodium acetate anhydrous were obtained from Riedel-deHäen; 2-(*N*-morpholino)ethanesulphonic acid monohydrate 98% (MES) from Alfa Aesar; phenol, 3-amino phenol (AP), 3- aminophenyl boronic acid (ABA) , bovine serum albumin (BSA), paraffin wax was from Sigma Aldrich, and potassium chloride from Merck. Carbon and Ag/AgCl ink were from Creative Materials, USA. Standard filter paper (cellulose, size 20 cm × 20 cm) was from Fanoia, Barcelona, Spain.

4.1.2.2 Solutions

Electrochemical cleaning and stabilization of the electrodes have been done using KCl solution (0.1M KCl in Milli-Q), and MES (1.0×10^{-2} mol/L, pH 5.0, KCl 0.1M) buffer respectively. Standard solution of phenol (3.55×10^{-3} mol/L), AP (1×10^{-2} mol/L) and ABA (1×10^{-2} mol/L) were prepared in sodium acetate buffer (1.0×10^{-2} mol/L, pH 5.0) for the electropolymerization. Electrochemical assays were performed with 5.0×10^{-3} mol/L $[Fe(CN)_6]^{3-}$ and 5.0×10^{-3} mol/L $[Fe(CN)_6]^{4-}$, prepared in MES buffer. Pseudo reference characteristics of the reference electrode and stability of the working electrode have been studied in HEPES buffer (1.0×10^{-4} mol/L, pH 7.2).

4.1.2.3 Instrumentation

Plastic tape (0.3 mm thick) coated with acrylic adhesive on one side (Arcare 8565) was obtained from Adhesives Research Inc., (Limerick, Ireland). Plastic mask was fabricated using a laser marker from Fenix Flyer (Synrad, USA). Rolling ball used was from Schmidt Technology, type EF117. The electrochemical measurements were conducted with a potentiostat/galvanostat from Metrohm Autolab and a PGSTAT302N (Utrecht, The Netherlands), equipped with a FRA module and controlled by Nova software. The homemade paper-based carbon-printed electrodes (HP C-PEs) were connected to a portable switch box, from DropSens (DRP-DSC), allowing their interface with the potentiostat/galvanostat. Electromotive force (EMF) was measured with a high input impedance (1015 W) EMF16 multichannel data acquisition device (Lawson Laboratories, Inc., Malvern) at room temperature. The standard reference electrode used was a Ag/AgCl

3 M KCl double-junction electrode (type 6.0726.100, Metrohm AG) containing 1 M LiAcO salt bridge (Herisau, Switzerland).

Raman measurements were performed in a Thermo Scientific DXR Raman spectrometer with confocal microscopy (Waltham, USA), with a 10 mW 532 nm excitation laser. Fourier transform infrared spectroscopy (FTIR) measurements were performed using a Thermo Scientific Smart iTR Nicolet iS10, coupled to a SAGA smart accessory, also from Thermo Scientific (Waltham, USA). Environmental scanning electron microscope (ESEM) images were obtained using a Quanta 600 (FEI Company) and atomic force microscopic (AFM) images were obtained using a Keysight 500 (Keysight, USA).

4.1.2.4 Plastic mask fabrication

The plastic mask was designed and drawn using CleWin 4.0.1 Layout Editor (PhoneiX Software, Netherlands). 30% laser power was applied on the plastic tape to make the plastic mask that was used to draw the electrodes over the wax-modified hydrophobic paper.

4.1.2.5 Design and fabrication process of HP C-PEs

The design of the HP C-PEs (three-electrode system) is presented in **Figure 4.1** (the smaller picture shows the design of the two-electrode system) with indication of different electrodes (reference, working and counter electrodes). The diameter of the working electrode was ≈ 3.50 mm and the spacing between electrodes was ≈ 1 mm. The length of the whole electrode system was 2.5 cm with 0.75 cm width.

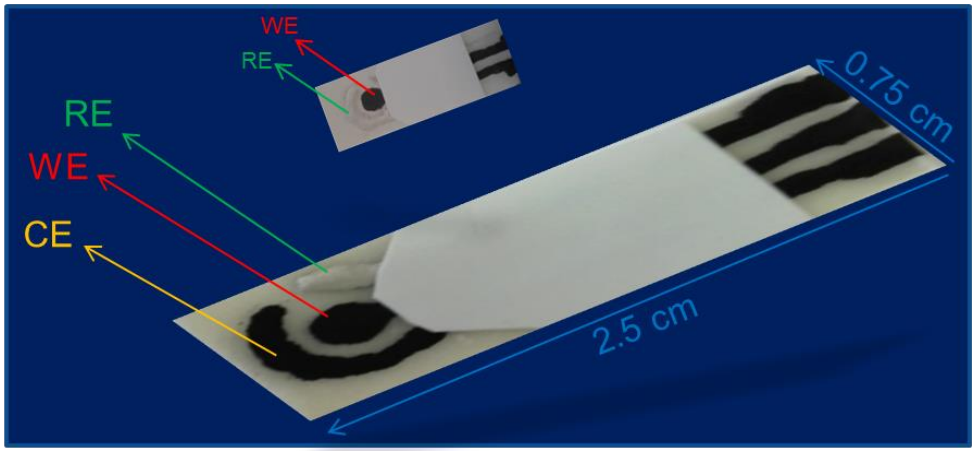

Figure 4.1. HP C-PEs (three-electrode design); RE: reference electrode, WE: working electrode, CE: counter electrode. The smaller picture on top shows the two-electrode design.

The fabrication process of the HP C-PEs consists of the following steps: 1. Modification of the filter paper (**Figure 4.2A**) with wax to make it hydrophobic (**Figure 4.2B**): grinded wax was scattered at above of the filter paper (0.037 g/cm^2) and another filter paper was kept down to the previous one to make support during the melting of wax. The total system was kept at the oven at 95°C for about 3h, and then cool down to room temperature. 2. Placing the plastic mask over the hydrophobic paper (**Figure 4.2C**) and drawing the electrodes system using a standard 2B graphite pencil. The sketch can be seen in **Figure 4.2D**, 3. Manually printing the electrodes along the pencil sketch using conductive carbon ink soaked at the tip of a rolling ball pen. The filter paper with the printed electrodes is then kept in the oven at 36°C overnight (**Figure 4.2E**). 4. Printing Ag/AgCl ink over the reference electrode part (using a rolling ball pen in a similar way than in step 3) and drying in the oven at 36°C by 30 minutes (**Figure 4.2F**), 5. Finally, the device was partly covered using plastic tape (**Figure 4.2G**) to remark a specific working area and to isolate this area from the connection part. The connection of the electrodes with the portable switch box is shown in **Figures 4.2H** and **I.**

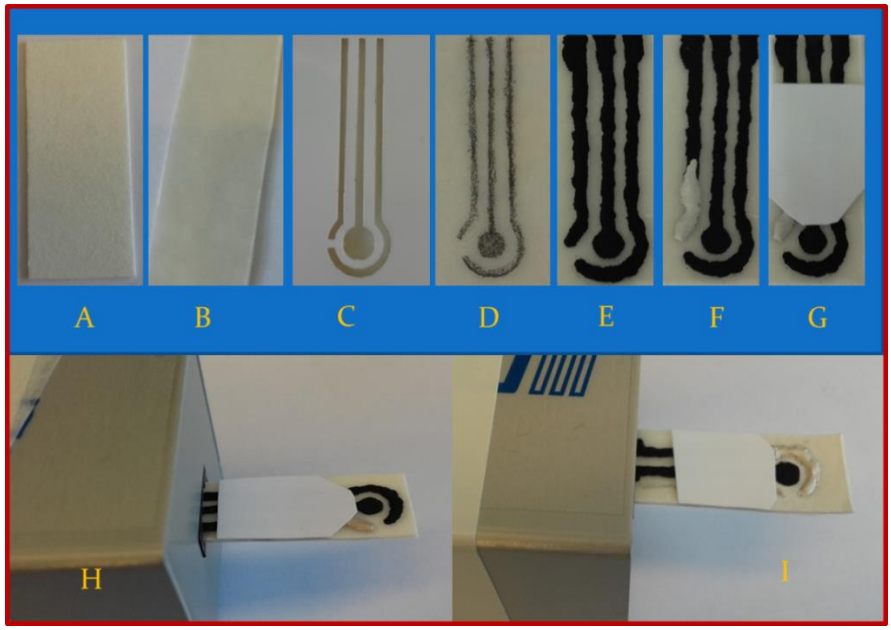

Figure 4.2. Schematic presentation of the process and fabrication of the device and its connection with the portable switch box: (A) filter paper; (B) hydrophobic filter paper; (C) plastic mask over the hydrophobic filter paper; (D) sketch of the electrodes; (E) carbon ink-printed electrode; (F) reference electrode (left) with Ag/AgCl ink; (G) final device partly covered by the plastic tape; (H) three-electrode and (I) two-electrode devices connected to a portable switch box.

4.1.2.6 Electrosynthesis of polymers on HP C- PEs

Prior to electropolymerization, HP C-PEs were cleaned using cyclic voltammetry (CV) (-2.0 to +2.0 V, 40 cycles, scan rate 100 mV/s, using KCl 0.1M in Milli-Q water) and stabilized electrochemically with MES buffer (conditioning) by CV (potential from -0.2 and 0.8 V, 10 cycles, scan-rate of 50 mV/s). Then 75 µL of phenol solution (3.55×10^{-3} mol/L prepared in acetate buffer 1.0×10^{-2} mol/L, pH 5.0) were deposited onto the HP C-PE to cover the three-electrodes for around 10s. Polymerization was then performed by CV between -0.2 and 1.2 V at a scan rate of 50 mV/s. For others monomers such as AP and ABA, the same procedure was followed for polymerization but the potential range was from -0.2 to 0.8 V for AP and from -0.2 to 1.2 V for ABA.

The surface was then thoroughly washed with Milli-Q water and electrochemically cleaned by 25 CV cycles in MES buffer (potential range from -0.2 to 0.8 V, scan rate 50 mV/s) to remove the remaining monomers and/or oligomers.

4.1.2.7 Electrochemical, spectroscopic and microscopic characterization

Electrochemical properties of the clean electrodes were checked observing the oxidation and reduction current peaks with different CV scan rates. The mechanical deformation of the device was studied by bending (≈ 90°) the electrode several times and following the redox behaviour at a scan rate of 50 mV/s.

Qualitative analyses were directly performed by FTIR and Raman spectroscopies on the HP C-PEs without any treatment of the polymeric films. FTIR analysis was performed before and after electropolymerization. In FTIR (from 400 to 4000 cm^{-1}) the number of scans was set to 256, the resolution to 8, apodization of Happ-Genzel, Mertz phase correction, and a background gain of 8. In Raman spectroscopy, the average signal-to-noise ratio (peak height/root mean square noise) was measured using standard polystyrene (full-range grating, 1 mW laser power at sample, 10 min photo bleaching time and 50 µm slit aperture). Electrochemical follow up of the surface modification was done by cyclic voltammetry (CV), square wave voltammetry (SWV), and electrochemical impedance spectroscopy (EIS) to check the polymer formation and their existence at the electrode surface. ESEM and AFM were employed to observe the modification of the filter paper by wax.

4.1.2.8 Electrochemical measurements

The redox probes in all CV and EIS measurements were 5.0 mmol/L $[Fe(CN)_6]^{3-}$ and 5.0 mmol/L $[Fe(CN)_6]^{4-}$ prepared in MES buffer at pH 5.0. In CV assays the potential range was from -0.5 to +0.7 V at 50 mV/s. In EIS, an open circuit potential was set using a sinusoidal potential perturbation of 0.01 V amplitude, and 50 logarithmically distributed frequency values over a frequency range of 0.01 Hz to100 kHz. In SWV assays the potential range was from -0.4 to +0.6 V.

4.1.2.9 Pseudo reference characteristics of the reference electrode and stability of the working electrode

Pseudo reference characteristics of the HP C-PEs reference electrode were studied in the two-electrode configuration by conditioning the electrode in HEPES buffer overnight and adding BSA (as a protein model for checking the performance in biochemical assays) in the potentiometric cell. The EMF response of the HP C-PEs reference electrode versus a standard reference electrode (Ag/AgCl 3 M KCl double-junction reference electrode) was recorded. Stability of the HP C-PEs working electrode was checked by recording its EMF response versus the HP C-PEs reference electrode.

4.1.3 Results and discussion

4.1.3.1 Modification of the filter paper

ESEM pictures of the original filter paper can be seen in **Figure 4.3A**. In **Figure 4.3A** we can see the original structure of cellulose. After wax modification the surface shows a much more homogeneous structure (**Figure 4.3B**). This is also supported by AFM images (**Figures 4.3C** and **D**). **Figure 4.4** shows the hydrophobic character of the modified paper by looking at a coloured droplet of water (10 mM of potassium ferri- and ferro- cyanide in water). The droplet does not squeeze throughout the paper with the indication of good hydrophobicity (contact angle, $\Theta_C = 90°$), which was necessary for the electrodes not being connected with the diffused liquid when the liquid sample is placed over the electrodes.

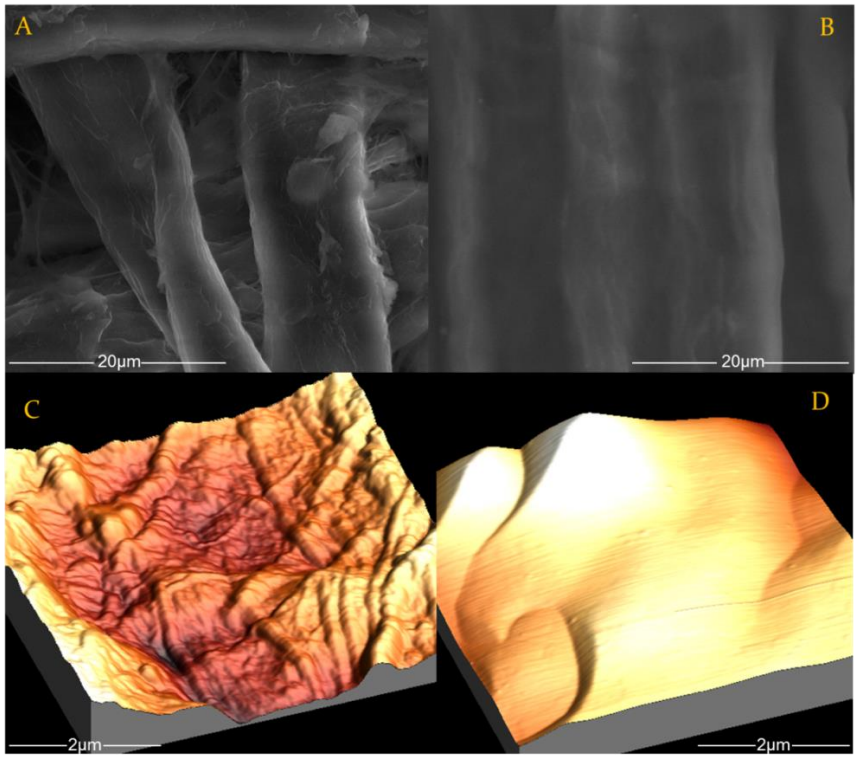

Figure 4.3. ESEM images before (A) and after (B) modification of the filter paper by wax, and AFM images before (C) and after (D) modification of the filter paper by wax.

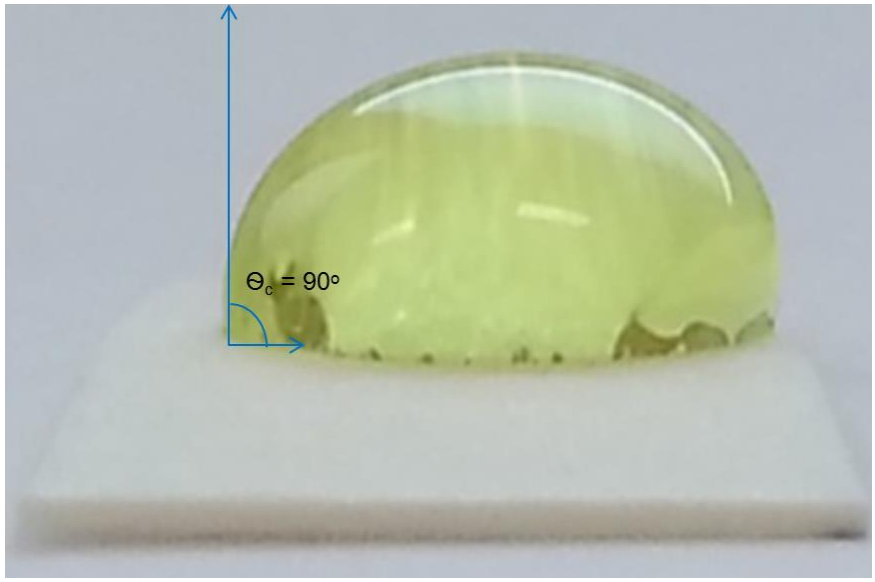

Figure 4.4. Hydrophobicity of the wax-modified filter paper (contact angle, Θ_C = 90°).

4.1.3.2 Electrochemical cleaning and conditioning

Figure 4.5 shows the electrochemical properties of the three-electrode system of HP C-PEs before and after cleaning. The CV of the non-cleaned system shows anodic and cathodic peak separation (Ep_a-Ep_c) of 0.40 V, and the difference of the anodic and the cathodic current peaks intensity (Ip_a-Ip_c) is 121 µA. The HP C-PEs was then electrochemically cleaned using a 0.1M KCl solution and conditioned in MES buffer, showing good electrical properties indicating a lower peak separation (Ep_a- Ep_c = 0.19 V) with higher current peaks difference (Ip_a-Ip_c = 233 µA). This result was supported by SWV and EIS. In case of SWV, the current peak was increased 230% (213 µA for the non-cleaned electrodes and 726 µA after cleaning and conditioning), where in EIS the charge transfer (R_{ct}) was decreased 930% (R_{ct} of 3048 Ω for the non-cleaned electrodes and 317 Ω after cleaning and conditioning). The most interesting and remarkable result can be seen in CV where the ratio of the cathodic and the anodic current (Ip_c/Ip_a) is 0.94 (after cleaning and conditioning the electrodes) which is a characteristic of the reversible performance of the fabricated device and that is similar to commercial electrodes (Ip_c/Ip_a = 0.84) (Fanjul-Bolado et al., 2008).

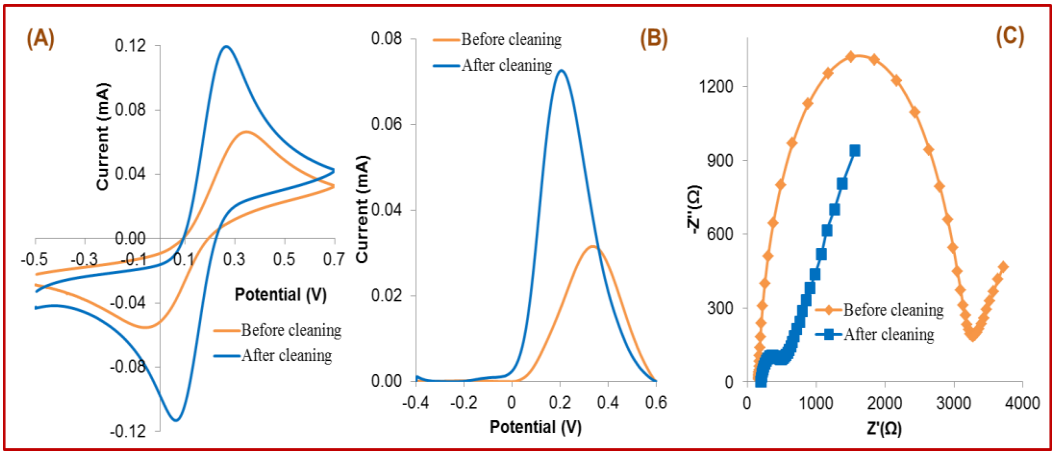

Figure 4.5. Electrochemical performance before and after the electrochemical cleaning of the fabricated HP C-PE; Electrochemical follow up in 5.0 mM $[Fe(CN)_6]^{3-}$ and 5.0 mM $[Fe(CN)_6]^{4-}$, in MES buffer pH 5.0, carried out by (A) CV, (B) SWV and (C) EIS (Nyquist plots) assays.

4.1.3.3 Electrochemical characterization

The scan rate study was performed using CV (**Figure 4.6**), and the peak separation (oxidation and reduction) was increased with increasing scan rate, what is indicative of slow electron-transfer kinetics associated with the use of nonconductive material on the surface of the carbon ink electrodes (Fosdick et al., 2014). Interestingly, the peak current as a function of the square root of the scan rate was linear (R^2 of 0.9981 and 0.9978 respectively for oxidation and reduction) with the evidence of diffusion-controlled behaviour of redox processes at HP C-Pes, as in the case of commercial electrodes (Fanjul-Bolado et al., 2008).

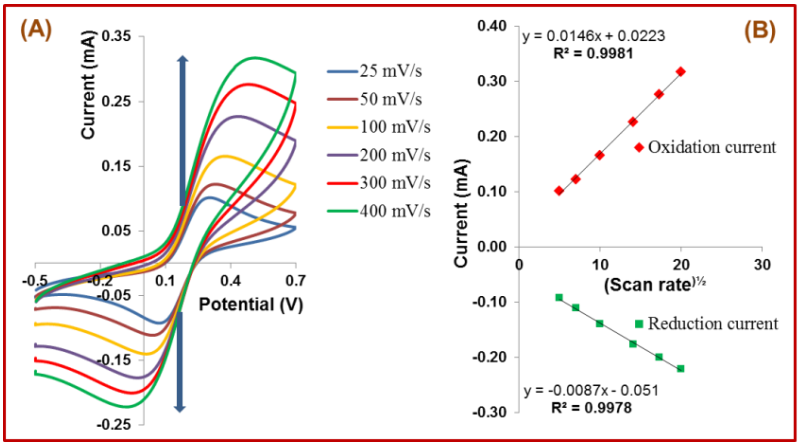

Figure 4.6. Electrochemical characterization of cleaned electrodes by scan rate (A) cyclic voltammograms with variable scan rate and (B) fitting of the oxidation and reduction current with the square root of scan rate (mV/s); 5.0 mM $[Fe(CN)_6]^{3-}$ and 5.0 mM $[Fe(CN)_6]^{4-}$, in MES buffer pH 5.0.

4.1.3.4 Mechanical deformation

HP C-PEs are rigid enough to allow easy connection with the portable switch box (**Figures 4.2H** and **4.2I)** but it was also flexible enough to bend (**Figure 4.7A**) without breaking. The bending properties have been observed by bending the cleaned and conditioned HP C-PEs several times and by the subsequent observation of the electrochemical properties by CV. The HP C-PEs can be bent at least 10 times without any significant change in the shape of the CV voltammogram (**Figure 4.7B**).

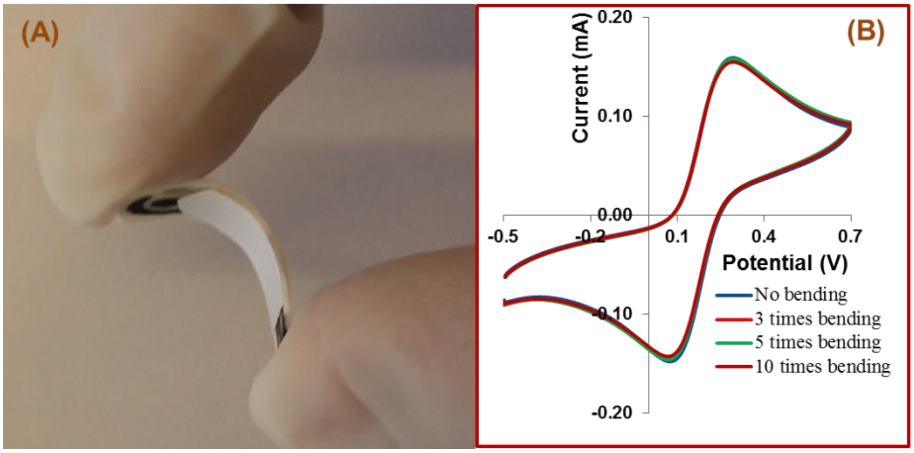

Figure 4.7. Bending characteristics of HP C-PEs (A) Bending test; (B) cyclic voltammograms after subsequent bending; 5.0 mM $[Fe(CN)_6]^{3-}$ and 5.0 mM $[Fe(CN)_6]^{4-}$, in MES buffer pH 5.0.

4.1.3.5 Electropolymerization

Different monomers have been employed to check electropolymerization on HP C-PE three-electrode devices. The results are presented in **Figure 4.8**. **Figure 4.8A** shows the CV curves (1–5 cycles) corresponding to the electropolymerization of phenol on HP C-PEs. During the anodic scan of the first cycle, a well-defined oxidative peak around 0.75 V is observed, while no reductive peak occurred during the cathodic scanning. This is indication of an irreversible reaction of polymerization. The peak current was around 65 µA in the first anodic scan, which decreased to around 15 µA in the second anodic scan. No oxidative peak was observed at the successive 4th and 5th anodic scan except the charging current which is highly expected due to the resistive and passive surface produced by the growth of polymers over the electrode surface. The resistive and passive surface is limited by the inability of electron transfer. The other monomers (AP, ABA) show similar behaviour of polymerization, and characteristic peaks were observed around 0.6 V for AP and 0.75 V for ABA (**Figures 4.8B** and **C**).

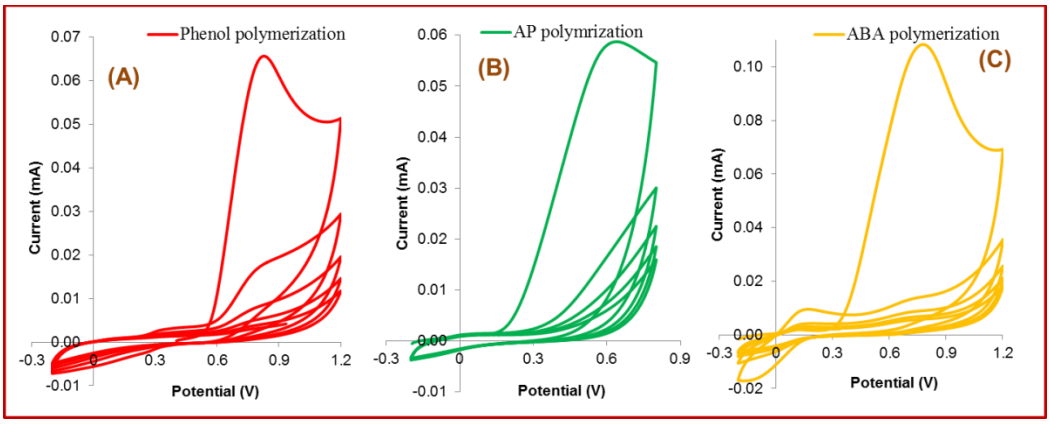

Figure 4.8. Electropolymerization of different monomers; (A) Phenol, (B) AP and (C) ABA using CV in sodium acetate buffer pH 5.0. Scan rate 50 mV/s.

The evidence of the existence of polymers on the electrode surface has been checked by comparing the surface blocking behaviour with respect to the clean electrode, using CV and SWV (**Figure 4.9**). **Figure 4.9** shows the redox peaks (in CV) and a high current of around 75 µA (in SWV) in the clean electrode, whereas after polymerization the surface of the electrodes is highly blocked as the redox peaks significantly decrease (in CV) and the intensity of current is significantly lower (in SWV).

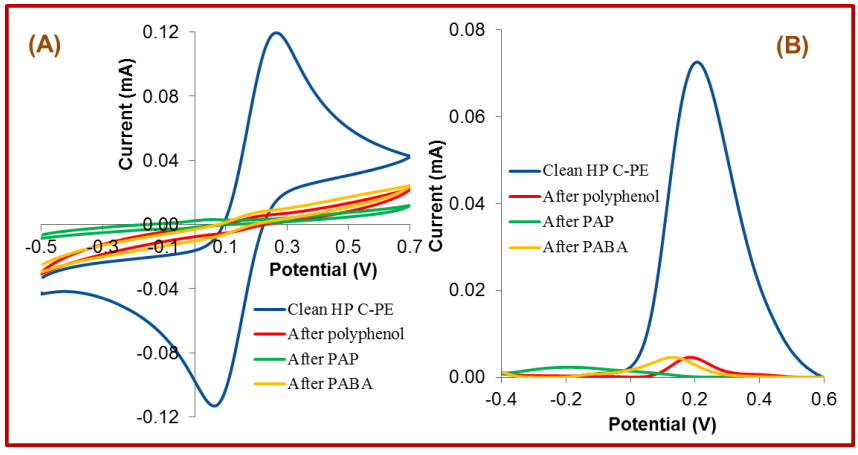

Figure 4.9. Follow up of surface modification due to electropolymerization by (A) CV and (B) SWV; 5.0 mM $[Fe(CN)_6]^{3-}$ and 5.0 mM $[Fe(CN)_6]^{4-}$, in MES buffer pH 5.0.

The existence of polymers over the surface of the working electrode of HP C–PEs can be checked by FTIR and Raman spectroscopy. Herein, the characterization of the phenol polymerization is presented as a representative example, with similar results for polyaminophenol (PAP) and poly(aminophenylboronic acid) (PABA).

The characteristic functional group in polyphenol is the hydroxyl group (–OH) (Gorinstein et al., 1993) at the end of the polymer and the expected amount of the hydroxyl group should be low due to the process of polymerization. FTIR reveals a characteristic broad peak at the region of 3200-3400 cm^{-1} with low intensity (expected due to the low amount of this functional group) after phenol polymerization, but that peak is missing in the clean HP C-PE (**Figure S4.1,** Supplementary Information). This is a good evidence for the presence of polyphenol over the surface of HP C-PE.

Raman spectroscopy supports the FTIR results by an increase of the I_D/I_G ratio (0.98) after polymerization, compared to the ratio of the clean electrode (I_D/I_G = 0.85) (**Figure S4.2,** Supplementary Information). This result is expected due to the increasing amount of sp^3 carbon after polymerization (due to presence of the –OH functional groups in the polymers) which increases the D peak intensity and is indicative of the existence of polyphenol at the electrode surface.

4.1.3.6 Pseudo reference characteristics of the reference electrode and stability of the working electrode

The HP C-PEs (two electrodes system) contains a Ag/AgCl reference electrode and a carbon working electrode. The pseudo reference characteristics of this reference electrode have been studied using potentiometric measurements with respect to a standard reference electrode (Ag/AgCl 3 M KCl double-junction reference electrode). The HP C-PE reference electrode was first stabilized and conditioned in HEPES buffer overnight, and then the EMF response was monitored against the standard reference electrode. The results show that the HP C-PE Ag/AgCl electrode is very stable, and the addition of a model protein BSA (125 ng/mL to 9.70 µg/mL) provokes no changes of EMF (**Figure 4.10A**).

The stability of the working electrode of HP C-PE (two electrodes system) was checked with respect to the pseudo reference electrode in HEPES buffer (**Figure 4.10B**).

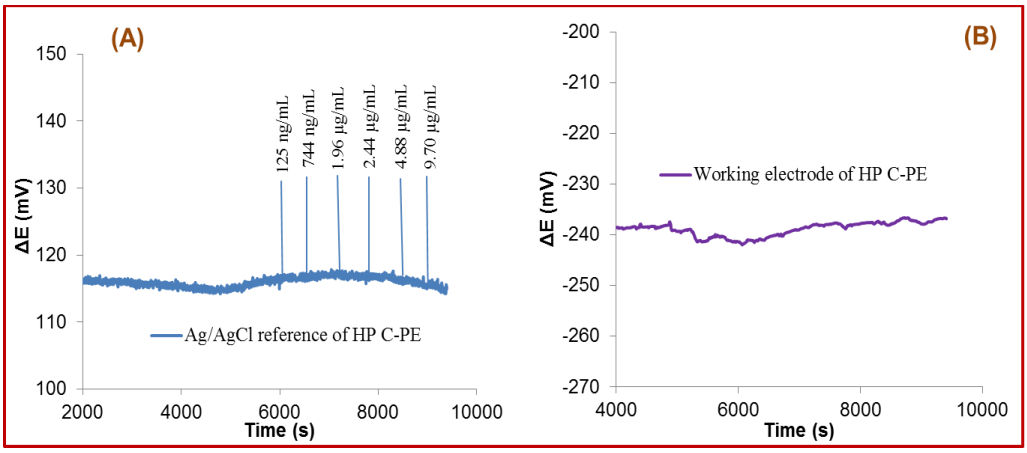

Figure 4.10. (A) ΔE changes of the Ag/AgCl electrode of HP C-PE with respect to standard Ag/AgCl double junction reference electrode (addition of different concentrations of BSA is indicated), (B) stability of the working electrode of HP C-PE with respect to the Ag/AgCl reference of HP C-PE. Measurements in HEPES buffer 10^{-4} M, pH 7.2.

4.1.4 Conclusions

Paper-based electrode fabrication is a promising technology and limitations still exist regarding the rigidity, flexibility and design of the electrode including the simplicity of fabrication with affordable cost. Herein, we have shown that manually homemade carbon-printed electrodes on paper-based substrates have been successfully fabricated with a simple, easy and cost-effective procedure. The fabricated electrodes are portable and can be used as disposable devices. We also show that the fabricated paper-based electrodes have special mechanical properties such as flexibility to bend but displaying enough rigidity to make easy and quick connection with portable connector boxes.

Acknowledgements

The Catalan Government and the European Research Council are acknowledged for the financial support of MARK PhD Fellowship (2013FI_B 00842) and Starting Grant, 3P's, GA 311086 respectively. The URV team thanks the financial support from the Spanish Ministerio de Economía y Competitividad (Project CTQ2010-18717).

4.1.5 References

Berkes, B.B., Bandarenka, A.S., Inzelt, G., 2015. Electropolymerization: Further insight into the formation of conducting polyindole thin films. J. Phys. Chem. C 119, 1996–2003.

Fanjul-Bolado, P., Hernández-Santos, D., Lamas-Ardisana, P.J., Martín-Pernía, A., Costa-García, A., 2008. Electrochemical characterization of screen-printed and conventional carbon paste electrodes. Electrochim. Acta 53, 3635–3642.

Fosdick, S.E., Anderson, M.J., Renault, C., Degregory, P.R., Loussaert, J.A., Crooks, R.M., 2014. Wire, mesh, and fiber electrodes for paper-based electroanalytical devices. Anal. Chem. 86, 3659–3666.

Gorinstein, S., Weisz, M., Zemser, M., Tilis, K., Stiller, A., Flam, I., Gat, Y., 1993. Spectroscopic analysis of polyphenols in white wines. J. Ferment. Bioeng. 75, 115–120.

Li, Z., Li, F., Hu, J., Wee, W., Han, Y., Pingguan-Murphy, B., Lu, T., Xu, F., 2015. Direct writing electrodes using ball pen for paper-based point-of-care testing. Analyst 140, 5526–5535.

Lin, Z., Takahashi, Y., Kitagawa, Y., Umemura, T., Shiku, H., Matsue, T., 2008. An addressable microelectrode array for electrochemical detection. Anal. Chem. 80, 6830–6833.

Lin, Z., Takahashi, Y., Murata, T., Takeda, M., Ino, K., Shiku, H., Matsue, T., 2009. Electrochemical gene-function analysis for single cells with addressable microelectrode/microwell arrays. Angew. Chem. Int. Ed. 48, 2044–2046.

Lipatov, A., Wymore, B.B., Fursina, A., Vo, T.H., Sinitskii, A., Redepenning, J.G., 2015. Electropolymerization of poly(phenylene oxide) on graphene as a top-gate dielectric. Chem. Mater. 27, 157–165.

Oh, J.-M., Chow, K.-F., 2015. Recent developments in electrochemical paper-based analytical devices. Anal. Methods 7, 7951–7960.

Samet, Y., Kraiem, D., Abdelhedi, R., 2010. Electropolymerization of phenol, o-nitrophenol and o-methoxyphenol on gold and carbon steel materials and their corrosion protection effects. Prog. Org. Coatings 69, 335–343.

Sjberg, P., Maattanen, A., Vanamo, U., Novell, M., Ihalainen, P., Andrade, F.J., Bobacka, J., Peltonen, J., 2016. Paper-based potentiometric ion sensors constructed on ink-jet

printed gold electrodes. Sensors Actuators B Chem. 224, 325–332.

Zhu, X., Ino, K., Lin, Z., Shiku, H., Chen, G., Matsue, T., 2011. Amperometric detection of DNA hybridization using a multi-point, addressable electrochemical device. Sensors Actuators B Chem. 160, 923–928.

4.1.6 Supplementary Information

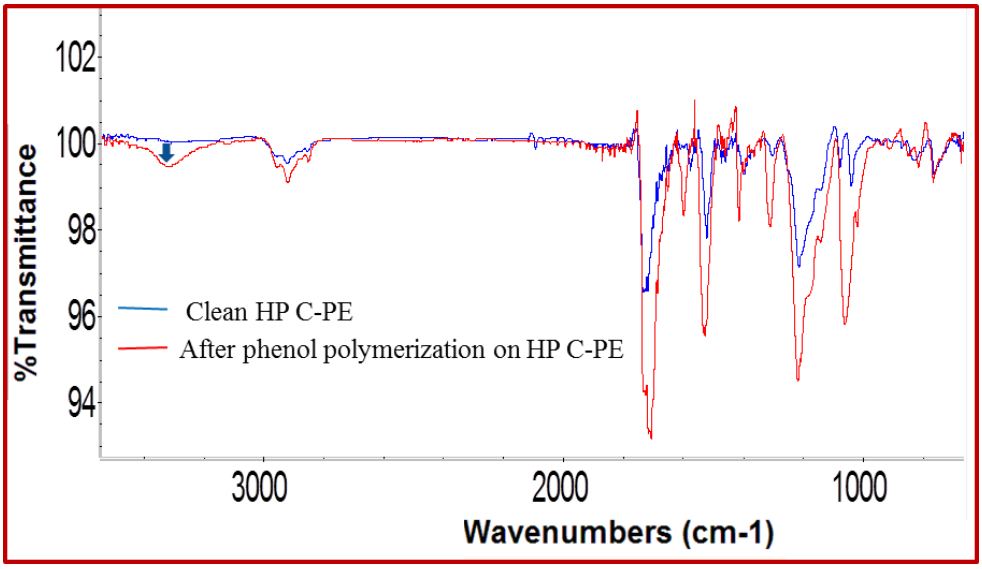

Figure S4.1. FTIR spectrum.

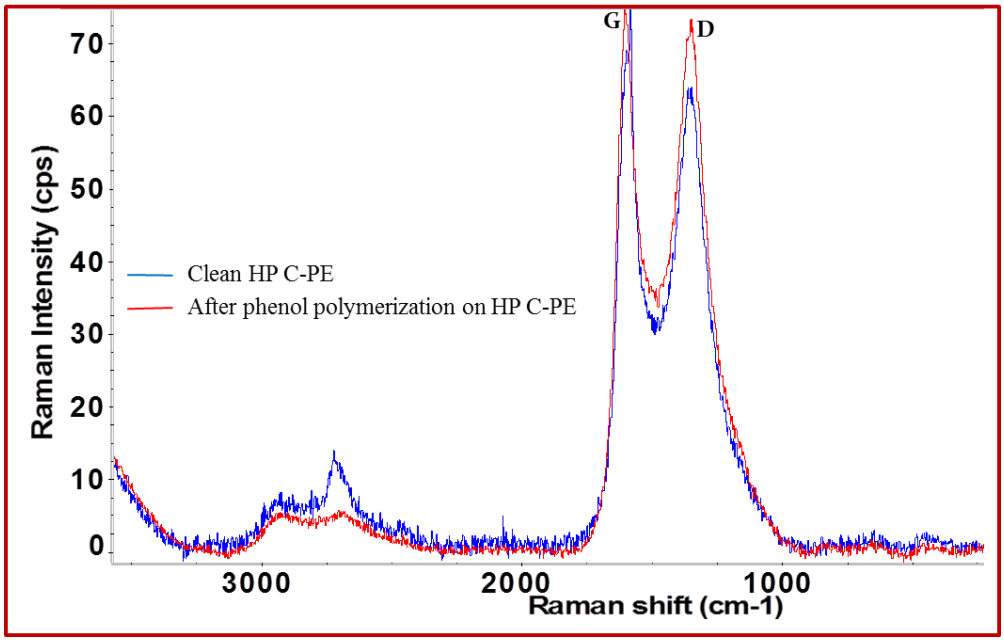

Figure S4.2. Raman spectrum.

UNIVERSITAT ROVIRA I VIRGILI
PLASTIC ANTIBODIES FOR THE DETECTION OF BACTERIAL PROTEINS AND MICROORGANISMS
Azizur Rahman Khan

Chapter 5

Molecular imprinting of flagella from *Proteus mirabilis*

UNIVERSITAT ROVIRA I VIRGILI
PLASTIC ANTIBODIES FOR THE DETECTION OF BACTERIAL PROTEINS AND MICROORGANISMS
Azizur Rahman Khan

This chapter discusses the imprinting of flagella (**Figure 5.1**) from *Proteus mirabilis* and the impedimetric, square wave voltammetric and/or potentiometric detection of the target. There are three sections. The first section (**5.1**) describes the detection of flagella from *Proteus mirabilis* by impedimetric and/or square wave voltammetric techniques. The second section (**5.2**) is the continuation of the first (**5.1**) and detects whole *Proteus mirabilis* cells. The third section (**5.3**) uses molecular imprinted receptors as a novel approach for the potentiometric detection of *Proteus mirabilis* flagella and their whole cells.

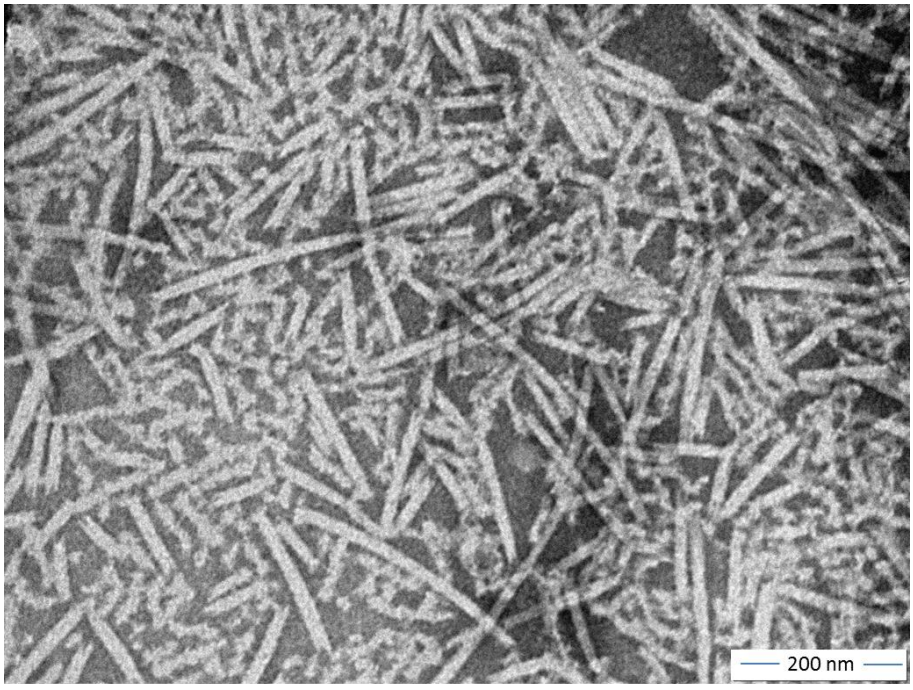

Figure 5.1. TEM images of flagella from *Proteus mirabilis.*

5.1 Artificial antibodies for the electrochemical detection of bacterial flagella from *Proteus mirabilis (Manuscript submitted).*

In this work, we successfully detect for the first time bacterial flagella from *Proteus mirabilis* using molecularly imprinted-based artificial receptors. These receptors acted as a sensing layer of the biosensors, assembled by imprinting flagella proteins on a polymeric backbone of electropolymerized phenol. In brief, flagella were absorbed onto a carbon support, phenol was electroplolymerized around it through the carbon conductive matrix to create the protein molecular molds and lastly flagella were removed by enzymatic and electrochemical action. Each removed flagella gave rise to an imprinted site with eventual rebinding ability.

Electrical impedance spectroscopy (EIS) and square wave voltammetry (SWV) were employed to measure the interaction of flagella with the sensing layer assembled on commercial screen-printed electrodes, offering low detection limits, high precision and selectivity towards the targeted protein; the detection limit was 8.00 pM by EIS and 11.43 pM by SWV. The artificial receptors were further assembled on home-made paper-printed electrodes, with the three electrodes system printed on a paper substrate, yielding the possibility of detecting flagella down to 7.02 pM with a disposable and cost-effective portable device.

From the best of our knowledge this is the first sensing device where molecularly imprinted artificial receptors are tailored on home-made electrode based on paper substrates while three electrodes are assembled together, which is a suitable approach for the fabrication of easy and cost-effective tailored electrodes.

Keywords: Molecularly imprinted polymers; Artificial receptors; Flagella; *Proteus mirabilis*; Screen-printed electrodes; Paper-printed electrodes; Electropolymerization; Disposable device.

5.1.1 Introduction

Bacteria are present in a variety of sources, including food, water, animals, environment as well as the human body. Detection of pathogenic bacteria is extremely important due to health and safety reasons. Detection of bacteria using biosensors has been proposed using a variety of analytical detection techniques such as reflectometric interference spectroscopy

(Merkl et al., 2014), fluorescence (Heyduk and Heyduk, 2010), quartz crystal microbalance (Guo et al., 2012; Wangmaung et al., 2014), electrochemical methods (Lu et al., 2013; Maalouf et al., 2007; Sporer and Teixeira, 2013; Zelada-Guillén et al., 2009) or surface plasmon resonance (SPR) (Nadkarni et al., 2002). Recently, the focus is set on detecting specific bacterial markers, referred to as pathogen-associated molecular patterns, rather than on whole cell detection (Yang and Bashir, 2008; Yang et al., 2003). These markers include, but are not limited to, intercellular entities such as DNA (Barlaan et al., 2005; Ikeda et al., 2006) or extracellular components such as lipopolysaccharides (LPS) or flagella (Jordana et al., 2014; Uzarski and Mello, 2012).

Flagella are located at the outer surface of bacteria and can act as markers to detect and/or identify bacteria. In this regard, clinical studies revealed the significant role of flagella for characterization and affiliation of anaerobic bacteria (Kodaka et al., 1982). Also, in natural aquatic environment flagella can be used as biomarkers (Grossart et al., 2001; Winstanley and Morgan, 1997), and they can also be used in mechanistic studies to observe the motility behavior of bacteria.

Different strategies have been made for staining and detecting bacterial flagella, including tannic acid-fuchsin method (Kodaka et al., 1982) and subsequent modifications (Clark W. A., 1976; Forbes, 1981), as well as silver staining methods (Kodaka et al., 1982). These approaches are satisfactory but involve complicated protocols. Also, each method has limitations, such as time, unstable reagents and fixation-induced alterations. Thus, there are still key issues that need to be considered in the development of rapid methods for the detection of bacteria and/or flagella with effective cost, simplicity, training, and accuracy (Wang et al., 2012). Alternative methods for the detection of bacterial flagella on-site would facilitate the characterization/quantification of clinical and environmental bacterial isolates.

Thus, this paper describes a novel, rapid and label-free method for the detection of bacterial flagella. It uses an artificial receptor as biorecognition element, as it may offer a promising alternative to antibodies and other biological receptors currently used in biosensors. The most generic and cost-effective technique for preparing synthetic receptors is molecular imprinting. It combines high affinity and specificity with robustness and low manufacturing costs, to generate molecularly imprinting polymers (MIPs), also known as artificial receptors (Whitcombe et al., 2011). As far as we know, several strategies have

been reported for the detection of bacterial flagella, but none of these make use of molecularly imprinted polymers.

Fabrication of MIP-based receptors for small molecules is quite straightforward and these receptors have been successfully used in extraction, separation, binding, detection, enzyme-like catalysis and drug delivery. But MIP-based receptors preparation for large molecules such as proteins is rather difficult although promising (Liu et al., 2014; Verheyen et al., 2011; Whitcombe et al., 2011). Therefore, the preparation of MIP-based materials for large templates such as flagella is even more difficult.

In molecular imprinting, monomeric structures are polymerized to form a well-organized structure surrounding the target (herein, the flagella), in a complex polymeric network via covalent and/or non-covalent interactions. Customized specific binding sites which conserve size, shape and orientation of the target (key-lock approaches) are created by the subsequent removal of the target from the polymeric network. The generated binding cavities are selectively used as recognition sites of the target, like in natural antibody and antigenic interactions. Hence, the material can be termed as artificial or man-made antibodies to capture specific target analytes (Haupt, 2003; Lingxin, 2016).

In this paper, we detect flagella from *Proteus mirabilis* as a proof of concept for the detection of flagella by using artificial antibodies as biorecognition element. *Proteus mirabilis* is a widely distributed bacterium in soils and water and has the ability to produce high levels of urease. It may be responsible for urinary tract infection with serious complications, including cystitis, acute pyelonephritis, fever, bacteremia, and death (Bahrani et al., 1991). As far as we know, there are no previous MIP-based biosensors for the detection of flagella. Therefore we are able to create a MIP using flagella as template for the first time, and the MIP-based biosensors are used for the impedimetric (EIS) and square wave voltammetric (SWV) detection of flagella from *Proteus mirabilis* with high selectivity and precision. Furthermore, the biorecognition element is assembled on home-made paper substrates, creating, to the best of our knowledge, the first device based on molecularly imprinted artificial receptors built on paper substrates while three electrodes are assembled together, thereby helping to the fabrication of easy cost-effective tailored electrodes.

5.1.2 Experimental section

5.1.2.1 Apparatus

The electrochemical measurements were conducted with a potentiostat/galvanostat from Metrohm Autolab and a PGSTAT302N (Utrecht, The Netherlands), equipped with a FRA module and controlled by Nova software. The single walled carbon nanotubes screen printed electrodes (SWCNTs-SPEs) were purchased from DropSens (Oviedo, Spain), and they were composed of a working electrode made of carboxylated SWCNTs, a counter electrode made of carbon and a reference electrode and electrical contacts made of silver. The diameter of the working electrode was 3.80 mm. The SWCNTs-SPEs were connected to a portable switch box, also from DropSens (DRP-DSC), allowing their interface with the potentiostat/galvanostat.

As alternative to commercial SWCNTs-SPEs, homemade paper-based carbon-printed electrodes (identified herein as HP C-PEs) were made on our laboratory by coating a filter paper with paraffin wax to make it hydrophobic and manually printing the three electrodes with carbon ink (Creative Materials, USA). One of the three electrodes was coated with Ag/AgCl (Creative Material, USA) to make the reference electrode. The final system was covered by a plastic mask which was connected to a portable switch box, also from DropSens (DRP-DSC), allowing their interface with the potentiostat/galvanostat.

Raman measurements were performed in Thermo Scientific DXR Raman spectrometer with confocal microscopy (Waltham, USA), with a 10 mW 532 nm excitation laser.

5.1.2.2 Reagents

All chemicals were of analytical grade and water was de-ionized or ultrapure Milli-Q laboratory grade was used throughout. Potassium hexacyanoferrate III, potassium hexacyanoferrate II trihydrate, and sodium acetate anhydrous were obtained from Riedel-deHäen; proteinase K from Fluka 99%; 2-(*N*-morpholino)ethanesulphonic acid monohydrate 98% (MES) from Alfa Aesar; phenol, bovine serum albumin (BSA), and protein A (PA) from *Staphylococcus aureus* was from Sigma Aldrich, and potassium chloride (KCl) from Merck.

5.1.2.3 Flagella from *Proteus mirabilis*

Proteus mirabilis was grown in Luria Broth at 37ºC for flagella purification. Cells were collected by centrifugation at 5000 × g, and suspended in 100 mM Tris (pH = 7.8) buffer.

Flagella were removed from the cells by shearing in a vortex with a glass bar for 3-4 min, and then passing repetitively (minimum six times) through a syringe. Cells were removed by centrifugation at 8000 × g for 30 min, and the supernatant centrifuged at 18000 × g for 20 min. From the remaining supernatant, the flagella were pelleted by ultracentrifugation at 100000 × g for 60 min, and resuspended in 100 mM Tris (pH = 7.8) plus 2 mM EDTA buffer. Such flagella enriched fraction was purified in a cesium chloride gradient by ultracentifugation at 60000 × g for 48 h. The band containing the flagella was collected, the cesium chloride removed by extensively dialysis against the same buffer (100 mM Tris 2 mM EDTA). Purified flagella were analysed by SDS-PAGE (**Figure S5.1**, Supplementary Information).

5.1.2.4 Solutions

Stock solutions of 1.22×10^{-5} mol/L flagella from *Proteus mirabilis* (FPM) were prepared in TRIS buffer (6.66×10^{-4} mol/L, pH 7.8) and stored at −20°C. Standards were obtained by accurate dilution of the previous solution in MES buffer (1.0×10^{-2} mol/L, pH 5.0, KCl 0.1 mol/L) depending of the applications. Electrochemical assays were performed with 5.0×10^{-3} mol/L $[Fe(CN)_6]^{3-}$ and 5.0×10^{-3} mol/L $[Fe(CN)_6]^{4-}$, prepared in MES buffer. The selectivity study was made by the competitive method in MES buffer and using BSA and PA (12.2×10^{-9} mol/L).

5.1.2.5 Electrochemical synthesis of imprinted and non-imprinted films

Prior to electropolymerization, the SWCNTs-SPEs were cleaned using chronoamperometry (+1.7 V for 60 s, with KCl 0.1 mol/L) and stabilized electrochemically with MES buffer by cyclic voltammetry (CV, potential from -0.2 to +0.8 V, 10 cycles, and scan-rate of 50 mV/s). In the case of HP C-PEs, the electrodes were cleaned by CV (potential from −2.0 to +2.0 V, 40 cycles, and scan-rate of 100 mV/s in KCl 0.1 mol/L), and stabilized electrochemically in the same way as for SWCNTs-SPEs.

For imprinting the flagella on SWCNTs-SPE, 10 µL of 1.22×10^{-6} mol/L FPM solution prepared in MES buffer was placed over the working electrode area for 30 min at room temperature, and gently washed next with Milli-Q water. Then 75 µL of phenol solution (3.55×10^{-3} mol/L prepared in acetate buffer 1.0×10^{-2} mol/L pH 5.0) was deposited onto the SWCNTs-SPEs to cover the three-electrodes for ~10 s, and polymerization was performed by CV between −0.2 and +0.8 V (scan-rate of 50 mV/s, 15 CV cycles was found to be

optimal). For HP C-PEs, the procedure was the same as for the SWCNTs-SPEs, but the potential range of electropolymerization was set from –0.2 to +1.2 V.

The resulting polymeric film (either in SWCNTs-SPEs or in HP C-PEs) was thoroughly washed with deionized water and was incubated with proteinase K (500 µg/mL in PBS pH 7.4) for 2.5 h at room temperature. The surface was then thoroughly washed with Milli-Q water and subject to subsequent electrochemical cleaning by 25 CV cycles in MES buffer (potential range –0.2 to 0.8 V, scan rate 50 mV/s). The synthesis of the artificial receptors based on molecularly imprinting polymers (MIPs) is schematically presented in **Figure 5.2**.

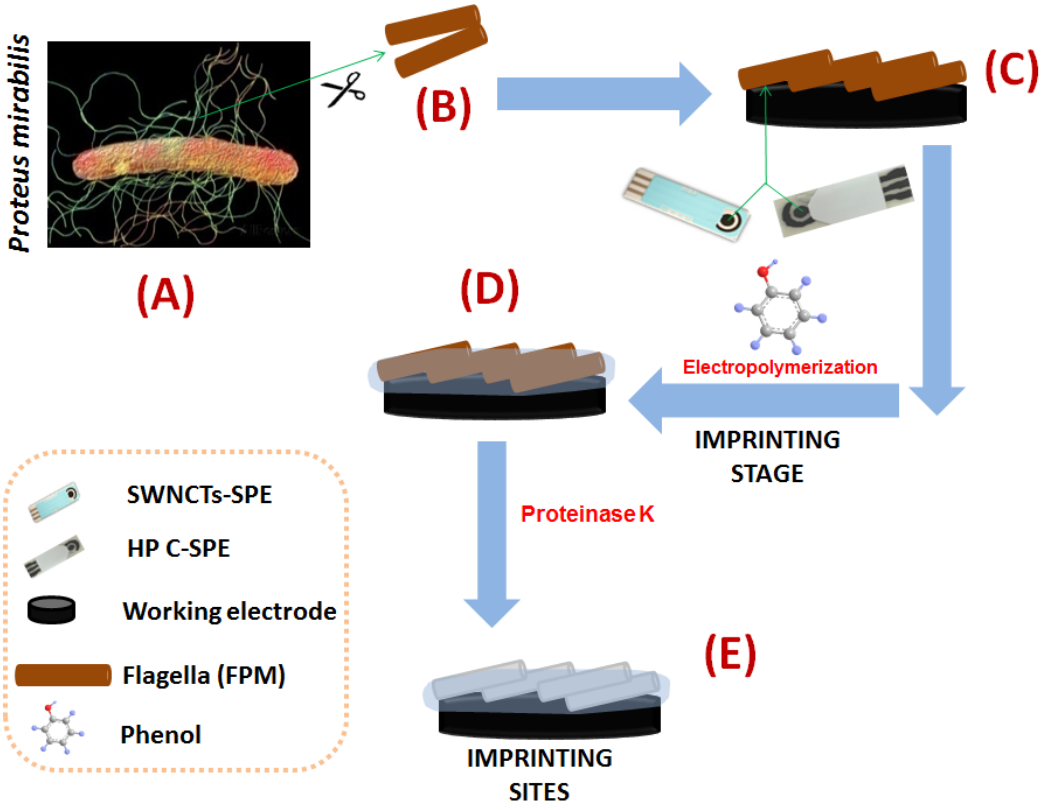

Figure 5.2. Schematic presentation of MIP synthesis: (A) *P. Mirabilis* with flagella, (B) Flagella (FPM), (C) Immobilized FPM at the working area of SWCNTs-SPE/HP C-PE, (D) Imprinting stage after electropolymerization of phenol, E) Binding sites formation after template removal by proteinase K.

In parallel, non-imprinting polymers (NIPs) were synthesized in a similar way but without the presence of FPM. All the steps involved in the fabrication of the imprinted and non-imprinted polymers were followed by CV, EIS and SWV.

5.1.2.6 Qualitative characterization of the films

Qualitative analyses of the several stages of the assembly of the biorecognition film were performed directly on the SWCNTs-SPE by Raman spectroscopy, without any treatment of MIP and NIP films. The spectra were collected by 1 mW laser power at sample, 10 min photo bleaching time, and 50 µm slit aperture.

5.1.2.7 Binding isotherm

The rebinding properties of MIP- and NIP-based biosensors on SWCNTs-SPEs were measured by calculating the apparent dissociation constant (K_D) using EIS and SWV assays. FPM standards ranging from pmol/L to µmol/L concentrations were prepared in MES buffer, and each standard was incubated 50 min before adding the redox probes for subsequent EIS and SWV measurements.

A Langmuir isotherm model (*Equation 5.1*) was applied to experimental data, as described in Moreira et al. 2013. In this equation, R_{ct} is the normalized charge transfer-density (kΩ/cm^2), S the concentration of FPM (in M), $R_{ct}^{máx}$ is the maximum charge transfer density observed (kΩ/cm^2) and K_D the concentration (in mol/L) of flagella required to give half of the maximum response produced by the device. K_D and $R_{ct}^{máx}$ were calculated from the fitting of the experimental data to the model in *Equation 5.1*. Concomitantly, the Langmuir isotherm model was applied to SWV data, in a similar way to that described for EIS.

$$R_{ct} = \frac{R_{ct}^{máx}}{1 + K_D / [S]} \qquad \textit{Equation 5.1}$$

5.1.2.8 Electrochemical assays

The redox probes in all CV and EIS measurements were 5.0 mmol/L $[Fe(CN)_6]^{3-}$ and 5.0 mmol/L $[Fe(CN)_6]^{4-}$ prepared in MES buffer at pH 5.0. In CV assays the potential range was from −0.5 to +0.7 V, at 50 mV/s. In EIS, an open circuit potential was set using a sinusoidal potential perturbation of 0.01 V amplitude, and 50 logarithmically distributed frequency

values over a frequency range of 0.01 Hz to100 kHz. In SWV assays the potential range was from –0.4 to +0.6 V.

Calibrations were performed by EIS and SWV measurements for FPM in the range from 0.12 nM to 1.22 µM. At each concentration level, 10 µL of FPM in MES buffer was exposed to the imprinted sensor surface for 50 min at room temperature. The values of precision corresponded to the standard deviation of triplicate experiments of different electrodes. Selectivity studies were conducted by using BSA and PA from *Staphylococcus aureus* in MES buffer at pH 5.0. Real sample analysis was done by spiking FPM in tap water (four times diluted in MES buffer) using the homemade paper based (HP C-PE) electrode.

5.1.3 Results and discussion

5.1.3.1. Polymer growth

The polymeric film acted as biorecognition element of the biosensor and was generated by electropolymerization. It was achieved by CV consecutive cycling (up to 15 cycles) on a phenol solution placed over the SPEs modified with a layer of flagella (in the case of MIP-based devices) or over bare SPEs (in the case of NIP-based devices), both for commercial SWCNTs-SPEs (**Figure 5.3A** and **B**) and HP C-PEs (**Figure 5.3C** and **D**).

The obtained cyclic voltammograms for SWCNTs-SPEs are displayed in **Figure 5.3A**. In brief, the anodic current peak in the direct scan corresponding to the oxidation of phenol is observed at +0.5 V for MIP films with low intensity of current, whereas NIPs showed a maximum peak position at around +0.6 V with higher intensity of current. The presence of the protein on the MIP layer was the responsible for the lower currents obtained, while the higher potential of the NIP layer evidenced slow electron transfer kinetics of the reaction, revealing changes in the rate of mass transport to the electrode surface. This is consistent with the fact that the oxidation of phenol occurred by irreversible direct electron transfer, accounting the absence of the reduction peak on the reverse scan.

The anodic currents were reduced in the second scan leading to the production of polyphenol. The CV data evidenced the formation of a non-conductive and electro-inactive polymeric film at the electrode surface, hindering the direct electron transfer and/or the diffusion of phenol molecules to the anode surface. Such current decrease was more intense in the NIP material (from 140 µA to 30 µA, from first to second scan) than in the MIP (from 100 µA to 60 µA). This was supported by the fact that the NIP electrode displayed higher currents at the beginning, meaning that a higher electrical stimulus was

driving the NIP polymerization forward. On the other hand, as the growing polymer is a non-conductive material, the electrical current dropped more for thicker layers of polymeric film. Consistently, as the number of successive cycles increased, the anodic peak current diminished, until a steady state was achieved (after 7 cycles for MIPs or 4 cycles in the case of NIPs).

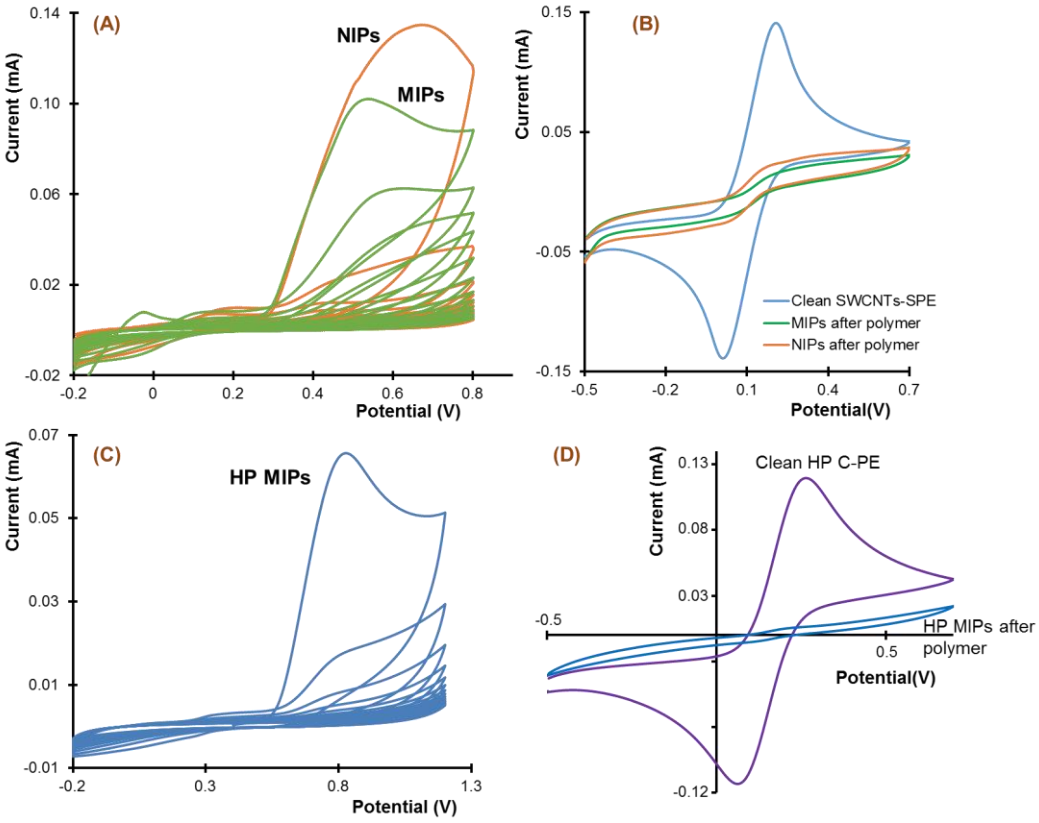

Figure 5.3. CV data for the (A) electrochemical synthesis of MIP and NIP films at SWCNTs-SPEs and (B) the electrical response of the so-obtained films in a standard iron redox probe of 5.0 mM $[Fe(CN)_6]^{3-}$ and 5.0 mM $[Fe(CN)_6]^{4-}$, in MES buffer pH 5.0, and the corresponding studies (C and D) with HP C-PEs.

After concluding the polymerization stage, the electrical output of MIP and NIP films was recorded using an iron redox probe. As may be seen in **Figure 5.3B**, the resulting CV data showed a significant current decrease in both MIP and NIP films, when compared to the

clean SWCNTs-SPEs. This behavior also evidenced the existence of polymer at the electrode surface.

The same procedure was applied to the MIP-based homemade electrodes prepared herein. The results obtained are shown in **Figure 5.3C** and **D**. Comparing to the commercial SWCNTs electrodes, the background electrical signal of the HP C-PEs was smaller in about 14.9 % (CV data in **Figures 5.3B** and **D**). This was due to the smaller physical area of the working electrode made in the laboratory; SWCNTs-SPEs had 45.36 mm^2 and HP C-PEs 38.48 mm^2. Apart from this, a similar behaviour to that of the SWCNTs electrodes was observed. The presence of the flagella protein on the clean HP C-PE reduced its intrinsic anodic current and shifted to peak potential of the monomer up to 0.8 V (**Figure 5.3C**). In addition, the consecutive CVs involved in the polymerization process promoted significant additional current decay, as expected (**Figure 5.3C** and **D**).

5.1.3.2 Template removal

The follow-up of the protein template exit from the polymeric material was made by EIS spectra and SWV, measured before and after FPM removal (**Figure 5.4**; clean SWCNTs-SPEs were also included for control purposes). EIS data fitted the Randles equivalent circuit. In this, the semicircles (observed at high frequency range) indicated a charge-transfer controlled process. The diameter of this semicircle equaled the charge-transfer resistance, R_{ct}, which controlled the electron-transfer kinetics of the redox-probe at the electrode interface (Panagopoulou et al., 2010). The linear behavior was given at the low frequency range and revealed a diffusion-controlled mass-transfer process (Suni, 2008), measured by the Warburg element (W). Overall, the electrical circuit in EIS consisted of a resistor element (solution resistance, R_s) in series with one parallel circuit comprising a charge transfer resistance, R_{ct}, with a Warburg element (W) and a double layer capacitance, C_{dl} (inset, **Figure 5.4A** and **B**) (Daniels, 2008; Ding et al., 2005a, 2005b).

After electropolymerization, MIPs showed higher EIS-based R_{ct} than NIPs, thought the polymerization was lower in MIPs than NIPs (**Figure 5.4A** and **B**). This is consistent with the fact that both FPM and polyphenol are coating the electrodes in MIP films, while only polyphenol is present in NIP-based electrodes. In addition, this behaviour is an ultimate indication that the presence of FPM alone increases the charge transfer resistance of the electrodes.

FPM removal was achieved by the proteolytic action of proteinase K. The peptide fragments generated by this process were then removed from the surface by subsequent chemical (washing) and electrochemical cleaning (consecutive CVs). As expected, the ultimate result of this process generated a decrease in the charge transfer resistance R_{ct} (**Figure 5.4A** and **B**). Such decrease correlated well with the protein exit from the sensing layer, as the previous addition of FPM to the electrode surface promoted a R_{ct} increase. In addition, as the NIP films also showed a small R_{ct} decrease (in smaller extent than MIP ones), a small

part of the R_{ct} reduction observed in the NIP film may be evidencing the exit of small polymer fragments and unreacted species that were not firmly attached to the electrode surface.

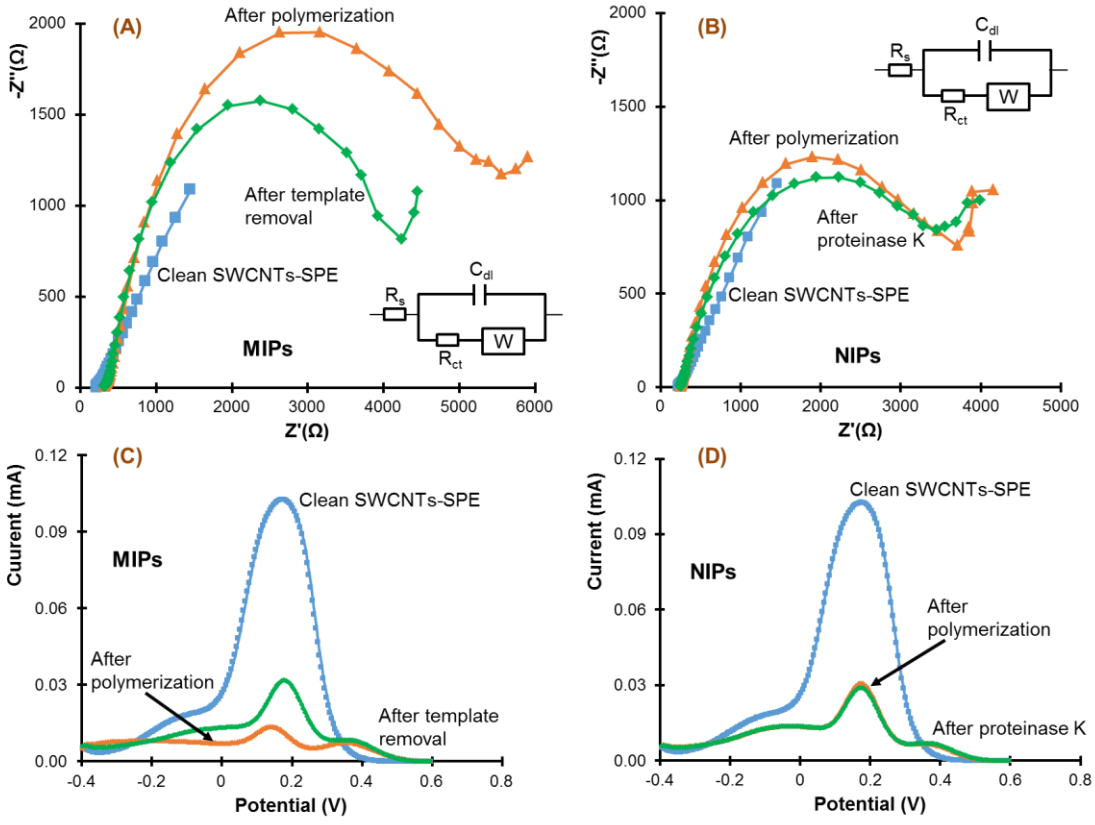

Figure 5.4. EIS (A, B) and SWV (C, D) data of clean SWCNTs-SPEs, MIP and NIP films, in a 5.0 mM $[Fe(CN)_6]^{3-}$ and 5.0 mM $[Fe(CN)_6]^{4-}$ solution, prepared in MES buffer pH 5.0.

SWV data is shown in **Figures 5.4C** and **D** and was also consistent with the behaviour observed in EIS. The electrical current generated by an iron redox probe on the MIP film holding the protein was much lower than on the NIP one, thereby confirming the presence of the protein within the polymer. In turn, the subsequent removal of the protein has led to a significant current increase in the MIP film; the NIP film was increased by only in a little amount and remained with lower currents than the MIP material.

The surface modification of HP C-PE-based MIPs was also followed by SWV, showing similar behaviour to the MIP films relying on SWCNTs-SPEs. These corresponding data has been added as supplementary material (**Figure S5.2**). Overall, the above data was a powerful evidence of the successful imprinting procedures, thereby generating the intended rebinding cavities. In parallel to the electrical readings, the chemical modifications occurring at the electrode surface were also followed-up by Raman spectroscopy.

5.1.3.3 Raman spectroscopy follow-up

The electropolymerized films of phenol are produced by *ortho*- or *para*- coupling of phenoxy radicals generated by oxidation of the phenolate anion. The necessary electrical conditions were established by CV, where the minimum voltage to promote the phenol oxidation on the underlying substrate is identified. Subsequent reactions to produce the intended polyphenol polymers were promoted by consecutive CV recordings (Samet et al., 2010; Yuqing et al., 2004). The resulting polymers were observed directly by Raman analysis with confocal microscopy, in order to have some qualitative data about the newly formed chemical structures.

The obtained spectra are presented in **Figure S5.3** (Supplementary Information). As the background support in all electrodes is carbon, the typical G and D and 2D bands appeared in spectra.

Regarding the D and G bands, the intensity ratio I_D/I_G of the clean SWCNTs-SPE was 1.078, whereas the ratios for MIP and NIP films were 1.069 and 1.068 respectively. Although the ratio values were quite similar, MIP and NIP peaks have a broader shape when compared to the clean SWCNTs-SPE control materials, providing the indication of surface coverage by carbon polymeric material. As expected, the polymeric-based devices (MIPs and NIPs) showed similar behavior in terms of broaden peak shape and which was consistent with the fact that the chemical composition of these films was similar. Although NIP films were expected to have a thicker film of polymeric material on top of the carbon

background, in terms of intensity ratio this difference would not be reflected in the Raman data.

Greater differences between control and polymeric materials (MIP and NIP) were observed in 2D peaks. In general, the 2D peak intensity is assigned as an inverse relationship with the surface layer and/or coverage. The control SWCNTs material had a higher Raman intensity, which decreased after creating a polymeric film on top of it.

Overall, the Raman spectra confirmed the chemical differences between control and polymeric materials, thereby corroborating the presence of the polyphenol film on top of the carbon background and that the presence of FPM at the imprinting stage had no effect on the final sensing layer. In addition, such similarity between MIP and NIP films also confirmed that the action of proteinase K had no effect during the template removal.

5.1.3.4 Main analytical features

The EIS and SWV responses of both MIP and NIP sensors to increasing concentrations of FPM is shown in **Figure 5.5**. The raw data of MIP and NIP films are shown in 5.5A and B for EIS assays and in 5.5D and E for SWV. The corresponding calibration curves are shown in 5.5C and F, respectively.

In general, the NIP-based devices presented a negligible response in the presence of increasing concentrations of FPM, both in EIS and in SWV assays (**Figure 5.5B** and **E**). This confirmed the lack of affinity of the non-imprinted polyphenol receptor surface towards the target protein (and therefore its unimportant contribution to the performance of the final device). Thus, the target FPM protein displays littler non-specific binding affinity towards the polyphenol surface.

On the contrary, the MIP devices showed very sensitive changes against increasing FPM concentrations (**Figures 5.5A** and **D**). In the EIS data (**Figure 5.5A**), the semicircles became larger, as the FPM concentration increased. This behaviour was probably due to the increase of the MIP surface thickness and passiveness caused by the captured FPM, which in turn hindered the electron transfer of a negatively charged iron redox probe molecules at the surface. The average slope of this process was 0.274 decade^{-1}·M^{-1} (860.53 Ω/decade·M^{-1} reverting the ratio of R_{ct}/Ro_{ct} by multiplying by Ro_{ct}) for a linear range over three orders of magnitude, from 0.12 nM up to 0.73 µM (**Figures 5.5C**). The detection limit (LOD) of MIP-based devices was 8.00 pM, assuming three times the standard deviation of the blank response. In SWV (**Figure 5.5D**), a similar behaviour to that observed

in EIS assays was present. The average slope was of -2.30 µA/decade M^{-1} (data was obtained converting again the current ratio into current units) with a similar linear range to that in EIS, from 0.12 nM up to 0.73 µM (**Figures 5.5F**). The LOD in this case is 11.06 pM, which is also very close to the EIS LOD.

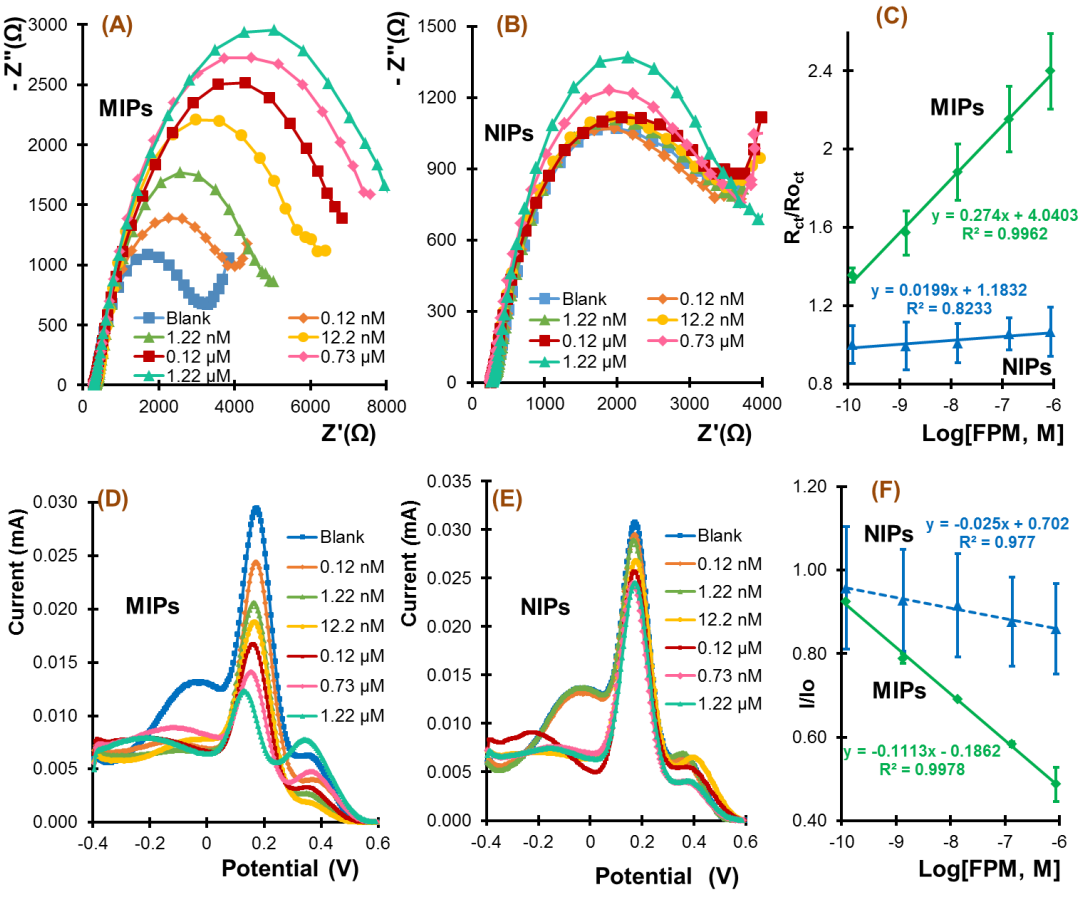

Figure 5.5. EIS (A, B and C) and SWV (D, E, and F) measurements of (A, D) MIP and (B, E) NIP-based devices upon increasing FPM concentrations, and (C, F) the corresponding calibration curves (typical values with error bars corresponding to 3 measurements from three independent devices), in 5.0 mM $[Fe(CN)_6]^{3-}$ and 5.0 mM $[Fe(CN)_6]^{4-}$, prepared in MES buffer, pH 5.0.

The precision of the analytical devices in EIS and SWV assays was assessed by the standard deviation of the collected data, considering three different assays, with three different devices, taken in different days. The corresponding standard deviations have been expressed as error-bars in the corresponding calibration curves, shown in **Figures 5.5C** and

F. Interestingly, SWV showed more precise data than EIS. Since SWV was also more rapid than EIS assays (because SWV measurements took ~5 s, while EIS measurements were ~7 min), this technique was chosen for further analysis with the homemade (HP C-PE) electrodes.

5.1.3.5 Binding isotherm

The artificial antibodies described herein were further evaluated in terms of affinity towards their target analyte, with the purpose of monitoring the strength of binding of FPM to its rebinding position on the artificially-generated polymeric site. This was made by monitoring the analytical data produced by incubating the rebinding sites on the MIP film with different concentrations of FPM and recording the differences generated in terms analytical signal. This data was further used to calculate an apparent dissociation constant (K_D) and the maximum binding of the target ($\Delta R_{ct}^{máx}$ *or* $\Delta I^{máx}$). K_D is the indication of the concentration of FPM at half of the maximum response. If K_D is a low value, a large binding affinity is present as the reaction approached the maximum response more rapidly, meanwhile a high K_D value indicates that the sensor does not efficiently bind to FPM.

In general, the isotherm analysis of a typical antibody/antigen behaviour generates the hyperbolic response (Ding et al., 2005a), shown in **Figure S5.4** (Supplementary Information), both for EIS and SWV data. Moreover, changes in K_D are sensitive to variations in protein access/binding (Rothwell et al., 2010; Sasso et al., 1990) and may be interpreted herein in terms of barriers to antigen-artificial receptors access.

In EIS (**Figure S5.4-A**), the MIP-based sensors presented $\Delta R_{ct}^{máx}$ and K_D of 9.68 kΩ/cm^2 and 6.60 nM, respectively. The R_{ct} and Ro_{ct} indicated, respectively, the normalized and baseline charge transfer resistance values of the sensor, and hence the signal density (ΔR_{ct} per unit area of electrode, where $\Delta R_{ct} = (R_{ct} - Ro_{ct})$) represented the binding adsorption for each concentration of FPM. The signal density of MIP-films increased after each addition of FPM (until saturation). In contrast, the NIP films had no significant signal variation throughout the FPM addition, showing no or random affinity towards the protein.

In SWV (**Figure S5.4-B**), the MIP-based sensors presented maximum binding ($\Delta I^{máx}$) of 23.40 µA/cm^2 with a dissociation constant of K_D 4.40 nM. *I* and *Io* indicated the normalized and baseline currents, respectively. The plot of signal density ($-\Delta I$ per unit area of electrode, where $-\Delta I = (I-Io)$) *versus* FPM concentration showed again that MIPs were

highly sensitive to FPM, whereas NIPs were rather insensitive. Interestingly, the results of SWV are closely related with the EIS-based results.

Overall, NIPs displayed almost negligible affinity towards FPM compared to MIP-based sensors. This showed a predictable and sensitive response of the MIPs against FPM concentration, since the differences between NIPs and MIPs were only the absence or presence of FPM tailored binding sites at the receptor surface.

5.1.3.6 Selectivity

The selectivity of the sensor was evaluated by EIS and SWV measurements (**Figure 5.6**) using the competitive assay (Moreira et al., 2013). In this assay, the target FPM protein was allowed to compete for the same surface with a foreign element that is expected to behave as an interfering species.

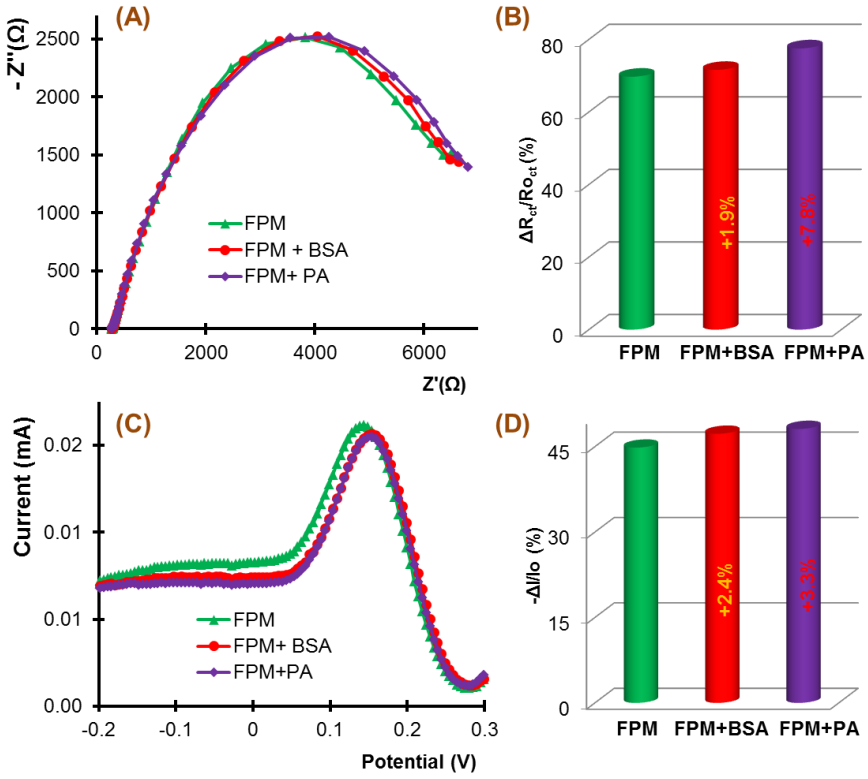

Figure 5.6. Selectivity study with (A) EIS & corresponding bar diagram (the percentage corresponds to the deviation in the response caused by the interference) (B); and with (C) SWV & corresponding bar diagram (the percentage corresponds to the response caused by the interference) (D).

The assay was done by setting the FPM concentration to 12.2 nM; the solutions of the interfering species (BSA, PA from *Staphylococcus aureus*) were equimolar of the FPM concentration. The response of MIP-based sensors was checked using solutions with only FPM or FPM plus the interfering species. The time and conditions were set as in the calibration of the sensors.

The average percentage of deviation produced by each interfering species in pure FPM solution were 1.9% for BSA and 7.8% for PA in EIS studies, and 2.4% for BSA and 3.3% for PA in SWV evaluations. The typical EIS-based spectra and SWV voltammograms obtained herein may be seen in **Figures 5.6A** and **B**, respectively.

Overall, negligible interfering was found from the competing proteins (BSA and PA), with current changes always below 10% in the nM protein level. Furthermore, and in agreement with the previous precision data, the sensors displayed better performance in term of selectivity when evaluated by SWV.

5.1.3.7 Application to real samples

As this work was meant for field water monitoring and low cost applications, the possibility of using the homemade paper-based devices (HP C-PE) under this context was tested herein. Tap water was used as sample, aiming to assess a possible application to the proposed devices and tested as a proof of concept for the detection of FPM. The results obtained are presented in **Figure 5.7**.

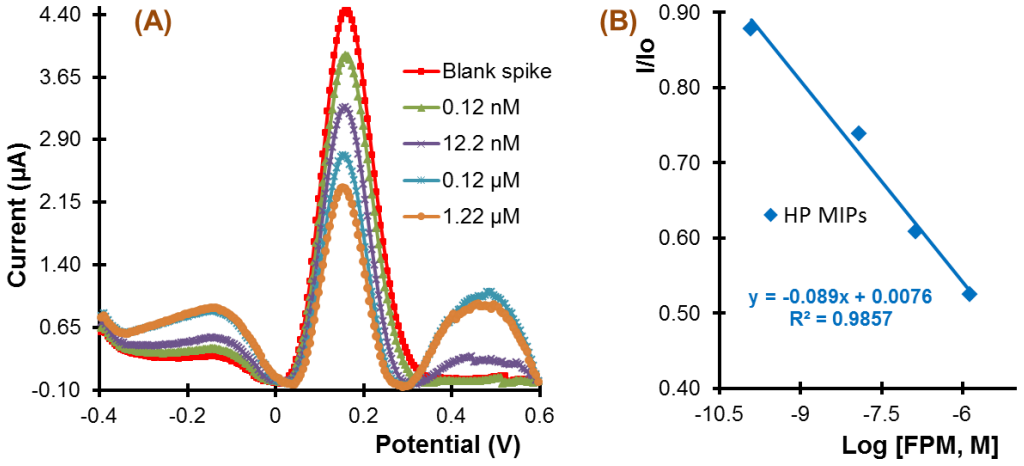

Figure 5.7. SWV based measurements (A) of MIP-based HP C-PE and the corresponding calibration curve (B) in 5.0 mM $[Fe(CN)_6]^{3-}$ and 5.0 mM $[Fe(CN)_6]^{4-}$ by spiking FPM in tap water within 0.12 nM and 1.22 µM.

In the absence of real contaminated water, the tap water was spiked and diluted four times in MES buffer due to the need of adding standards. The resulting solutions were

monitored, as in a calibration where the background was a real water sample artificially contaminated. In general, the obtained results pointed out good features in terms of concentration range of linear response (0.12 nM to 1.2 µM), LOD (7.02 pM) and slope (-0.395 µA/decade·M^{-1}, the slope was obtained converting again the current ratio to current units). Comparing these results with the FPM calibration curve in MES buffer pH 5.0, the LOD is of the same order magnitude.

The most interesting information from this experiments is that the home-made disposable device (HP C-PE) showed sensing performance for detecting FPM from tap water with very similar analytical parameters to the ones obtained using SWCNTs-SPE in MES buffer, which would be a great advance to make home-made easy tailored electrodes that are cost-effective and portable bio-sensing devices.

5.1.4 Conclusions

In this paper, an artificial receptor based on molecular imprinting for the direct electrochemical detection of bacterial flagella is presented for the first time. The non-imprinted devices showed random binding, making this sensor especially suitable for the detection of bacterial surface proteins. In addition, and to the best of our knowledge, the homemade device (HP C-PE) is the first home-made paper-based approach for making electrochemically-based artificial protein receptors, which would be a cost-effective portable device and would be a useful tool in the field of electrochemical research and diagnostic in developing countries.

This device displays a good precision, high selectivity, low detection limit, cost-effectiveness, offering also the advantages of disposability and portability, simple instrumentation and easy preparation for the detection of flagella from the outer surface of *P. mirabilis.* This device can be seen as one of the initial steps for the detection of bacteria using molecularly imprinted polymer-based devices.

Acknowledgements

The Catalan Government and the European Research Council are acknowledged for the financial support of MARK PhD Fellowship (2013FI_B 00842) and Starting Grant, 3P's, GA 311086 respectively. The URV team thanks the financial support from the Spanish Ministerio de Economía y Competitividad (Project CTQ2010-18717).

5.1.5 References

Bahrani, F.K., Johnson, D.E., Robbins, D., Mobley, H.L.T., 1991. *Proteus mirabilis* flagella and MR/P fimbriae : isolation, purification, N-terminal analysis, and serum antibody response following experimental urinary tract infection. Infect. Immun. 59, 3574–3580.

Barlaan, E.A., Sugimori, M., Furukawa, S., Takeuchi, K., 2005. Electronic microarray analysis of 16S rDNA amplicons for bacterial detection. J. Biotechnol. 115, 11–21.

Clark W. A., 1976. A simplified leifson fagella stain. J. Clin. Microbiol. 3, 632–634.

Daniels, J.S., 2008. Label-free impedance biosensors: opportunities and challenges. Electroanalysis 19, 1239–1257.

Ding, S.J., Chang, B.W., Wu, C.C., Lai, M.F., Chang, H.C., 2005a. Electrochemical evaluation of avidin-biotin interaction on self-assembled gold electrodes. Electrochim. Acta 50, 3660–3666.

Ding, S.J., Chang, B.W., Wu, C.C., Lai, M.F., Chang, H.C., 2005b. Impedance spectral studies of self-assembly of alkanethiols with different chain lengths using different immobilization strategies on Au electrodes. Anal. Chim. Acta 554, 43–51.

Forbes, L., 1981. Rapid flagella stain. J. Clin. Microbiol. 13, 807–809.

Grossart, H., Riemann, L., Azam, F., 2001. Bacterial motility in the sea and its ecological implications. Aquat Micrbial Ecol 25, 247–258.

Guo, X., Lin, C., Chen, S., Ye, R., Wu, V.C.H., 2012. A piezoelectric immunosensor for specific capture and enrichment of viable pathogens by quartz crystal microbalance sensor , followed by detection with antibody-functionalized gold nanoparticles. Biosens. Bioelectron. 38, 177–183.

Haupt, K., 2003. Imprinted polymers —Tailor-made mimics of antibodies and receptors. Chem. Commun. 171–178.

Heyduk, E., Heyduk, T., 2010. Fluorescent homogeneous immunosensors for detecting pathogenic bacteria. Anal. Biochem. 396, 298–303.

Ikeda, M., Yamaguchi, N., Tani, K., Nasu, M., 2006. Detection of food poisoning bacteria in fresh vegetables using DNA microarray. J. Heal. Sci. 52, 36–42.

Jordana, S.L., Oliveira, M.D.L., Melo, C.P. De, Andrade, C.A.S., 2014. Impedimetric sensor of bacterial toxins based on mixed (concanavalin A)/polyaniline films. Colloids Surfaces B Biointerfaces 117, 549–554.

Kodaka, H., Armfiled, A.Y., Lombard, G.L., Dowell, V.R., J R. et al, 1982. Practical procedure for demonstrating bacterial flagella. J. Clin. Microbiol. 16, 948–952.

Lingxin, S., 2016. As featured in: molecular imprinting : perspectives and applications. Chem. Soc. Rev. 45, 2137–2211.

Liu, J., Deng, Q., Tao, D., Yang, K., Zhang, L., Liang, Z., Zhang, Y., 2014. Preparation of protein imprinted materials by hierarchical imprinting techniques and application in selective depletion of albumin from human serum. Sci. Rep. 4:5487, 1–6.

Lu, L., Chee, G., Yamada, K., Jun, S., 2013. Electrochemical impedance spectroscopic technique with a functionalized microwire sensor for rapid detection of foodborne pathogens. Biosens. Bioelectron. 42, 492–495.

Maalouf, R., Fournier-wirth, C., Coste, J., Chebib, H., Saı, Y., Vittori, O., Errachid, A., Cloarec, J., Martelet, C., Jaffrezic-renault, N., Cnrs, U.M.R., Cnrs, U.M.R., Lyon, E.C. De, Collongue, G. De, 2007. Label-free detection of bacteria by electrochemical impedance spectroscopy : comparison to surface plasmon resonance. Anal. Chem. 79, 4879–4886.

Merkl, S., Vornicescu, D., Dassinger, N., Keusgen, M., 2014. Detection of whole cells using reflectometric interference spectroscopy. Phys. Status Solidi A 1422, 1416–1422.

Moreira, F.T.C., Sharma, S., Dutra, R.A.F., Noronha, J.P.C., Cass, A.E.G., Sales, M.G.F., 2013. Smart plastic antibody material (SPAM) tailored on disposable screen printed electrodes for protein recognition: application to myoglobin detection. Biosens. Bioelectron. 45, 237–244.

Nadkarni, M.A., Martin, F.E., Jacques, N.A., Hunter, N., 2002. Determination of bacterial load by real-time PCR using a broad-range (universal) probe and primers set. microbiology 148, 257–266.

Panagopoulou, M.A., Stergiou, D. V, Roussis, I.G., Prodromidis, M.I., 2010. Impedimetric biosensor for the assessment of the clotting activity of rennet. Anal. Chem. 82, 8629–8636.

Rothwell, S.A., Killoran, S.J., O'Neill, R.D., 2010. Enzyme immobilization strategies and electropolymerization conditions to control sensitivity and selectivity parameters of a polymer-enzyme composite glucose biosensor. Sensors 10, 6439–6462.

Samet, Y., Kraiem, D., Abdelhedi, R., 2010. Electropolymerization of phenol, o-nitrophenol and o-methoxyphenol on gold and carbon steel materials and their corrosion protection effects. Prog. Org. Coatings 69, 335–343.

Sasso, S. V, Pierce, R.J., Walla, R., Yacynych, A.M., 1990. Electropolymerized 1,2-diaminobenzene as a means to prevent interferences and fouling and to stabilize immobilized enzyme in electrochemical biosensors. Anal. Chem. 62, 1111–1117.

Sporer, C., Teixeira, V., 2013. Highly sensitive detection of pathogen *Escherichia coli* O157 : H7 by electrochemical impedance spectroscopy. Biosens. Bioelectron. 45, 174–180.

Suni, I.I., 2008. Impedance methods for electrochemical sensors using nanomaterials. TrAC -Trends Anal. Chem. 27, 604–611.

Uzarski, J.R., Mello, C.M., 2012. Detection and classification of related lipopolysaccharides via a small array of immobilized antimicrobial peptides. Anal. Chem. 84, 7359–7366.

Verheyen, E., Schillemans, J.P., Van Wijk, M., Demeniex, M.-A., Hennink, W.E., Van Nostrum, C.F., 2011. Challenges for the effective molecular imprinting of proteins. Biomaterials 32, 3008–3020.

Wang, Y., Ye, Z., Ying, Y., 2012. New trends in impedimetric biosensors for the detection of foodborne pathogenic bacteria. Sensors 12, 3449–3471.

Wangmaung, N., Chomean, S., Promptmas, C., Mas-oodi, S., 2014. Silver quartz crystal microbalance for differential diagnosis of plasmodium falciparum and plasmodium vivax in single and mixed infection. Biosens. Bioelectron. 62, 295–301.

Whitcombe, M.J., Chianella, I., Larcombe, L., Piletsky, S.A., Noble, J., Horgan, A., 2011. The rational development of molecularly imprinted polymer-based sensors for protein detection. Chem. Soc. Rev. 40, 1547–1571.

Winstanley, C., Morgan, J.A.W., 1997. The bacterial flagellin gene as a biomarker for detection, population genetics and epidemiological analysis. Microbiology 143, 3071–3084.

Yang, L., Bashir, R., 2008. Electrical/electrochemical impedance for rapid detection of foodborne pathogenic bacteria. Biotechnol. Adv. 26, 135–150.

Yang, L., Ruan, C., Li, Y., 2003. Detection of viable Salmonella typhimurium by impedance measurement of electrode capacitance and medium resistance. Biosens. Bioelectron. 19, 495–502.

Yuqing, M., Jianrong, C., Xiaohua, W., 2004. Using electropolymerized non-conducting polymers to develop enzyme amperometric biosensors. Trends Biotechnol. 22, 227-231.

Zelada-Guillén, G.A., Riu, J., Düzgün, A., Rius, F.X., 2009. Immediate detection of living bacteria at ultralow concentrations using a carbon nanotube based potentiometric aptasensor. Angew. Chem. Int. Ed. 48, 7334-7337.

5.1.6 Supplementary Information

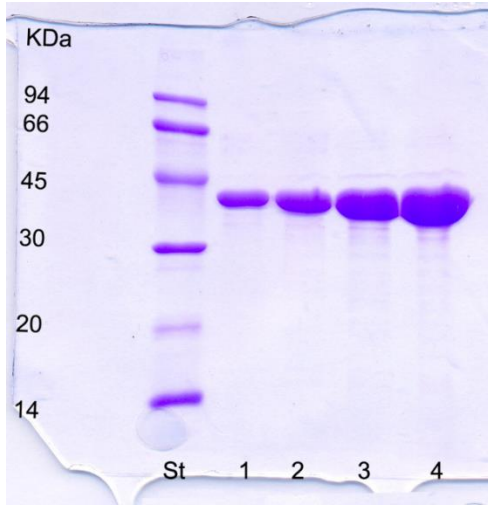

Figure S5.1. SDS-PAGE analysis of purified flagella.1) 0,5 µL 2) 1 µL 3) 2 µL 4) 4 µL

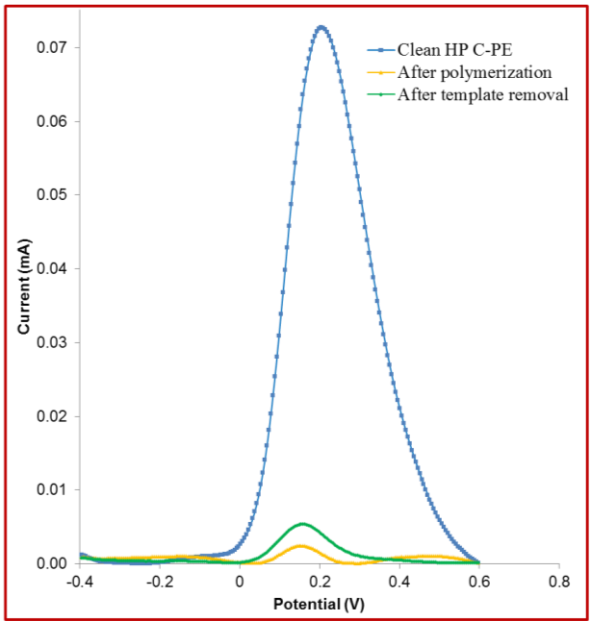

Figure S5.2. SWV data of clean HP C-PE, and MIP film, in a 5.0 mM $[Fe(CN)_6]^{3-}$ and 5.0 mM $[Fe(CN)_6]^{4-}$ solution, prepared in MES buffer pH 5.0.

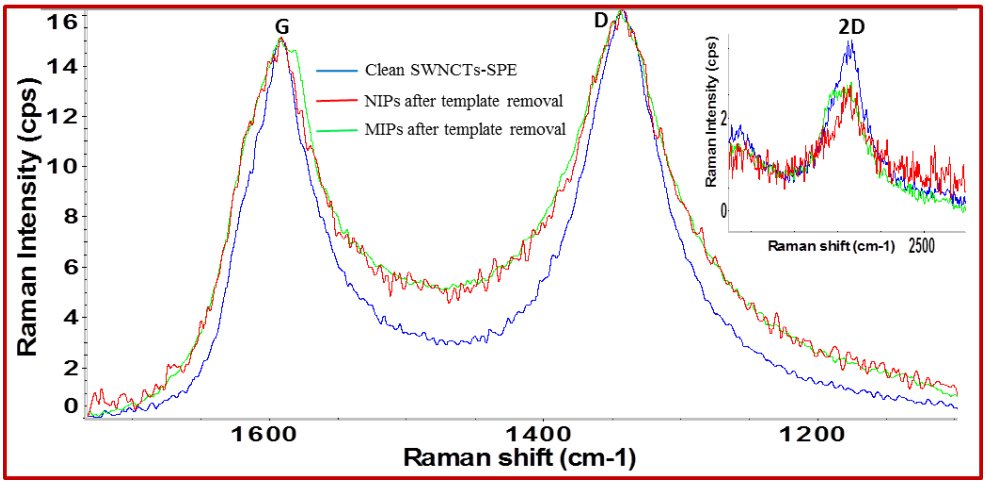

Figure S5.3. Raman spectra of the MIP and NIP materials and the control clean SWCNTs-SPE, highlighting D, G and 2D (inset) bands. The D, G and 2D band were observed at ~347, ~594 and ~2671 cm^{-1} respectively.

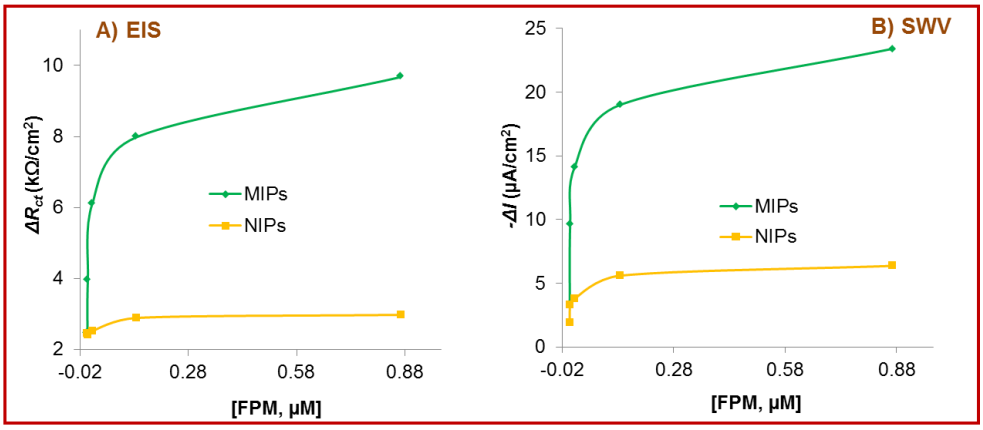

Figure S5.4. Langmuir isotherm plot. (A) EIS and (B) SWV data plotting the FPM concentration against signal variation and maximum binding capacity ($\Delta R_{ct}^{máx}$ *and* $I_{máx}$) of MIPs and NIPs.

5.2 Detection of *Proteus mirabilis*

Bacterial flagella were successfully detected in section **5.1**. This is because imprinted materials perfectly preserve the size and shape of the target flagella from *Proteus mirabilis.* As a proof of concept, MIPs created by imprinting of flagella from *Proteus mirabilis* (section **5.1**) can have the ability to capture and detect the whole *Proteus mirabilis* cell since the outer surface of *Proteus mirabilis* contains those flagella. The images of the whole cell of *Proteus mirabilis* can be seen at **Figure 5.8**.

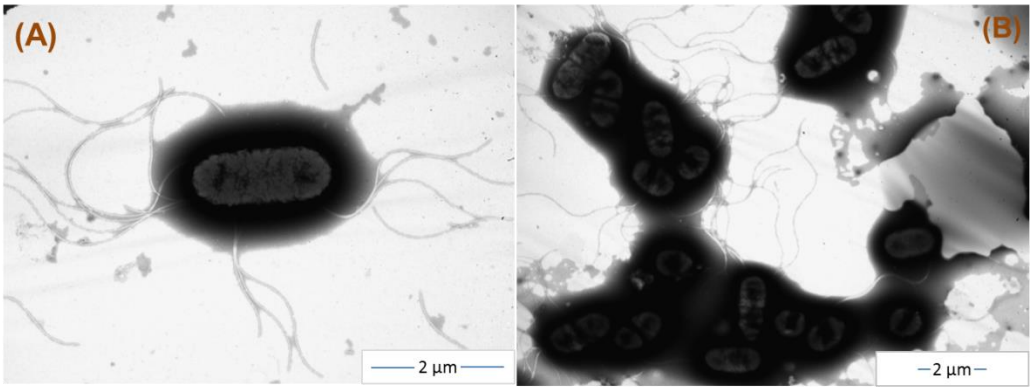

Figure 5.8. TEM images of whole cell of PM with high (A) and low (B) magnification: length of PM ≈ 3 µm and width ≈ 2µm. The curve lines represent the flagella at the outer surface of PM.

Although the flagella from whole living bacteria may be longer than the isolated flagella, the repeating structure of the flagella is exactly the same in all cases. Therefore, the receptors fabricated in section **5.1** might be candidates to bind with *Proteus mirabilis* (PM), which could be termed as epitope imprinting for the detection of the target. In this section, the sensing devices were fabricated over SWCNTs-SPEs using the same protocol as in section **5.1**. Representative results from impedimetry (EIS) can be seen in **Figure 5.9.**

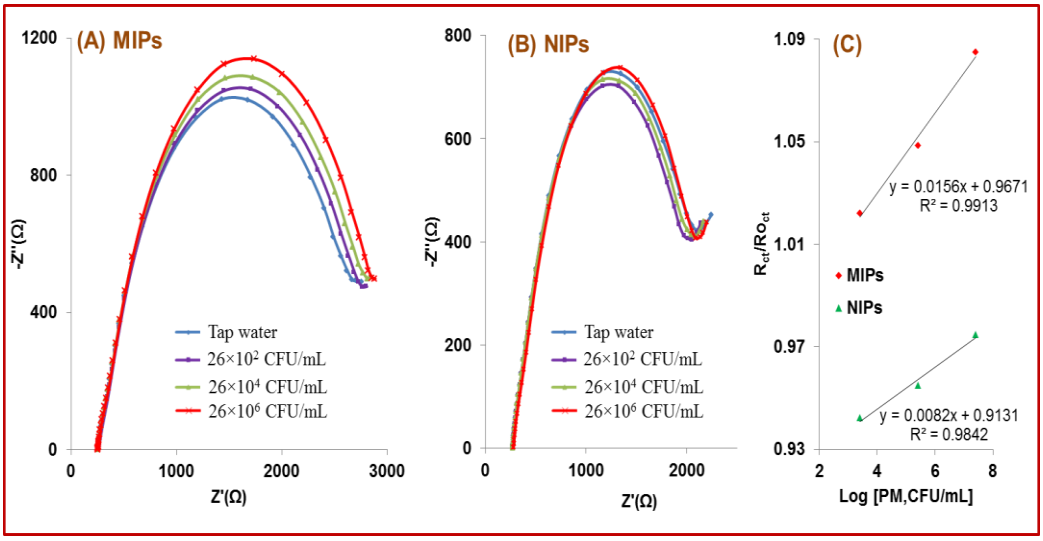

Figure 5.9. EIS-based response of *Proteus mirabilis* in (A) MIPs and (B) NIPs, and corresponding calibration curves (C); calibration was performed by dilution of the cell with sterilized tap water; exposure time was 1 h at room temperature.

In **Figure 5.9**, the charge transfer resistance (R_{ct}) of MIPs increases with PM concentration and the sensitivity is 38.55 Ω/decade [PM, CFU/mL] (data was obtained by converting the ratio of the charge transfer resistance into unit). The detection limit was observed to be 368 CFU/mL, considering three times the standard deviation of the blank response. In the case of the NIPs, the charge transfer resistance with respect to PM concentration decreased after the initial addition of PM (**Figure 5.9B**) and then increased, although the slope was not as steep as with MIPs (**Figure 5.9A, B** and **C**). This lesser increase in the charge transfer resistance (R_{ct}) of NIPs is probably due to the mass transfer effect of the large target (PM). However, to increase the sensors performance further optimization is needed.

5.3 Potentiometric biosensors for the detection of flagella and whole cell of *Proteus mirabilis*

In previous sections of this chapter we used square wave voltammetry and/or impedimetry to detect flagella and *Proteus mirabilis*. This section includes potentiometric detection of flagella and/or *Proteus mirabilis*. It is globally well-known that potentiometry has some advantages over other electrochemical techniques in terms of accuracy, fast response time, sensitivity and low-cost (Novell et al., 2012). The most widely used potentiometric sensors are ion-selective electrodes (ISEs). The sensing layer of ISEs is the ion-selective membrane that contains the ionophore, the true receptor of the ion-selective membrane. The ion-selective membrane is the analogue to MIPs in MIP-based biosensors. Traditionally the fabrication of the ion-selective membrane involves the mixing of the ionophores with suitable additives and/or plasticizers to fabricate the cocktail membrane that will be deposited over the electrode surface (Almeida et al., 2012; Rebelo et al., 2014; Solsky, 1990). The main drawback is that this process is time-consuming. But herein we electrochemically synthetized the sensing layer of MIP-based sensors over Au-SPEs in a similar way than in section **5.1**. Pyrrole was chosen as the monomer to entrap the target and to form the corresponding MIP. The resulting conductive polypyrrole is expected to act as the transducer part in the potentiometric biosensor.

5.3.1 Experimental

5.3.1.1 Equipment and instrumentation

High-input impedance voltmeter (1015 Ω), model EMF-16 Lawson Laboratories Inc. (Malvern, PA, USA). The standard reference electrode used was a Ag/AgCl 3 M KCl double-junction electrode containing a 1 M LiAcO electrolyte bridge, type 6.0729.100, Metrohm AG (Herisau, Switzerland). The electrochemical measurements were conducted with a potentiostat/galvanostat from Metrohm Autolab and a PGSTAT302N (Utrecht, The Netherlands), equipped with a FRA module and controlled by Nova software. The Au-SPEs were purchased from DropSens (Oviedo, Spain), and composed by a working electrode made of gold, a counter electrode made of gold and a reference electrode made of silver (electrical contacts were also made of silver). The diameter of the working electrode was 4.00 mm. The Au-SPEs were connected to a portable switch box, also from DropSens (DRP-DSC), allowing their interface with the potentiostat/galvanostat.

5.3.1.2 Reagents and solutions

All chemicals were of analytical grade and water was de-ionized or ultrapure Milli-Q laboratory grade. Sulfuric acid (98%), potassium hexacyanoferrate III, potassium hexacyanoferrate II trihydrate, sodium acetate anhydrous, trypsin, pyrrole (98%), 2-(*N*-morpholino)ethanesulphonic acid monohydrate 98% (MES), bovine serum albumin (BSA), protein A from *Staphylococcus aureus* (PA), glucose oxidase (GOx), 4-(2-hydroxyethyl)-1-piperazineethanesulfonic acid (HEPES), tris(hydroxymethyl)aminomethane and potassium chloride (KCl) were from Sigma Aldrich. Flagella from *Proteus mirabilis* (FPM) was obtained from Department of Microbiology, University of Barcelona. Stock solutions of 1.22×10^{-5} mol/L flagella from *Proteus mirabilis* (FPM) were prepared in TRIS buffer (6.66×10^{-4} mol/L, pH 7.8) and stored at –20˚C. Standards were obtained by accurate dilution of the previous solution in HEPES buffer (1.0×10^{-4} mol/L) at different pH (5, 7.3 or 8.3) depending on the applications. TRIS buffer (5.0×10^{-2} mol/L, $CaCl_2$ 1.0×10^{-3} mol/L pH 8.0) was used for trypsin solution preparation. The selectivity study was made by the matched potential method in HEPES (1.0×10^{-4} mol/L, pH 7.3) buffer using BSA, PA and GOx.

5.3.1.3 Electrochemical synthesis of molecularly imprinted (MIP) and non-imprinted polymer (NIP) films

Prior to the electropolymerization, the Au-SPEs electrodes were cleaned with ethanol followed by electrochemical cleaning with 0.5 M H_2SO_4 (CV from −0.2 to 1.2 V, 15 cycles at a scan-rate of 50 mV/s). Then FPM were deposited at the working area of the Au-SPE: 10 µL of 2.44×10^{-6} mol/L FPM solution prepared in MES buffer was exposed to the working area of the electrodes for 30 min at room temperature and gently washed with Milli- Q water. 75 µL of pyrrole solution (1×10^{-3} mole/L) in acetate buffer (1×10^{-2} mole/L, pH 5.0) was placed to cover the three electrodes and polymerization was performed by CV from -0.2 to 1.2 V (scan rate 0.05 V/s, 15 CV cycles was found to be the optimal). Flagella were removed by adding trypsin (500 µg/mL in TRIS buffer, 37°C, and 2.5 h) and by the subsequent electrochemical cleaning in MES buffer (10 CV cycles from -0.6 to 1 V, scan rate 50 mV/s). The fabrication of the MIP-based biosensors is schematically presented in **Figure 5.10.**

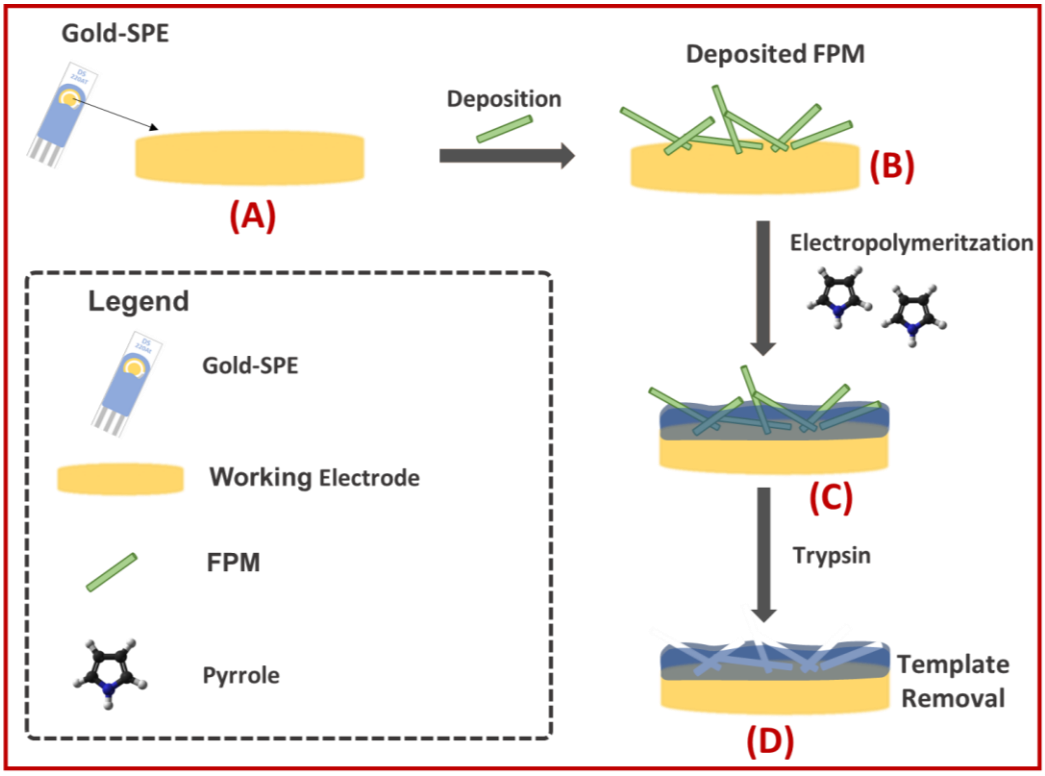

Figure 5.10. Schematic representation of the fabrication of the biosensor. (A) working area of Au-SPE, (B) deposited FPM, (C) imprinting stage after electropolymerization of pyrrole, (D) binding sites formation after template removal by trypsin.

In parallel, non-imprinted polymers (NIPs) were synthesized in a similar mode, but without the presence of FPM.

5.3.1.4 Electrochemical characterization of the films

The polymer growth and the surface characteristics of MIP and NIP-films were followed by CV, EIS and SWV. The redox probes in all CV and EIS measurements were 5.0 mmol/L $[Fe(CN)_6]^{3-}$ and 5.0 mmol/L $[Fe(CN)_6]^{4-}$ prepared in MES buffer (1.0×10^{-2} mol/L, KCl 0.1M, pH 5.0). In CV assays, the potential ranged from –0.5 to +0.7 V with a scan rate of 50 mV/s. In EIS, an open circuit potential was set using a sinusoidal potential perturbation of 0.01 V amplitude and 50 frequency values logarithmically distributed over a frequency range of 0.1 Hz to100 kHz. In SWV the potential range was from –0.1 to 0.6 V.

5.3.1.5 Potentiometric measurements

In the case of potentiometric measurements the working electrode of Au-SPE (with the MIP/NIP on the top of it) was used against the standard reference electrode (Ag/AgCl 3M KCl double-junction reference electrode). The working electrode was stabilized in HEPES buffer at a fixed pH before starting the calibration. All the potentiometric measurements for FPM detection were carried out at room temperature and in stirred solutions. EMF values of each electrode were measured in HEPES buffer (1.0×10^{-4} mol/L) at different pH (5.0, 7.3 or 8.3). The best performance of the sensors during the calibration stage was found at pH 7.3 and these results are presented herein. For the detection of *Proteus mirabilis* potentiometric measurements were performed in sterilized HEPES buffer, pH 7.3.

5.3.2 Results and discussion

5.3.2.1 Electrochemical imprinting

A typical cyclic voltammogram recorded during the MIP and NIP electropolymerization is presented in **Figure 5.11A.**

The CV shows two oxidation peaks (a higher first one at ~0.7 V and then a lower second one at ~1.0 V) during NIP-film fabrication. The first high intense peak is due to the polymerization of pyrrole onto the clean Au-electrode and the second peak is probably due to further polymerization onto the already polypyrrole-modified Au-electrode. Since the surface is already partially covered by polypyrrole, the intensity is lower in this second peak. In the case of MIPs, the first peak shifted ~0.9 V towards more positive values and the second peak diminishes and/or is superimposed with the capacitance current. This is probably because to the low current intensity due to the surface coverage by FPM before starting polymerization. CV shows a decreasing current during the oxidation process (MIP at ~0.9 V and NIP at ~0.7 V and 1.0 V) from the 1st cycle to the 9th cycle, indicating the deposition of the polymer onto the electrode surface. This is also confirmed by the disappearance of the redox peaks of the ferro/ferricyanide probe with respect to the clean Au-SPE (**Figure 5.11B**).

During the anodic oxidation of pyrrole, the intensity of current is higher in the case of NIPs in the first cycles which is indicative of the surface coverage by FPM (in the case of MIPs) before electropolymerization. Furthermore, the decreasing trend of current is slower in MIPs than NIPs. This is due to the faster polymer growth in the case of NIPs since the

surface was cleaned before electropolymerization. Since the MIPs surface was initially covered by FPM, the polymerization process is slower than in the NIPs case.

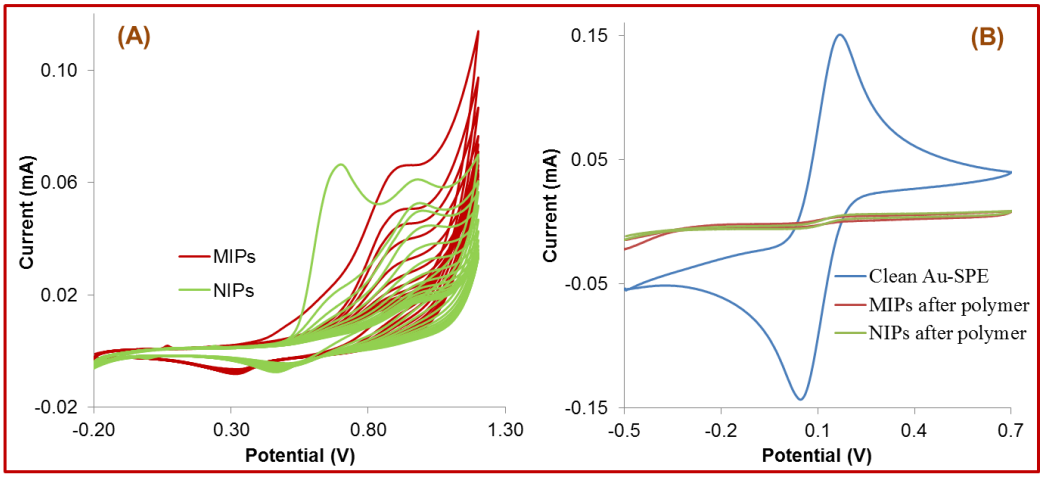

Figure 5.11. (A) Cyclic voltammetry-based synthesis of MIPs and NIPs, and the corresponding surface blocking test (B) carried out by CV in 5.0 mM $[Fe(CN)_6]^{3-}$ and 5.0 mM $[Fe(CN)_6]^{4-}$, in MES buffer pH 5.0.

5.3.2.2 EIS and SWV-based characterization

EIS and SWV were also employed for the characterization of the films (**Figure 5.12**). In the case of EIS, the interpretation of data was carried out by the Randles equivalent circuit, which is already described in section **5.1**.

Figure 5.12A shows the EIS response of the MIP and NIP-films before and after the addition of trypsin, which implies the removal of the template in MIP-films. Interestingly, after polymerization MIPs showed higher charge-transfer resistance, R_{ct} (16.67 kΩ) than NIPs (9.79 kΩ) even though polymerization was lower in case of MIPs. This is because the MIPs surface is covered by both the polymer and the FPM, while NIPs surface is only covered by the polymer. After the protein removal by the action of trypsin and the subsequent electrochemical cleaning, the R_{ct} value of MIPs and NIPs significantly decreased to a value of 1.83 and 2.59 kΩ respectively. The decrement, as expected, is higher in MIPs (89.01%) than in NIPs (73.53%) and is also an evidence of the creation of imprinted sites. In the case of MIPs, the decrement is probably related to two factors: firstly, the removal of the template and secondly, the removal of non-bound monomers and/or

oligomers, while only the second factor is responsible for the NIPs R_{ct}-value decrement. The SWV results (**Figure 5.12B**) seems to support this explanation.

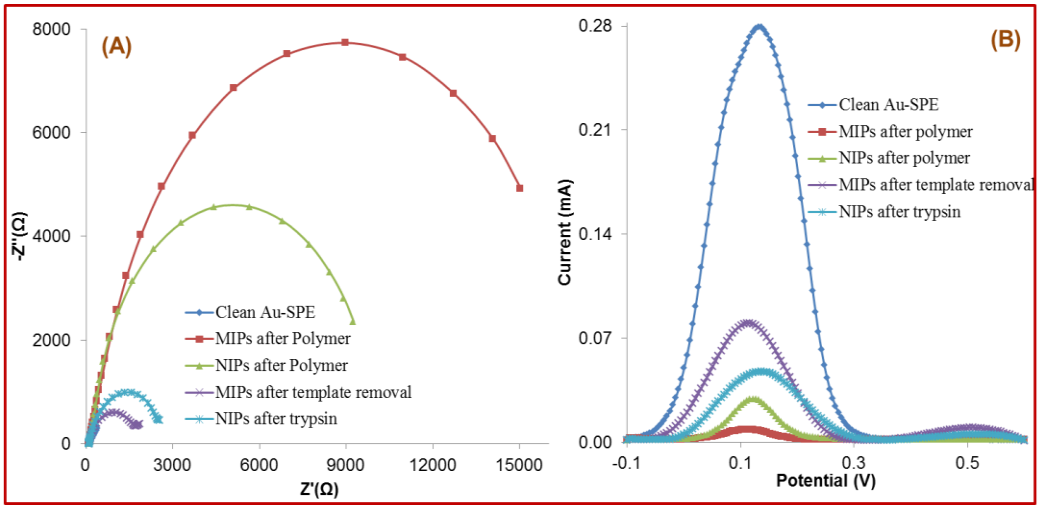

Figure 5.12. (A) Electrochemical characterization of MIP and NIP-films by (A) EIS (Nyquist plots) and by (B) SWV assays with 5.0 mM $[Fe(CN)_6]^{3-}$ and 5.0 mM $[Fe(CN)_6]^{4-}$ in MES buffer pH 5.0.

5.3.2.3 Sensors performance for the detection of flagella

Figure 5.13 shows the potentiometric performance of the sensors (in HEPES buffer pH 7.3) for the detection of FPM. Both devices (MIPs and NIPs) showed no response at lower concentration of FPM (1.2 to 0.13 nM). Later, from 1.3 nM to 31.2 nM MIPs showed a higher decreasing trend of EMF than NIPs. The response of MIPs is probably due to the imprinting sites in MIPs and also to some non-specific adsorption of flagella. The response of NIPs comes only from the non-specific adsorption of flagella by polypyrrole. However, the linear response of MIP-devices was from 3.8 to 31.2 nM while in case of NIP was from 9.9 to 31.2 nM.

The limits of detection (LODs) were 2.48 nM and 5.21 nM for MIP and NIP-devices (considering the cross-section of the two extrapolated linear parts in the calibration curve) respectively. The response time was between 12 s and 15 s for both MIP and NIP-devices (inset of **Figure 5.13A**).

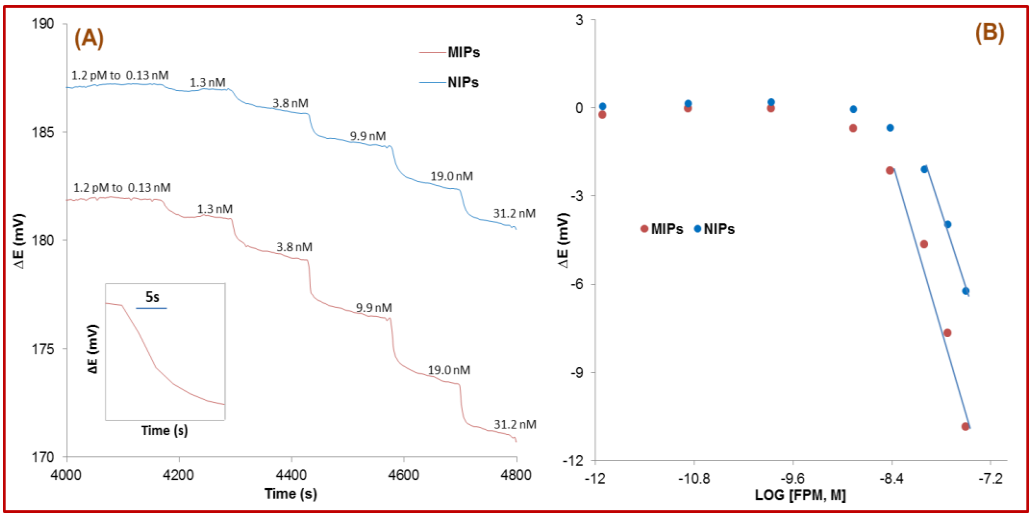

Figure 5.13. Potentiometric measurements of (A) MIP and NIP-based sensors and the corresponding calibration curves (B) in HEPES buffer pH 7.3. Inset in (A) shows the response time.

5.3.2.4 Regeneration of the sensors

Sensors were regenerated using trypsin and electrochemical cleaning (using the same protocol using for the template removal during the process of fabrication of the sensors) after the potentiometric calibration. EIS was employed to observe the surface characteristic of the MIP and NIP films after calibration and regeneration. After calibration, the R_{ct} value increased (MIPs 53.75 kΩ, NIPs 12.42 kΩ) in both devices but MIPs showed a higher increment than NIPs (**Figure 5.14A**) which is consistent with the calibration. Since the response was higher with MIPs it probably means that there is a higher binding load of flagella with MIPs than NIPs. After regeneration the R_{ct} value of both MIP and NIP-devices significantly decreased (**Figure 5.14B**) (MIPs 810 Ω, NIPs 792.80 Ω). The decrement of the R_{ct} value of MIPs is 98.46 % whereas in case NIPs it is 93.61%. This was due to the removal of the bound target (and/or the removal also of the non-specific adsorbed target) along with the probable removal of some polymers digested by trypsin and/or by the action of the electrochemical cleaning during the sensor regeneration. However, after regeneration of the sensors the R_{ct} value of MIPs was little bit higher than NIPs, probably due to the existence of some target proteins still into the imprinted sites of MIPs.

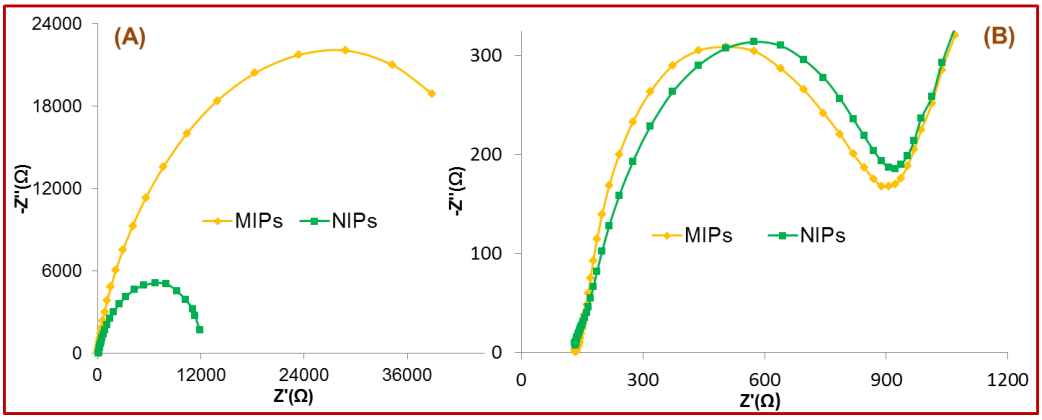

Figure 5.14. EIS-based surface follow-up after calibration (A) and regeneration (B) of the MIP and NIP-devices; 5.0 mM $[Fe(CN)_6]^{3-}$ and 5.0 mM $[Fe(CN)_6]^{4-}$, in MES buffer pH 5.0.

5.3.2.5 Selectivity

There are several approaches to assess selectivity in potentiometry, including separated solutions, mixed solutions or matched potential methods. The latter one is the only method enabling the evaluation of neutral species and the evaluation of electrodes that do not display Nernstian behavior. Thus, the selectivity of the FPM sensors was assessed by the matched potential method (Tavares et al., 2013). In brief, a known concentration of FPM was added into a reference solution containing a defined concentration of FPM (M1), and the corresponding potential change (ΔE) was recorded. Next, the interfering protein solution was added to the previous reference solution until the same potential change (ΔE) was reached, and the required concentration was marked as M2. The logarithm of the ratio (M1/M2) is the measure of the interference and termed as the selectivity coefficient (log*K*). It is technically very difficult to reach the exact required ΔE and herein we considered the closer value obtained. The MIP and NIP-based sensors both were suffering from non-specific adsorption of target flagella (which can be seen by comparing the calibration curves of MIPs and NIPs, **Figure 5.13B**) but the most interesting behavior of both sensors is that they show negligible interference effect over others proteins such as BSA, PA and GOx. However, MIPs show better selectivity than NIPs which was probably due to the presence of imprinting sites in MIPs to specifically bind with the target. The selectivity coefficient of MIP and NIP-based devices are summarized in the **Table 5.1**.

Table 5.1. Selectivity coefficient of MIP and NIP-based devices against various proteins

Selectivity coefficient	MIPs	NIPs
$\log K_{BSA}$	-4.586	-3.692
$\log K_{PA}$	-4.967	-2.967
$\log K_{GOx}$	-2.525	-2.037

5.3.2.6 Detection of *Proteus mirabilis*

The sensors were further tested to detect whole cell of *Proteus mirabilis* (PM) (**Figure 5.15**). The results show that both MIP and NIP-based sensors have no affinity towards PM up to 15×10^6 CFU/mL. However, at higher concentration values (from 31×10^6 CFU/mL to 151×10^6 CFU/mL) both sensors show response toward PM but the change of EMF value was really low (MIP 1.71 mV and NIP 1.19 mV). This is probably due to the mass transfer effect because of the large size of bacteria.

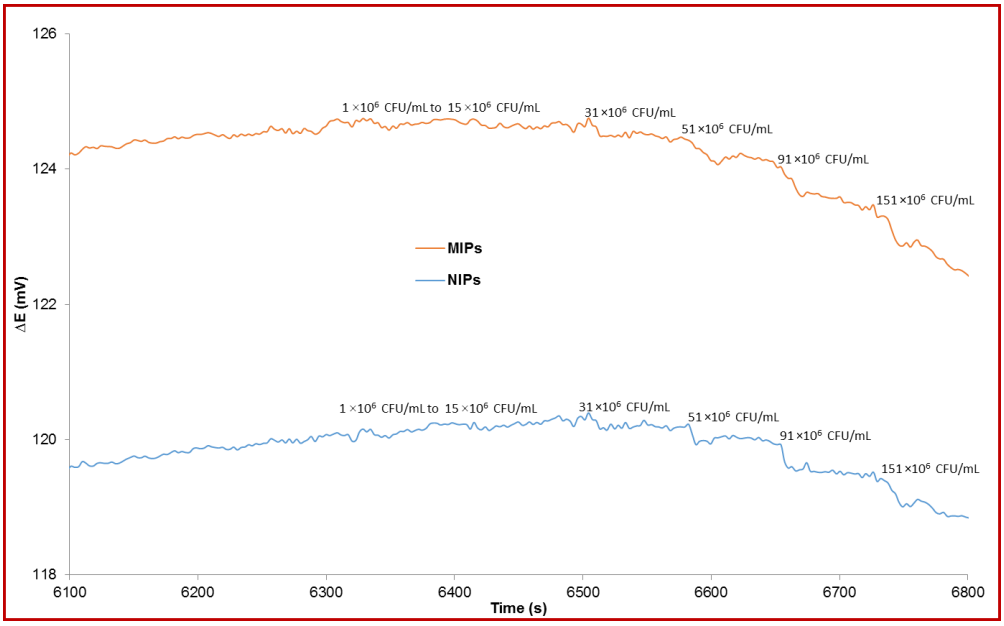

Figure 5.15. Potentiometric measurements of MIP and NIP-based sensors for the detection of *Proteus mirabilis* in sterilized HEPES buffer, pH 7.3.

The obtained results were not good which is probably due to a lack of expression of flagella by the bacteria and/or a complex structure at the outer surface of bacteria, and hence further optimization is needed. Maybe also some transducer element (such as carbon nanotubes or graphene) could be incorporated into the MIP structure to enhance the transduction characteristics of MIPs in order to detect the biorecognition event between the bacteria and the MIP.

5.3.3 Conclusions

In this section, potentiometric detection of flagella and whole cell of *Proteus mirabilis* were described as a proof-of-concept with the aim to fabricate cocktail-free regenerable potentiometric biosensors based on artificial receptors. This approach is a similar process than the fabrication of potentiometric ISEs (but using ion-selective membranes instead of molecularly imprinted polymers), which ISEs cannot be used in the detection of large targets such as proteins or microorganisms. Herein, we were able to detect flagella up to the nanomolar level but the sensors suffer from nonspecific adsorption of flagella. An interesting fact is that both sensors (MIPs and NIPs) show good selectivity with respect to various proteins which may come from the variable charges of different proteins. The sensors were further extended to the detection of whole cell of *Proteus mirabilis* but this detection was not successful. This was probably due to the large and complex structure of whole cells and hence optimization is required.

5.3.4 References

Almeida, S.A.A., Truta, L.A.A.N.A., Queirós, R.B., Montenegro, M.C.B.S.M., Cunha, A.L., Sales, M.G.F., 2012. Optimizing potentiometric ionophore and electrode design for environmental on-site control of antibiotic drugs: application to sulfamethoxazole. Biosens. Bioelectron. 35, 319–26.

Novell, M., Parrilla, M., Crespo, G.A., Rius, F.X., Andrade, F.J., 2012. Paper-based ion-selective potentiometric sensors. Anal. Chem. 84, 4695–4702.

Rebelo, T.S.C.R., Santos, C., Costa-Rodrigues, J., Fernandes, M.H., Noronha, J.P., Sales, M.G.F., 2014. Novel prostate specific antigen plastic antibody designed with charged binding sites for an improved protein binding and its application in a biosensor of potentiometric transduction. Electrochim. Acta 132, 142–150.

Solsky, R.L., 1990. Ion-selective electrodes. Anal. Chem. 62, 21R–33R.

Tavares, A.P.M., Moreira, F.T.C., Sales, M.G.F., 2013. Haemoglobin smart plastic antibody material tailored with charged binding sites on silica nanoparticles : its application as an ionophore in potentiometric transduction. RSC Adv. 3, 26210–26219.

Chapter 6

Conclusions

UNIVERSITAT ROVIRA I VIRGILI
PLASTIC ANTIBODIES FOR THE DETECTION OF BACTERIAL PROTEINS AND MICROORGANISMS
Azizur Rahman Khan

The present chapter contains the main conclusions of this thesis. The specific conclusions about the individual procedures carried out during the thesis have been discussed at the end of each chapter. This chapter is divided into two parts: the first gives the scientific conclusions directly related to the work carried out including some trends for the future work; and the second makes a personal analysis of the attributes and skills acquired during this PhD period, given that the main objective of the doctoral thesis is to train the PhD student to become a full researcher.

6.1 Scientific conclusions

The doctoral thesis was designed to explore the concept of fabricating artificial receptors based on molecular imprinting. These promising materials were used as new biosensing materials and platforms as an alternative to expensive and non-robust natural receptors, which may open up new horizons on diagnostic and point-of-care devices. Novel synthetic receptors with an affinity for bacterial surface proteins and for the whole cell have been studied in an attempt to construct stable, affordable, robust, cost-effective and portable biosensors. The main empirical findings are summarized within the respective chapters:

In Chapter 3 (***Molecular imprinting of protein A from Staphylococcus aureus)***, bacterial surface proteins of *Staphylococcus aureus* were imprinted to create MIPs to be used for the detection of protein A using electrochemical techniques. Potentiometric detection was not successful but impedimetric detection was correctly performed (section **3.1**).

In Chapter 4 (***Fabrication of homemade paper-based electropolymerized printed electrodes***), we report the design of a home-made device based on paper substrates that includes the configuration for three or two electrodes. The electrochemical characteristics of this low-cost device are comparable to those of commercial electrodes. These electrodes offer several advantages: the support is made of paper, which is inexpensive, they are bendable, they are lightweight, they are not fragile and they can be disposed of after a single use.

In Chapter 5 ***(Molecular imprinting of flagella from Proteus mirabilis***), flagella from *Proteus mirabilis* were imprinted for the first time and successfully detected using sensing devices based on commercial screen-printed electrodes and homemade disposable paper-printed electrodes, while impedimetry and/or square wave voltammetry were used as

detection techniques (section **5.1**). These sensors were also used to detect the whole cell of *Proteus mirabilis* but further optimization is required (section **5.2**). Moreover, a new approach was successfully used for the cocktail-free and regenerable potentiometric detection of flagella from *Proteus mirabilis* for the first time (**5.3**). The performance of the sensors also encouraged direct detection of whole cell of *Proteus mirabilis* but results were not positive probably due to the complex structure of the whole cell and the lack of further optimization.

6.2. Acquisition of attributes and skills

During my PhD studies, in addition to acquiring scientific knowledge, I have also acquired certain competences that will help me in my future career. In this thesis I have outlined the development of my research project. Firstly, I focused on learning the main features of artificial receptors based on molecularly imprinted polymers (a new, and therefore challenging, field for me), and how this field is related to analytical chemistry, which was my specific research area. I made an in-depth study of the literature in order to understand the concepts and terminology involved. Secondly, I made a careful selection of the relevant literature and reviewed it to obtain what was most useful for my own work. This has helped me to develop critical reading skills. I have also acquired the ability to initiate research projects and to define the framework and variables involved. These skills were necessary for my experimental work, which involved understanding what MIPs are, developing a new approach for MIP-based sensors for detecting specific proteins and microorganisms, and critically evaluating my results, both within and across a changing disciplinary environment. The experimental work of this thesis was conducted in collaboration with other members of the research group, and so I have learned to work as a member of a team. At the same time, I have attended several congresses where I had to present and discuss our scientific results. I also visited a foreign research group, and had the chance to observe similar and different ways of putting science into practice, which also gave me some experience in collaboration strategies. Moreover, I have written up the results of our work and published in international scientific journal. Through these scientific contributions, I have acquired the ability to communicate results effectively both orally and in writing, and have gained an understanding of the relevance and value of my research to the national and international scientific communities.

Appendices

- **Abbreviations**
- **List of figures**
- **Scientific contribution**

UNIVERSITAT ROVIRA I VIRGILI
PLASTIC ANTIBODIES FOR THE DETECTION OF BACTERIAL PROTEINS AND MICROORGANISMS
Azizur Rahman Khan

Appendix I. Abbreviations

ΔE – Potential change

R_{ct} – Charge transfer resistance

ΔR_{ct} – Relative charge transfer resistance

R_S –Solution resistance

C_{dl} – Double layer Capacitance

CV – Cyclic voltammetry

SWV– Square wave voltammetry

D_0 – Diffusion coefficient

E_0 – Standard potential

EIS – Electrochemical impedance spectroscopy

EMF – Electromotive force

Ep_a – Anodic peak potential

Ep_c – Cathodic peak potential

F – Faraday constant (96485 C/mol)

MPM – Matched potential method

GOx – Glucose oxidase

AP – 3-Aminophenol

ABA – 3-Aminophenyl boronic acid

BSA – Bovine serum albumin

PA – Protein A from *Staphylococcus aureus*

FPM – Flagella from *Proteus mirabilis*

PM – *Proteus mirabilis*

TEM – Transmission electron micrscope

ESEM – Environmental scanning electron microscope

FTIR – Fourier transform infrared spectroscopy

Hz – Hertz (frequency unit)

Ip_a – Anodic peak current

Ip_c – Cathodic peak current

ISE – Ion-selective electrode

log*K* – Selectivity coefficient

LOD – Limit of detection

MWCNT – Multi-walled carbon nanotube

n – Number of electrons transferred per molecule diffusing to the electrode surface

R – Universal gas constant (8.314 J/K·mol)

RE – Reference electrode

WE – Working electrode

CE – Counter electrode

SPE – Screen printed electrodes

SWCNT – Single-walled carbon nanotube

K_D – Dissociation Constant

W – Warburg diffusion element

Z' – Imaginary component of impedance

Z''– Real component of impedance

ω – Angular frequency

ϕ – Phase shift

ΔG – Free energy change

AC – Alternating current

ATR – Attenuated total reflectance

AFM – Atomic Force Microscopy

APZ – Aminophenoxazone

HEPES – 4-(2-Hydroxyethyl)-1-piperazineethanesulfonic acid

ELISA – Enzyme linked immunosorbent assay

FRA – Frequency response analysis

MES – 2-(*N*-morpholino) ethanesulfonic acid

MI – Molecular imprinting

MIP – Molecularly imprinted polymer

NIP – Non imprinted polymer

PBS – Phosphate buffered saline

PAP – Polyaminophenol

PABA – Poly(aminophenylboronic acid)

QCM – Quartz crystal microbalance

TRIS – Tris(hydroxymethyl)aminomethane

TSB – Tryptic soy broth

TSA – Tryptic soy agar

PEG – Poly(ethyleneglycol)

Appendix II. List of figures

Figure 3.5. Selectivity test of the sensor by competitive method; signal for (A) only PA, (B) mixture of PA and BSA 1: 0.1 (in M), and (C) mixture of PA and BSA 1: 1 (in M).

Figure 3.6. EIS measurements of (A) MIPs based sensor and the corresponding calibration curves (B) in 5.0 mM $[Fe(CN)_6]^{3-}$ and 5.0 mM $[Fe(CN)_6]^{4-}$ by spiking PA in tap water.

Figure S3.1. Raman spectrum at different stages of the sensors fabrication, (A) MIPs; (B) NIPs; inset: zoom of MIPs D peaks.

Figure S3.2. FTIR Spectrum at different stages of the sensors fabrication.

Figure S3.3. ESEM images at different stages of the sensors fabrication, (A) Clean SWNCTs SPE, (B) MIP after polymerization and (C) MIP after template removal.

Figure 4.1. HP C-PEs (three-electrode design); RE: reference electrode, WE: working electrode, CE: counter electrode. The smaller picture on top shows the two-electrode design.

Figure 4.2. Schematic presentation of the process and fabrication of the device and its connection with the portable switch box: (A) filter paper; (B) hydrophobic filter paper; (C) plastic mask over the hydrophobic filter paper; (D) sketch of the electrodes; (E) carbon ink-printed electrode; (F) reference electrode (left) with Ag/AgCl ink; (G) final device partly covered by the plastic tape; (H) three-electrode and (I) two-electrode devices connected to a portable switch box.

Figure 4.3. ESEM images before (A) and after (B) modification of the filter paper by wax, and AFM images before (C) and after (D) modification of the filter paper by wax.

Figure 4.4. Hydrophobicity of the wax-modified filter paper (contact angle, $\Theta_C = 90°$).

Figure 4.5. Electrochemical performance before and after the electrochemical cleaning of the fabricated HP C-PE; Electrochemical follow up in 5.0 mM $[Fe(CN)_6]^{3-}$ and 5.0 mM $[Fe(CN)_6]^{4-}$, in MES buffer pH 5.0, carried out by (A) CV, (B) SWV and (C) EIS (Nyquist plots) assays.

Figure 4.6. Electrochemical characterization of cleaned electrodes by scan rate (A) cyclic voltammograms with variable scan rate and (B) fitting of the oxidation and reduction current with the square root of scan rate (mV/s); 5.0 mM $[Fe(CN)_6]^{3-}$ and 5.0 mM $[Fe(CN)_6]^{4-}$, in MES buffer pH 5.0.

Figure 4.7. Bending characteristics of HP C-PEs (A) Bending test; (B) cyclic voltammograms after subsequent bending; 5.0 mM $[Fe(CN)_6]^{3-}$ and 5.0 mM $[Fe(CN)_6]^{4-}$, in MES buffer pH 5.0.

Figure 4.8. Electropolymerization of different monomers; (A) Phenol, (B) AP and (C) ABA using CV in sodium acetate buffer pH 5.0. Scan rate 50 mV/s.

Figure 4.9. Follow up of surface modification due to electropolymerization by (A) CV and (B) SWV; 5.0 mM $[Fe(CN)_6]^{3-}$ and 5.0 mM $[Fe(CN)_6]^{4-}$, in MES buffer pH 5.0.

Figure 4.10. (A) ΔE changes of the Ag/AgCl electrode of HP C-PE with respect to standard Ag/AgCl double junction reference electrode (addition of different concentrations of BSA is indicated), (B) stability of the working electrode of HP C-PE with respect to the Ag/AgCl reference of HP C-PE. Measurements in HEPES buffer 10^{-4} M, pH 7.2.

Figure S4.1. FTIR spectrum.

List of figures

Figure 5.10. Schematic representation of the fabrication of the biosensor. (A) working area of Au-SPE, (B) deposited FPM, (C) imprinting stage after electropolymerization of pyrrole, (D) binding sites formation after template removal by trypsin.

Figure 5.11. (A) Cyclic voltammetry-based synthesis of MIPs and NIPs, and the corresponding surface blocking test (B) carried out by CV in 5.0 mM $[Fe(CN)_6]^{3-}$ and 5.0 mM $[Fe(CN)_6]^{4-}$, in MES buffer pH 5.0.

Figure 5.12. (A) Electrochemical characterization of MIP and NIP-films by (A) EIS (Nyquist plots) and by (B) SWV assays with 5.0 mM $[Fe(CN)_6]^{3-}$ and 5.0 mM $[Fe(CN)_6]^{4-}$ in MES buffer pH 5.0.

Figure 5.13. Potentiometric measurements of (A) MIP and NIP-based sensors and the corresponding calibration curves (B) in HEPES buffer pH 7.3. Inset in (A) shows the response time.

Figure 5.14. EIS-based surface follow-up after calibration (A) and regeneration (B) of the MIP and NIP-devices; 5.0 mM $[Fe(CN)_6]^{3-}$ and 5.0 mM $[Fe(CN)_6]^{4-}$, in MES buffer pH 5.0.

Figure 5.15. Potentiometric measurements of MIP and NIP-based sensors for the detection of *Proteus mirabilis* in sterilized HEPES buffer, pH 7.3.

Appendix III. Scientific contributions

- **Journal directly resulting from this doctoral thesis:**

M. Azizur R. Khan, Felismina T.C. Moreira, Jordi Riu and M. Goreti F. Sales, Plastic antibody for the electrochemical detection of bacterial surface proteins, *Sensors and Actuators B: Chemical*, 233 (2016) 697-704.

M. Azizur R. Khan, A. Rita Aires Cardoso, M. Goreti F. Sales, Susana Merino, Juan M. Tomás, F. Xavier Rius and Jordi Riu, Artificial antibodies for the electrochemical detection of bacterial flagella from *Proteus mirabilis* (*Submitted*).

M. Azizur R. Khan, C.A.C. Vieira, M. Goreti F. Sales, F. Xavier Rius and Jordi Riu, Fabrication of homemade paper-based electropolymerized printed electrodes (*Submitted*).

Journal indirectly resulting from this doctoral thesis:

Zewdu Mesele, *M. Azizur R. Khan*, Pascal Blondeau and Jordi Riu, Antibody and aptamer based chemiresistor: a comparative study for the detection of lysozyme (*Manuscript in preparation*).

- **Conference attendance and poster presentation directly resulting from this doctoral thesis:**

Md. Azizur Rahman Khan, A. Rita Aires Cardoso, Susana Merino, M. Goreti F. Sales and Jordi Riu, Plastic antibody for the electrochemical detection of bacterial Flagella, Biosensors 2016 conference, Gothenburg, Sweden, PP.1.271.

Md. Azizur Rahman Khan, Jordi Riu, Susana Merino and M. Goreti F. Sales, Molecularly–imprinted polymers for the electrochemical detection of bacterial Flagella, Graduate student symposium on molecular imprinting 2015, Medway School of Pharmacy, Kent, United Kingdom, PP.09, Page 46.

Md. Azizur Rahman Khan, Felismina Moreira, M. Goreti F. Sales and Jordi Riu, Molecularly–imprinted polymers for the electrochemical detection of bacterial surface proteins, VII workshop on analytical nanoscience and nanotechnology NyNa 2015, University of Salamanca, Salamanca, Spain, PP.69, Page 243.

UNIVERSITAT ROVIRA I VIRGILI
PLASTIC ANTIBODIES FOR THE DETECTION OF BACTERIAL PROTEINS AND MICROORGANISMS
Azizur Rahman Khan

UNIVERSITAT ROVIRA I VIRGILI
PLASTIC ANTIBODIES FOR THE DETECTION OF BACTERIAL PROTEINS AND MICROORGANISMS
Azizur Rahman Khan

UNIVERSITAT ROVIRA I VIRGILI
PLASTIC ANTIBODIES FOR THE DETECTION OF BACTERIAL PROTEINS AND MICROORGANISMS
Azizur Rahman Khan

UNIVERSITAT ROVIRA I VIRGILI